ON HIGHER–ORDER MIXED–INTERPOLATED GENERAL SHELL FINITE ELEMENTS

by

Miguel Luiz Bucalem

Engenheiro Civil
Escola Politécnica da Universidade de São Paulo (December 1984)

Mestre em Engenharia
Escola Politécnica da Universidade de São Paulo (June 1987)

Submitted to the Department of Civil Engineering
in partial fulfillment of the requirements
for the degree of

Doctor of Philosophy in Structural Engineering

at the

MASSACHUSETTS INSTITUTE OF TECHNOLOGY

February 1992

Signature of Author.... .....
Department of Civil Engineering
February 21, 1992

Certified by.....
Klaus-Jürgen Bathe
Professor of Mechanical Engineering
Thesis Supervisor

Accepted by. .....
Eduardo Kausel
Chairman, Departmental Committee on Graduate Students

ON HIGHER–ORDER MIXED–INTERPOLATED GENERAL SHELL FINITE ELEMENTS

by

Miguel Luiz Bucalem

Submitted to the Department of Civil Engineering
on February 21, 1992, in partial fulfillment of the
requirements for the degree of
Doctor of Philosophy in Structural Engineering

Abstract

The use of shell finite elements has become an important ingredient in the analysis and design of shell structures. This thesis is concerned with the development of new plate bending and general nonlinear shell elements that are suitable for engineering design applications. Therefore the requirements of our formulations have been simplicity, effectiveness and, above all, reliability.

In the first part of the work a family of Reissner–Mindlin mixed–interpolated plate bending elements is studied. The elements are based on the **M**ixed **I**nterpolation of **T**ensorial **C**omponents (MITC) approach in which the transverse shear strain components are interpolated and tied to the displacement field. This family of elements has a sound mathematical foundation that assures the convergence of the discretizations with optimal error bounds. A detailed numerical convergence study of displacement and stresses is also presented. Special attention is given to the accuracy of the transverse shear stress predictions and the effect of element geometric distortions on the performance of the elements.

In the second part of the thesis two mixed-interpolated general nonlinear shell elements — a 9-node element and a 16-node element — are presented. They are also based on the MITC approach in which the covariant strain component fields for the in–plane and shear actions are interpolated and tied to the displacement field. Both elements do not exhibit either membrane or shear locking.

The reliability and effectiveness of the newly developed shell elements were assessed by solving a number of well established test problems. Both elements perform very well and the 16-node mixed interpolated element shows a substantial improvement with respect to its displacement based counterpart.

Thesis Supervisor: Klaus-Jürgen Bathe
Title: Professor of Mechanical Engineering

Dedication

To my parents Wilson and Beatriz and to my wife Tamara

Acknowledgements

I would like to express my respect and deep gratitude to Professor Klaus–Jürgen Bathe for his invaluable guidance throughout my stay at M.I.T.. His exceptional attitude towards teaching and his enthusiasm regarding research are examples that I will endeavor to follow. His support, encouragement and trust have given me the strength and stability to develop my research.

I would like also to express my sincere appreciation to Professor Eduardo Kausel and Professor Jerome J. Connor. As members of my doctoral committee, they provided valuable advice and encouragement.

I am indebted to Professor Franco Brezzi from University of Pavia, Italy, from whose work I have learned so much. Our meeting by the occasion of the ADINA conference, in July 91, although short, was very meaningful and has been a source of inspiration.

Many thanks are due to the past and present colleagues of the Finite Element Research Group. Their friendly attitude and help made our work place comfortable and stimulating. In particular, I would like to thank Kenshiro Kato, Adrian Eterović, Seong–Wook Cho, Chanwut Nitikitpaiboon, Nam–Sua Lee, Paolo Gaudenzi, Olivier Comps and Aécio Lira for sharing with me their ideas, knowledge and friendship.

I would like also to acknowledge ADINA R & D, Inc. for their collaboration during this research. Their staff members have always been very helpful and the use of the ADINA Finite Element Systems has been important for the development of this work.

Professor Decio Leal de Zagottis through his brilliant teaching has introduced me to the field of solid mechanics and incited my interest to pursue graduate studies. He was

my advisor for my Master's work and has always encouraged, helped and guided me on my scholastic pursuits. I am most grateful for his assistance.

I am also thankful to the professors of my home university that have given me, in many occasions, advice, assistance and encouragement. In particular, I should mention Victor Manoel de Souza Lima, Henrique Lindenberg Neto, Waldemar Hachich, João Cyro André, Carlos E. N. Mazzilli, Carlos Alberto Soares, Paulo M. Pimenta and Paulo Boulos.

Truly unbounded thanks are due to my family. My father Wilson has given me throughout these years an extraordinary moral support. His encouragement for my coming to M.I.T. was a tremendous act of generosity since it implied many sacrifices for him. My mother Beatriz has always given me unconditional support. My wife Tamara has been always present. She helped me overcome all the difficulties along the way. Her love, patience, sacrifice and emotional support were essential for the completion of my studies.

I finally would like to acknowledge the Conselho Nacional de Desenvolvimento Científico e Tecnológico for providing me the scholarship for my graduate studies at M.I.T. and the Escola Politécnica da Universidade de São Paulo for conceding me an extended leave of absence.

Contents

List of Figures

List of Tables

Chapter 1

Introduction

There is no need to discuss the importance of shell structures. Their efficient load–carrying capabilities made their use widespread in a variety of engineering applications [1]. The continuous development of new structural materials leads to ever increasingly complex shell designs that require careful analysis.

Although analytical techniques are very important, the use of numerical methods to solve shell mathematical models of complex structures has become an essential ingredient in the design process. The finite element method has been the fundamental numerical procedure for the analysis of shells.

Ideally, the structural designer or analyst should be able to concentrate on the mechanical behavior of the structure and pay close attention to the underlying design issues. The finite element procedure should be used merely as a tool to obtain the solution of the mathematical model chosen to describe the structure. Unfortunately, this is not what usually happens in shell finite element analysis. Frequently, the analyst is required to be an expert in shell element technology to use confidently his/her finite element results. This is mainly due to the proliferation of elements that do not always work *i.e.*, are not reliable. In our research the development of reliable finite elements has always been a requirement. Although this may seem a very basic condition, the literature has plenty of proposed elements that perform effectively in some cases but fail severely in others.

Nevertheless, their use with "care" is recommended.

An important consideration discussed in Reference [2] is that shell finite elements tend to be integrated in CAD (Computer Aided Design) systems, exposing design engineers, that are relatively inexperienced with the details of shell element technology to the use of such elements. In this setting, the recommendation that a particular element should be used with care is meaningless, and the reliability of the elements is a strict requirement. Also, in such an environment, shell elements that are just adequate for a certain class of problems *i.e.*, for thin shell situations or for specific shell geometries and/or loading conditions are not as suitable as general shell elements.

The research activity in the area of finite elements for plates and shell structures spans a period of over two decades and continues to be very intense. A review of the current state of the art can be found in Reference [1]. Although we do not intent to present here a comprehensive review of what has been accomplished in shell element technology, we plan to briefly mention some key aspects of this research area before concentrating on the approach that we have followed in developing our plate and shell elements.

The first step is to select an appropriate mathematical model. The thin shell theories that developed from the fundamental work of Love [3], and lead to the Koiter–Sanders theory [4; 5], have been used as mathematical models to propose shell elements. Also, a number of simplified thin shell theories that are derived by imposing restrictions either on the shell geometry or the loading conditions, or both, have been used to formulate shell elements. Many of such shell elements are discussed in Reference [6] where a catalogue of elements is presented.

The approach of degenerating the shell from a three–dimensional solid is a very attractive alternative to the use of a thin shell theory. In this approach the shell behavior is described by imposing judiciously chosen kinematic and mechanical assumptions on the three–dimensional continuum mechanics conditions. The resulting theory corresponds for plate bending situations to the Reissner–Mindlin plate theory. This approach has been first presented, in the context of shell element formulations, by Ahmad *et. al.* [7] and has

a number of key features that make it very suitable for shell finite element constructions, namely:

- The formulation is applicable to any shell geometry.
- The formulation is adequate for thin and thick situations.
- The formulation leads to C^0 conforming displacement based elements.
- The formulation uses only engineering nodal point degrees of freedom such as displacements and rotations.

Shell elements based on this approach have been formulated for general nonlinear analysis (material and geometric nonlinear) by Ramm [8] and Bathe and Bolourchi [9]. A very lucid and thorough presentation of these elements can be found in Reference [10].

Although the pure displacement based formulation of these elements has all the above-mentioned appealing features, which are very desirable if the elements are to be used in engineering practice, they do suffer from the serious deficiency of membrane and shear locking. The locking effects are devastating for lower–order elements, and even for higher–order elements they severely reduce the potential predictive capability of the elements.

A number of approaches and techniques have been proposed to overcome these difficulties. The simplest one, however unsuccessful, is the use of uniform and selective reduced integration. In general the URI (uniform reduced integrated) elements possess spurious zero energy modes, and although in some cases they may provide accurate solutions, in other cases a global mechanism may form due to the collective action of the spurious zero energy modes causing rank deficiency (or almost rank deficiency) of the global stiffness matrix. Even if a global mechanism does not arise, a near–mechanism might be activated which leads to unacceptable answers. The recommendation of disregarding solutions that have been affected by spurious energy modes is not easy to observe since, when the solution of the problem is not known, the judgement of whether a solution is "good" or not is very difficult to make. The SRI (selective reduced integrated)

elements, although to a smaller degree, suffer from the same deficiencies as the URI elements and in some case show very low convergence rates. Both types of elements are quite sensitive to geometric distortions. The above considerations make clear that the use of reduced integration is an unreliable technique to deal with locking effects. Nevertheless, the literature is rich in uniform and selective reduced integrated elements for plates and shells. We refer here just to the early works on reduced integration [11; 12; 13]. We note that in some cases it is possible to show a total equivalence between the use of reduced integration and a mixed formulation [14; 15]. In such an event reduced integration may be an efficient way of implementing a mixed method but the analysis of whether it is a good formulation or not has to be made in the context of mixed methods.

Belytschko and co-workers developed the concept of spurious mode control [16; 17] in an attempt to use reduced integration and avoid the possibility of having spurious zero energy modes. Although successful in suppressing the spurious modes, their formulation is not transparent, requiring the use of some numerically adjusted factors.

The MITC (**M**ixed **I**nterpolation of **T**ensorial **C**omponents) approach has successfully overcome the difficulties regarding locking encountered by the degenerated displacement based elements still preserving their desirable properties.

The MITC concept was first introduced for shell elements by Dvorkin and Bathe [18]. In this work a general 4–node shell element for nonlinear analysis, referred to as the MITC4 element, was proposed. The subsequent developments undertaken with the MITC approach for general shell analysis are discussed in more detail in Chapter 4.

Although 8 and 9-node shell elements were developed with the MITC and similar approaches [2; 19; 20; 21], it has usually been implied that the 16–node displacement based element avoids membrane and shear locking and is a good performer. Our experiences with this element show that in some problems it displays a very low convergence rate and when curved and distorted it may present a locking behavior. The above evidence would already justify efforts towards developing a 16-node mixed interpolated element. Moreover, numerical studies [22] have indicated that higher–order Lagrangian elements are

very efficient to predict stresses in two–dimensional analysis. In addition, in shell analysis, the higher–order elements provide a better approximation of the curved geometry of the shell.

Another important topic that has received a great deal of attention is the development of plate bending elements. The literature in this subject is abundant and a comprehensive review is not pursued here. For a partial account on this subject we refer to [23] and appropriate sections of Reference [6].

Of course, general shell elements degenerate to linear plate bending elements when the shell is flat, the analysis is linear and the plate is subjected to transverse loading only. Reliable and effective general shell elements when applied to plate bending problems should avoid shear locking and provide accurate predictions. This is a requirement which is addressed in Chapter 5. However, the Reissner–Mindlin plate bending model [24; 25] is very important and *per se* justifies a special treatment regarding its finite element discretizations.

The MITC4 element [18; 26] has been mathematically analyzed in the context of the Reissner–Mindlin plate model. It has been shown [27] that this element has optimal error bounds for the displacement variables even for the limit case when the thickness goes to zero. The initiative, which started with the mathematical analysis of the MITC4 element, has continued and led to the development of a family of MITC elements for Reissner-Mindlin plates that has a strong mathematical foundation. We have been involved in this effort and the developments are presented in Chapter 2.

Summarizing, the major objective of this work was the development of reliable and effective higher–order mixed–interpolated plate bending and general nonlinear shell elements. The organization of the thesis is as follows.

In Chapter 2 we summarize the mathematical theory of the MITC plate bending elements, show the element developments and present a thorough numerical assessment of the performance of this family of elements.

In Chapter 3, we study the membrane and shear locking behavior of the one–dimensional

analogues of the degenerated displacement based shell elements *i.e.*, the isobeam elements. The objective is to use this simplified setting to gain insight into and understanding of the locking behavior (mainly membrane locking) of curved shell elements.

In Chapter 4 we discuss the requirements that our formulations for general shell elements should comply with, we review the work that has been carried out earlier with the MITC approach and we propose two higher–order elements for general nonlinear shell analysis.

Finally, in Chapter 5 a series of benchmark and established test problems are used to assess the predictive capabilities of the newly proposed mixed–interpolated higher–order shell elements.

Chapter 2

A Family of Reissner–Mindlin Mixed–Interpolated Plate Bending Elements

The mixed interpolation of the tensorial components has been a successful approach to formulate Reissner–Mindlin plate bending elements that are effective and free of shear locking. Although in recent years many researchers have taken similar approaches to propose plate bending elements [28; 29; 30; 1], there are differences in the element formulations and the MITC elements are the only ones that have a good mathematical foundation.

As mentioned already in Chapter 1 the MITC4 was the first MITC element proposed. Although it was formulated directly as a general shell element for nonlinear analysis, of course, it degenerates to a plate bending element when subjected to the appropriate conditions [26]. In this case in certain geometries it is similar to the elements proposed by MacNeal [28] and Hughes and Tezduyar [29].

Insight into element behavior and the use of numerical experiments were the main ingredients employed in the construction of the MITC4 element. Subsequently, this element was mathematically analyzed [27] for the plate bending problem and shown to

be free of shear locking and to have optimal error bounds for the displacement variables for any thickness of the plate. This mathematical analysis was expanded [31; 32] and a set of properties about the finite element discretizations were identified. When these properties are satisfied, optimal convergence behavior is assured. Therefore a procedure for the design of new elements that comply with the requirements of the mathematical analysis was formulated and, in fact, new elements were proposed [31; 32; 33; 34].

The mathematical theory of the MITC elements is quite general and it is, to our knowledge, the only mathematical analysis available of the convergence characteristics of Reissner–Mindlin plate bending elements. However, there are still a few issues not accounted for in the theory. One of these issues is the fact that the mathematical analysis is only valid for rectangular decompositions of the domain. General quadrilateral and triangular isoparametric elements are formulated using the mixed interpolation of the covariant strain component fields in natural element coordinates. This extension has not yet been theoretically analyzed, therefore it is important to assess numerically the effect of element distortions both in the accuracy of the predictions and in the convergence rates. In Section 2.3 we present results concerning element geometric distortions. The optimality of the shear strain predictions is another point in which the mathematical theory is still not complete. The transverse shear strains are usually the most difficult strain components to predict for Reissner–Mindlin plate elements and deserve a great deal of our attention. The numerical results, as will be seen shortly, are very encouraging in this respect. We should also mention that progress has recently been made in the mathematical analysis regarding the transverse shear strain predictions. In Reference [35] near–optimal error bounds for the transverse shear strains were derived for the higher–order MITC elements.

The organization of this chapter is as follows. In the next section we summarize the mathematical theory of the MITC elements. In section 2.2 we present the MITC element formulations *i.e.*, the MITC4, MITC9 and MITC16 quadrilateral elements and the MITC7 and MITC12 triangular elements. Finally, in section 2.3 we show numerical

results obtained with the above elements including a detailed numerical convergence study.

2.1 The Plate Bending Problem and its Discretizations

We consider the sequence of problems P_t in which the thickness t goes to zero and the load has the form $t^3 p(x_1, x_2)$ per unit mid-surface area with $p(x_1, x_2)$ given and fixed. A typical problem of this sequence has then the form

$$\min_{\underline{\theta}, w} \left\{ \frac{t^3}{2} a(\underline{\theta}, \underline{\theta}) + \frac{\lambda t}{2} \int_\Omega |\underline{\theta} - \underline{\nabla} w|^2 \, d\Omega - t^3 \int_\Omega p \, w \, d\Omega \right\} \tag{2.1}$$

which divided by t^3 becomes

$$\min_{\underline{\theta}, w} \left\{ \frac{1}{2} a(\underline{\theta}, \underline{\theta}) + \frac{\lambda t^{-2}}{2} \int_\Omega | \underline{\theta} - \underline{\nabla} w |^2 \, d\Omega - \int_\Omega p \, w \, d\Omega \right\} \tag{2.2}$$

Here $\frac{t^3}{2} a(\underline{\theta}, \underline{\theta})$ is the bending internal energy and $\frac{\lambda t}{2} \int_\Omega | \underline{\theta} - \underline{\nabla} w |^2 \, d\Omega$ is the shear energy [10].

A finite element is effective if the solution to any problem in the sequence (uniformly in t) yields good approximations. A detailed analysis of the MITC4 element for the solution of Equation (2.2) was presented in Reference [27].

However, a simplified test on whether an element is effective was proposed in Reference [31]: since we are interested in the limit behavior for $t \to 0$ we might restrict ourselves to the limit problem $t = 0$. It is clear that if an element is uniformly good for $t \to 0$ it will also be good for $t = 0$, but the converse is not necessarily true. Intuitively the test ($t = 0$) makes sense and as can be seen in References [27] and [35] the test is indeed very

useful. Hence we can concentrate on the limit problem of Equation (2.2), which can be written as

$$\min_{\substack{\underline{\theta},w \\ \underline{\theta}=\underline{\nabla}w}} \left\{ \frac{1}{2} a(\underline{\theta},\underline{\theta}) - \int_\Omega p\, w\, d\Omega \right\} \tag{2.3}$$

The members of the family of elements that we are going to discuss here are constructed like the MITC4 and MITC8 elements of references [26] and [2]. In particular we have to choose

(i) a finite element space $\underline{\Theta}_h$ for the approximation of the rotations,

(ii) a finite element space W_h for the approximation of the transverse displacement,

(iii) a finite element space $\underline{\Gamma}_h$ for the approximation of the shear strains and, finally,

(iv) a "reduction operator" R_h which interpolates piecewise smooth functions into $\underline{\Gamma}_h$.

Accordingly, the discrete version of Equation (2.2) becomes

$$\min_{\underline{\theta}_h,w_h} \left\{ \frac{1}{2} a(\underline{\theta}_h,\underline{\theta}_h) + \frac{\lambda t^{-2}}{2} \int_\Omega \mid R_h(\underline{\theta}_h - \underline{\nabla} w_h) \mid^2 d\Omega - \int_\Omega p\, w_h\, d\Omega \right\} \tag{2.4}$$

and the corresponding limit problem ($t = 0$) is

$$\min_{\substack{\underline{\theta}_h,w_h \\ R_h(\underline{\theta}_h-\underline{\nabla}w_h)=\underline{0}}} \left\{ \frac{1}{2} a(\underline{\theta}_h,\underline{\theta}_h) - \int_\Omega p\, w_h\, d\Omega \right\}. \tag{2.5}$$

The aim is now to find choices for $\underline{\Theta}_h, W_h, \underline{\Gamma}_h$ and R_h such that Equation (2.5) has a unique solution which converges, as the mesh parameter $h \to 0$, to the solution of

Equation (2.3) with optimal error bounds.

The construction of the appropriate choices starts by recognizing that for every pair $\underline{\theta}, w$ with

$$\underline{\theta} = \underline{\nabla} w, \tag{2.6}$$

of smooth functions, we want to find a corresponding pair $\underline{\theta}^I \in \underline{\Theta}_h$ and $w^I \in W_h$ with

$$R_h(\underline{\theta}^I - \underline{\nabla} w^I) = \underline{0} \tag{2.7}$$

which approximates $(\underline{\theta}, w)$ with optimal error bounds. It is clear that, if this can be done (and if R_h is a good approximation of the identity, as you expect from a decent interpolation operator) then the minimum of a quadratic functional (as is $\frac{1}{2}a(\underline{\theta}, \underline{\theta}) - \int_\Omega p\ w\ d\Omega$) over the set of pairs satisfying Equation (2.7) will be a good approximation to the minimum of the same functional over the set of pairs satisfying Equation (2.6).

The first step of the element formulation is therefore to find $\underline{\theta}^I$ and w^I. Our crucial assumption for the function $w_h \in W_h$ is that

$$R_h(\underline{\nabla} w_h) = \underline{\nabla} w_h \qquad \forall w_h \in W_h \tag{2.8}$$

so that Equation (2.7) becomes

$$R_h \underline{\theta}^I = \underline{\nabla} w^I \tag{2.9}$$

Now, by setting for a general vector valued function $\underline{\phi}$,

$$\mathrm{rot}\underline{\phi} = \frac{\partial \phi_2}{\partial x_1} - \frac{\partial \phi_1}{\partial x_2}, \tag{2.10}$$

we recognize that a necessary condition for Equation (2.9) to hold is that

$$\mathrm{rot}(R_h \underline{\theta}^I) = 0 \tag{2.11}$$

Since the rot operator is formally very close to the divergence operator, we are facing a situation very similar to the one that is encountered in the solution of the Stokes problem of incompressible fluids. There (for the Stokes problem) we have a smooth function $\underline{u}$ with div $\underline{u} = 0$, and want to find a finite element approximation $\underline{u}_h$ which satisfies div $\underline{u}_h = 0$. Such finite element approximation must be judiciously constructed, and much attention has been focused on this task. Consequently, we can find in the literature (see e.g. Reference [36]) many pairs $(\underline{U}_h, P_h)$ of velocity-pressure approximations such that the discretization of the Stokes problem

$$\left.\begin{array}{l} \text{find } \underline{u}_h \in \underline{U}_h \text{ and } p_h \in P_h \text{ such that} \\ \int_\Omega \underline{\underline{\nabla}}\, \underline{u}_h : \underline{\underline{\nabla}}\, \underline{v}_h d\Omega - \int_\Omega p_h \text{ div } \underline{v}_h d\Omega = \int_\Omega \underline{f} \cdot \underline{v}_h d\Omega \quad \forall \underline{v}_h \in \underline{U}_h \\ \int_\Omega q_h \text{div } \underline{u}_h d\Omega = 0, \qquad \forall q_h \in P_h \end{array}\right\} \tag{2.12}$$

is well-posed, stable and has optimal convergence properties to the continuous solution. A sufficient condition for that is the inf-sup condition:

$$\exists\ \beta > 0 \quad \text{such that} \quad \inf_{q_h \in P_h} \sup_{\underline{v}_h \in \underline{U}_h} \frac{\int_\Omega q_h \text{ div } \underline{v}_h d\Omega}{\| q_h \|_{L^2} \| \underline{v}_h \|_{H^1}} \geq \beta. \tag{2.13}$$

With this example in mind, we try something similar. For a given $\underline{\theta} = \underline{\nabla} w$ smooth, we look for $\underline{\theta}^I$ as the discrete solution of

$$\left.\begin{array}{l} \text{find } (\underline{\theta}^I, q^I) \text{in } (\underline{\Theta}_h, Q_h) \text{ such that} \\ \int_\Omega \underline{\underline{\nabla}}\, \underline{\theta}^I : \underline{\underline{\nabla}}\, \underline{\eta}_h d\Omega - \int_\Omega q^I \text{ rot } \underline{\eta}_h d\Omega = \int_\Omega \underline{\underline{\nabla}}\, \underline{\theta} : \underline{\underline{\nabla}}\, \underline{\eta}_h d\Omega, \quad \forall \underline{\eta}_h \in \underline{\Theta}_h \\ \int_\Omega q_h \text{ rot } \underline{\theta}^I d\Omega = 0, \quad \forall q_h \in Q_h \end{array}\right\} \tag{2.14}$$

In Equation (2.14), $\underline{\Theta}_h$ is the finite element space that we are going to choose for the approximation of rotations while Q_h is an auxiliary "pressure space" that will never enter the Reissner-Mindlin plate element formulation (it is not present in Equation (2.4)). Hence our first step is the choice of a pair of finite element spaces $\underline{\Theta}_h, Q_h$ such that:

$$\exists\, \beta > 0 \quad \text{such that} \quad \inf_{q_h \in Q_h} \sup_{\underline{\eta}_h \in \underline{\Theta}_h} \frac{\int_\Omega q_h \text{ rot } \underline{\eta}_h d\Omega}{\| q_h \|_{L^2} \| \underline{\eta}_h \|_{H^1}} \geq \beta. \tag{2.15}$$

In perfect analogy with what is done for the Stokes problem, Equation (2.12), it is now easy to see that if Equation (2.15) holds true, the problem given by Equation (2.14) has a unique solution $\underline{\theta}^I, q^I$ and that $\underline{\theta}^I \to \underline{\theta}, q^I \to 0$ (with optimal order) as $h \to 0$. We discard q^I (we have no use for it) and keep the precious $\underline{\theta}^I$. On our way to Equation (2.9) we have reached an intermediate step: we constructed a $\underline{\theta}^I$ in $\underline{\Theta}_h$, close to $\underline{\theta}$ and satisfying

$$\int_\Omega q_h \text{ rot } \underline{\theta}^I d\Omega = 0 \quad \text{for all} \quad q_h \in Q_h. \tag{2.16}$$

We have now to choose the reduction operator R_h together with its "arrival space" $\underline{\Gamma}_h$. We want R_h (and $\underline{\Gamma}_h$) to be such that Equation (2.16) implies Equation (2.11). This will surely be true if the following diagram

$$\begin{array}{ccc} (H_0^1)^2 & \xrightarrow{\text{rot}} & L^2 \\ R_h \downarrow & & \downarrow \pi_h \\ \underline{\Gamma}_h & \xrightarrow{\text{rot}} & Q_h \end{array} \tag{2.17}$$

commutes. In Equation (2.17) π_h is the orthogonal projection (in $L^2(\Omega)$) into Q_h. Note that Equation (2.17) implies in particular that, for every $\underline{\gamma}_h$ in $\underline{\Gamma}_h$ we have rot $\underline{\gamma}_h \in Q_h$. Note also that Equation (2.16) can be written as

$$\pi_h(\text{rot } \underline{\theta}^I) = 0. \tag{2.18}$$

If the diagram given in Equation (2.17) commutes, then we have

$$\text{rot}(R_h \underline{\theta}^I) = \pi_h(\text{rot } \underline{\theta}^I) \tag{2.19}$$

and equations (2.18) and (2.19) imply the desired Equation (2.11). Hence our second step is to choose R_h and $\underline{\Gamma}_h$ in such a way that the diagram given in Equation (2.17) commutes. On the other hand this diagram (or rather its analogue with "div" instead of "rot") is *the* crucial step in the approximation of linear elliptic problems with mixed methods and we can easily find in the literature (see e.g. Reference [36]) many choices of triplets $(\underline{\Gamma}_h, Q_h, R_h)$ which are convenient. Note the special role of the auxiliary space Q_h : it never enters the actual computations but it is the only *link* between our first step (choice of $\underline{\Theta}_h$ and Q_h satisfying Equation (2.15)) and our second step (choice of $\underline{\Gamma}_h, Q_h, R_h$ satisfying Equation (2.17)).

Now that we have Equation (2.11) satisfied, we can start looking for w^I. As we have seen, if the domain is simply connected, Equation (2.11) implies that $R_h \underline{\theta}^I$ is the gradient of some function: we want this function to belong to W_h. This condition, together with assumption given by Equation (2.8), completely characterizes W_h. Actually we must have

$$\underline{\nabla} W_h = \{\underline{\gamma}_h \in \underline{\Gamma}_h \text{ such that rot } \underline{\gamma}_h = 0\}. \tag{2.20}$$

In other words, Equation (2.20) tells us that we have no more freedom in the choice of W_h. On the other hand, if Equation (2.20) holds, then Equation (2.11) will imply the existence of a $w^I \in W_h$ such that

$$R_h \underline{\theta}^I = \underline{\nabla} w^I \tag{2.21}$$

that is Equation (2.9). If moreover (as is always the case in practice) R_h is a good approximation of the identity, then we have

$$\underline{\nabla} w^I = R_h \underline{\theta}^I \simeq \underline{\theta}^I \simeq \underline{\theta} = \underline{\nabla} w \tag{2.22}$$

and w^I will be a good approximation of w.

Let us finally summarize the three basic steps of our element construction:

1st Step. Choose $\underline{\Theta}_h, Q_h$ so that Equation (2.15) holds.

2nd Step. Choose $\underline{\Gamma}_h, R_h$ such that the diagram given in Equation (2.17) commutes.

3rd Step. Choose W_h according to Equation (2.20).

Remark As can be seen, in the construction of $\underline{\theta}^I$ we discarded the "pressure part" q^I of the solution of Equation (2.14). Hence what is really only needed is that Equation (2.14) produces a good "velocity" $\underline{\theta}^I$; specifically, if the discretization produces spurious checkerboard modes in the variable q^I, this will not be a difficulty as long as $\underline{\theta}^I$ is a good approximation of $\underline{\theta}$. In a sense, then, Equation (2.15) is too strong, since it ensures good stability and accuracy *both* for $\underline{\theta}^I$ and q^I. Some attractive choices of finite elements for the Stokes problem (as the widely used bilinear velocities/constant pressure $(Q_1 - P_0)$ element) are known to produce good results for velocities and poor results for

pressures (see Reference [37] for a proof of this observation in some particular cases), and it follows that the plate bending complements of such elements should not be discarded *a priori* (for example, the MITC4 element being the plate bending complement of the $Q_1 - P_0$ element provides very good results, see Section 2.3). □

In the following section we summarize the elements that we find attractive and for which we present numerical results and convergence studies in Section 2.3.

2.2 The MITC Plate Bending Elements

The MITC element formulations comprise the choice of the spaces $\underline{\Theta}_h$, W_h, $\underline{\Gamma}_h$ and the tying used – as expressed by R_h – between the interpolations in $\underline{\Gamma}_h$ and the transverse shear strain components as evaluated from $\underline{\Theta}_h$ and W_h.

We present below the choices for each element considered using the Cartesian coordinates x, y, thus considering uniform rectangular and triangular decompositions. The same interpolations are used in natural coordinates for the covariant strain components in general elements [2; 26; 18; 38; 33; 34].

2.2.1 The MITC4 Element

For the 4–node element we use [26; 18]

$$\underline{\Theta}_h = \{\underline{\eta} |\ \underline{\eta} \in (H_0^1(\Omega))^2,\ \underline{\eta}|_K \in (Q_1)^2 \quad \forall K\} \tag{2.23}$$

$$W_h = \{\zeta |\ \zeta \in H_0^1(\Omega),\ \zeta|_K \in Q_1 \quad \forall K\} \tag{2.24}$$

where Q_1 is the set of polynomials of degree ≤ 1 in each variable and K is the current element in the discretization. The space $\underline{\Gamma}_h$ is given by

$$\underline{\Gamma}_h = \{\underline{\delta}|\ \underline{\delta}|_K \in TR(K)\ \ \forall K,$$
$$\underline{\delta} \cdot \underline{\tau} \text{ continuous at the interelement boundaries}\} \tag{2.25}$$

where $\underline{\tau}$ is the tangential unit vector to each edge of the element and

$$TR(K) = \{\underline{\delta}|\ \delta_1 = a_1 + b_1 y,\ \delta_2 = a_2 + b_2 x\} \tag{2.26}$$

The space $TR(K)$ is a sort of "rotated Raviart–Thomas" space of order zero [39]. The reduction operator R_h is given by

$$\int_e (\underline{\eta} - R_h\underline{\eta}) \cdot \underline{\tau}\, ds = 0 \quad \text{for all edges } e \text{ of } K \tag{2.27}$$

This 4-node plate bending element is the complement of the 4/1 element for incompressible analysis [40] and the theoretically predicted error estimates using uniform meshes are

$$\|\underline{\theta} - \underline{\theta}_h\|_1 \ \leq c\,h \tag{2.28}$$
$$\|\underline{\nabla} w - \underline{\nabla} w_h\|_0 \ \leq c\,h \tag{2.29}$$

In equation (2.28) and similar equations below it, "c" denotes a constant (different in each equation and dependent on the actual problem considered) that is independent of h, and $\|\cdot\|_0$ and $\|\cdot\|_1$ denote Sobolev norms. Specifically, for a vector valued function $\underline{\phi}$ with $\underline{\phi}^T = [\phi_1\ \phi_2]$ we have

$$\|\underline{\phi}\|_0 \ = \ \left[\int_\Omega ((\phi_1)^2 + (\phi_2)^2)\, d\Omega\right]^{1/2} \tag{2.30}$$

$$\|\underline{\phi}\|_1 = \left[\int_\Omega ((\phi_1)^2 + (\phi_2)^2 + (\phi_{1,1})^2 + (\phi_{1,2})^2 + (\phi_{2,1})^2 + (\phi_{2,2})^2)\, d\Omega\right]^{1/2} \tag{2.31}$$

Note that for this element we do not have yet theoretical convergence results available for the transverse shear strains. Some results concerning the convergence of the shear strains have recently been obtained for the following higher-order elements [35].

In general, the predicted rates in $\|\cdot\|_0$ for the shear strains are one order less than the corresponding rates, given below, for the rotations in the $\|\cdot\|_1$ norm.

2.2.2 The MITC7 Element

For the 7–node triangular element we use [38; 32]

$$\underline{\Theta}_h = \{\underline{\eta} |\ \underline{\eta} \in (H_0^1(\Omega))^2,\ \underline{\eta}|_T \in (S_7(T))^2 \quad \forall T\} \tag{2.32}$$

$$W_h = \{\zeta |\ \zeta \in H_0^1(\Omega),\ \zeta|_T \in P_2 \quad \forall T\} \tag{2.33}$$

where T is the triangular element in the discretization, P_2 is the space of complete second–order polynomials (corresponding to a 6–node element), and S_7 is

$$S_7(T) = \{\varphi |\ \varphi \in P_3,\ \varphi|_e \in P_2 \text{ on each edge } e \text{ of } T\} \tag{2.34}$$

where P_3 is the space of complete third–order polynomials. The space $\underline{\Gamma}_h$ is given by

$$\underline{\Gamma}_h = \{\underline{\delta} |\ \underline{\delta}|_T \in TR_1(T) \quad \forall T,\ \underline{\delta} \cdot \underline{\tau} \text{ continuous at the interelement boundaries}\} \tag{2.35}$$

where

$$TR_1(T) = \{\underline{\delta} |\ \delta_1 = a_1 + b_1 x + c_1 y + y(dx + ey);$$
$$\delta_2 = a_2 + b_2 x + c_2 y - x(dx + ey)\} \tag{2.36}$$

The space $TR_1(T)$ is a kind of "rotated Raviart–Thomas" space of order one [39]. The reduction operator R_h is given by

$$\int_e (\underline{\eta} - R_h\underline{\eta}) \cdot \underline{\tau}\, p_1(s) ds = 0 \quad \forall e \text{ edge of } T,\ \forall p_1(s) \in P_1(e) \tag{2.37}$$

$$\int_T (\underline{\eta} - R_h\underline{\eta}) dx dy = \underline{0} \tag{2.38}$$

where P_1 is the space of polynomials of degree ≤ 1.

This 7-node plate bending element is the complement of the Crouzeix-Raviart element for incompressible analysis [40] and the theoretically predicted error estimates using uniform meshes are

$$\|\underline{\theta} - \underline{\theta}_h\|_1 \leq c\, h^2 \tag{2.39}$$
$$\|\underline{\nabla} w - \underline{\nabla} w_h\|_0 \leq c\, h^2 \tag{2.40}$$

2.2.3 The MITC9 Element

For the 9–node element we use [31; 38; 32].

$$\underline{\Theta}_h = \{\underline{\eta} |\ \underline{\eta} \in (H_0^1(\Omega))^2,\ \underline{\eta}|_K \in (Q_2)^2 \quad \forall K\} \tag{2.41}$$

$$W_h = \{\zeta |\ \zeta \in H_0^1(\Omega),\ \zeta|_K \in Q_2^r \quad \forall K\} \tag{2.42}$$

where Q_2 is the set of polynomials of degree ≤ 2 in each variable corresponding to a nine node element, and $Q_2{}^r$ is the usual serendipity reduction of Q_2 corresponding to an eight node element. Note that $Q_2{}^r$ can also be written as $Q_2 \cap P_3$.

The space $\underline{\Gamma}_h$ is given by

$$\begin{aligned}\underline{\Gamma}_h = \{\underline{\delta} |\ \underline{\delta}|_K \in G_1(K) \quad \forall K,\\ \underline{\delta} \cdot \underline{\tau} \text{ continuous at the interelement boundaries}\}\end{aligned} \tag{2.43}$$

where

$$\begin{aligned} G_1(K) = \{\underline{\delta} |\ \delta_1 &= a_1 + b_1 x + c_1 y + d_1 xy + e_1 y^2; \\ \delta_2 &= a_2 + b_2 x + c_2 y + d_2 xy + e_2 x^2\} \end{aligned} \tag{2.44}$$

The space G_1 is some kind of rotated Brezzi–Douglas–Fortin–Marini space [41]. The reduction operator R_h is given by

$$\int_e (\underline{\eta} - R_h \underline{\eta}) \cdot \underline{\tau}\, p_1(s) ds = 0 \quad \forall e \text{ edge of } K,\ \forall p_1(s) \in P_1(e) \tag{2.45}$$

$$\int_K (\underline{\eta} - R_h \underline{\eta}) dx dy = \underline{0} \tag{2.46}$$

This 9-node plate bending element is the complement of the 9/3 element for incompressible analysis [42] and the theoretically predicted error estimates using uniform meshes are

$$\|\underline{\theta} - \underline{\theta}_h\|_1 \leq c h^2 \tag{2.47}$$

$$\|\underline{\nabla} w - \underline{\nabla} w_h\|_0 \leq c h^2 \tag{2.48}$$

2.2.4 The MITC12 Element

The MITC12 element is an extension of the MITC7 element. Here we use

$$\underline{\Theta}_h = \{\underline{\eta} |\ \underline{\eta} \in (H_0^1(\Omega))^2,\ \underline{\eta}|_T \in (S_{12}(T))^2 \quad \forall T\} \tag{2.49}$$

$$W_h = \{\zeta |\ \zeta \in H_0^1(\Omega),\ \zeta|_T \in P_3 \quad \forall T\} \tag{2.50}$$

where

$$S_{12}(T) = \{\varphi |\ \varphi \in P_4,\ \varphi|_e \in P_3 \text{ on each edge } e \text{ of } T\} \tag{2.51}$$

where P_4 is the space of complete fourth–order polynomials. The space $\underline{\Gamma}_h$ is given by

$$\begin{aligned} \underline{\Gamma}_h = \{\underline{\delta} |\ \underline{\delta}|_T \in TR_2(T) \quad \forall T, \\ \underline{\delta} \cdot \underline{\tau} \text{ continuous at the interelement boundaries}\} \end{aligned} \tag{2.52}$$

where

$$\begin{aligned} TR_2(T) = \{\underline{\delta} |\ \delta_1 &= a_1 + b_1 x + c_1 y + d_1 x^2 + e_1 xy \\ &\quad + f_1 y^2 + y(gx^2 + hxy + iy^2); \\ \delta_2 &= a_2 + b_2 x + c_2 y + d_2 x^2 + e_2 xy \\ &\quad + f_2 y^2 - x(gx^2 + hxy + iy^2)\} \end{aligned} \tag{2.53}$$

The space $TR_2(T)$ is a kind of "rotated Raviart–Thomas" space of order two [39]. The reduction operator R_h is given by

$$\int_e (\underline{\eta} - R_h \underline{\eta}) \cdot \underline{\tau}\, p_2(s) ds = 0 \quad \forall e \text{ edge of } T,\ \forall p_2(s) \in P_2(e) \tag{2.54}$$

$$\int_T (\underline{\eta} - R_h\underline{\eta}) \cdot \underline{p_1} dxdy = 0 \ \forall \underline{p_1} \in (P_1(T))^2 \tag{2.55}$$

The theoretically predicted error estimates for the MITC12 element are

$$\|\underline{\theta} - \underline{\theta}_h\|_1 \leq c\,h^3 \tag{2.56}$$

$$\|\underline{\nabla} w - \underline{\nabla} w_h\|_0 \leq c\,h^3 \tag{2.57}$$

2.2.5 The MITC16 Element

The MITC16 element is an extension of the MITC9 element. Here we use

$$\underline{\Theta}_h = \{\underline{\eta} |\ \underline{\eta} \in (H_0^1(\Omega))^2,\ \underline{\eta}|_K \in (Q_3)^2 \quad \forall K\} \tag{2.58}$$

$$W_h = \{\zeta |\ \zeta \in H_0^1(\Omega),\ \zeta|_K \in Q_3 \cap P_4 \quad \forall K\} \tag{2.59}$$

where Q_3 is the space of polynomials of degree ≤ 3 in each variable corresponding to a 16–node element. The space $\underline{\Gamma}_h$ is given by

$$\begin{aligned} \underline{\Gamma}_h = \{\underline{\delta} |\ \underline{\delta}|_K \in G_2(K) \quad \forall K, \\ \underline{\delta} \cdot \underline{\tau} \text{ continuous at the interelement boundaries}\} \end{aligned} \tag{2.60}$$

where

$$\begin{aligned} G_2(K) = \{\underline{\delta} |\ \delta_1 &= a_1 + b_1 x + c_1 y + d_1 x^2 + e_1 xy \\ &\quad + f_1 y^2 + g_1 x^2 y + h_1 x y^2 + i_1 y^3; \\ \delta_2 &= a_2 + b_2 x + c_2 y + d_2 x^2 + e_2 xy \end{aligned}$$

$$+f_2y^2 + g_2x^2y + h_2xy^2 + i_2x^3\} \tag{2.61}$$

The space G_2 is some kind of rotated Brezzi–Douglas–Fortin–Marini space [41]. The reduction operator R_h is given by

$$\int_e (\underline{\eta} - R_h\underline{\eta}) \cdot \underline{\tau}\, p_2(s)ds = 0 \quad \forall e \text{ edge of } K,\ \forall p_2(s) \in P_2(e) \tag{2.62}$$

$$\int_K (\underline{\eta} - R_h\underline{\eta}) \cdot \underline{p_1} dxdy = 0 \quad \forall \underline{p_1} \in (P_1(K))^2 \tag{2.63}$$

The theoretically predicted error estimates for the MITC16 element are

$$\|\underline{\theta} - \underline{\theta}_h\|_1 \leq c\,h^3 \tag{2.64}$$

$$\|\underline{\nabla} w - \underline{\nabla} w_h\|_0 \leq c\,h^3 \tag{2.65}$$

2.3 Numerical Results and Convergence Study

We present in this section some example analyses performed with the elements of Section 2.2. However, before we give the results let us note:

- The element matrices are all evaluated using full numerical Gauss integration (hence no reduced integration is used).
- The elements do not contain any spurious zero energy mode.
- The elements pass the patch test, see Figure 2-1 for an example solution. (Actually the MITC9 element shows a small difference to the analytical solution, but we can say that the patch test is practically passed [38]).

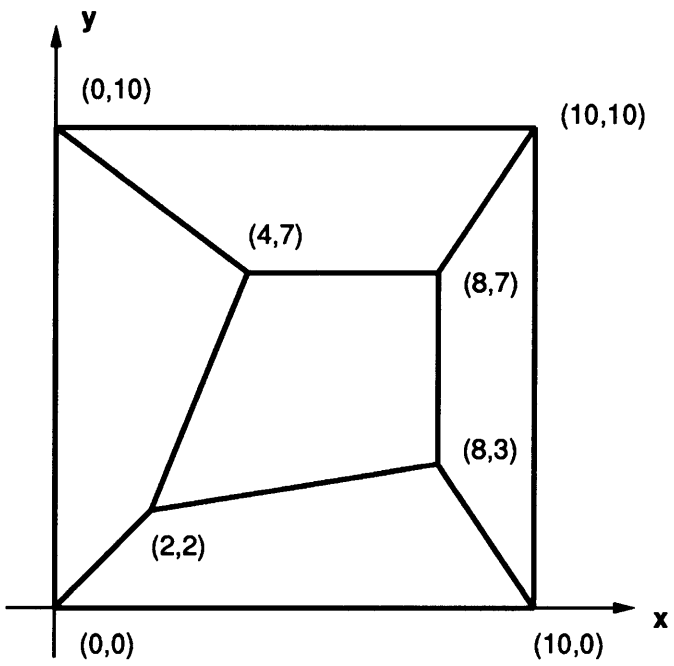

Figure 2-1: Patch of elements used in patch test, thickness/length = 1/1000. Support conditions correspond to only eliminating the rigid body modes. For triangular elements, one quadrilateral element is replaced by two triangular elements.

2.3.1 Analysis of a Simply–Supported Square Plate

We consider the transverse shear stress predictions in the analysis of a square plate subjected to uniform pressure. In this problem the transverse shear stresses display a strong boundary layer [43]. Therefore this is an adequate test problem to assess the predictive capability of the elements regarding transverse shear stresses for engineering problems in which these stresses vary rapidly.

Only a quarter of the plate needs to be discretized and we obtained a reference solution using graded meshes of 16–node displacement based elements (in undistorted form). The 10×10 graded mesh is shown in Figure 2-2 and the 20×20 was obtained by subdividing each element of the 10×10 mesh into four new elements. The solutions obtained with these meshes showed negligible differences.

In figures 2-3 and 2-4 we show the predictions, along the edge of the plate from the corner, obtained with the MITC4 and MITC9 elements and the reference solution. The stresses are evaluated at the corner of the elements using $\underline{\Gamma}_h$ spaces. The MITC element predictions show a good convergence to the reference solution. We note that at a sufficient distance from the corner the solution corresponds to the Kirchhoff solution. We also remark that the grading of the meshes has a very important effect for this type of analysis.

2.3.2 Convergence in the Analysis of an "Ad-hoc Problem"

We consider the problem of a square Reissner-Mindlin plate of side lengths two units, see Figure 2-5. The interior loading is p=0 and the imposed boundary displacement and section rotations correspond to:

$$w = \sin kxe^{ky} + \sin ke^{-k} \tag{2.66}$$

$$\theta_x = k \cos kxe^{ky} \tag{2.67}$$

$$\theta_y = k \sin kxe^{ky} \tag{2.68}$$

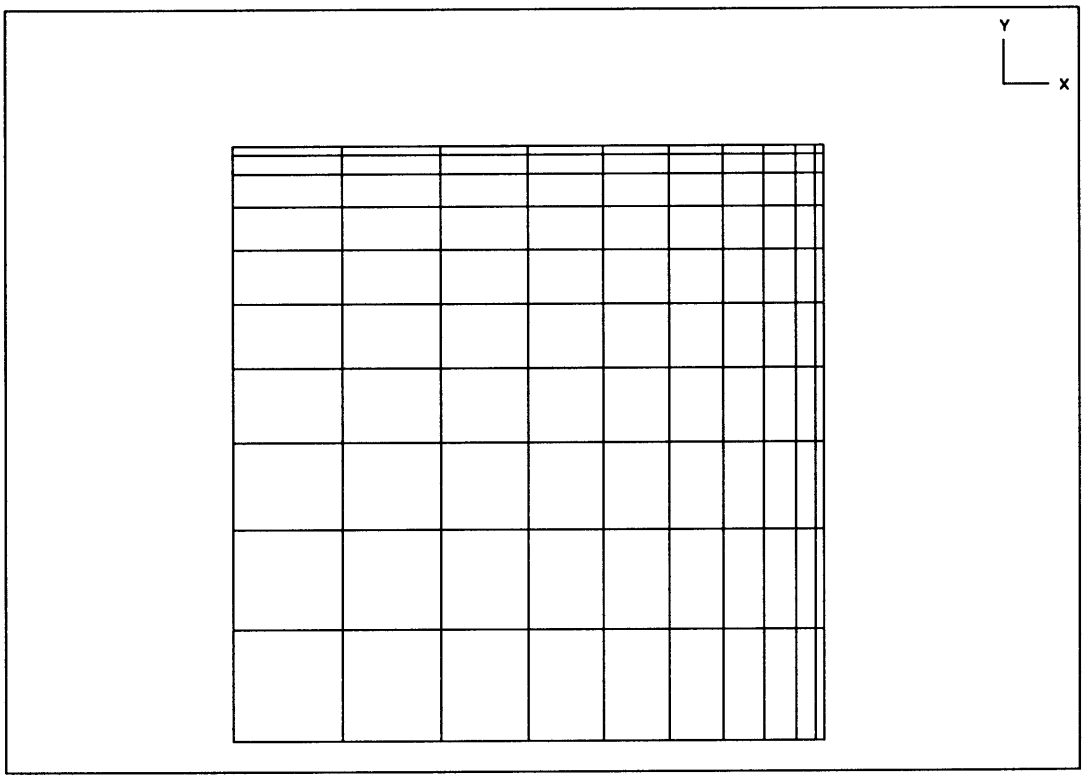

Figure 2-2: 10×10 graded mesh used in analysis of simply–supported plate, thickness/length = 1/100

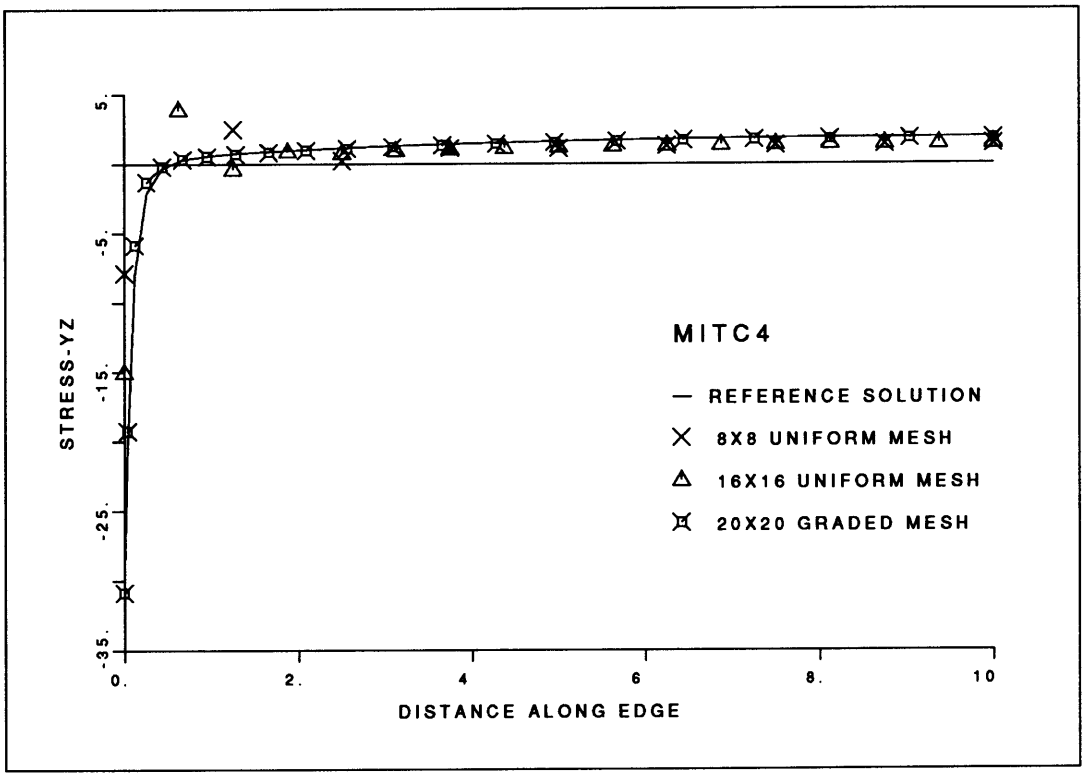

Figure 2-3: Shear stress predictions near corner of simply-supported plate subjected to pressure loading using MITC4 elements

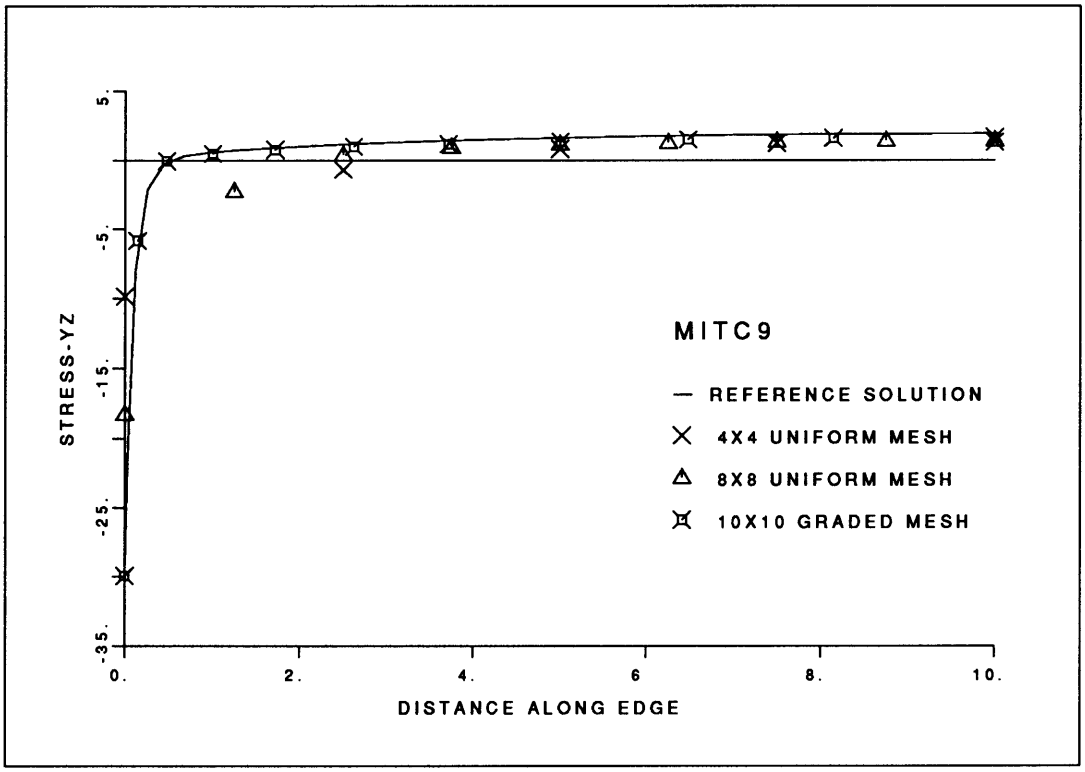

Figure 2-4: Shear stress predictions near corner of simply–supported plate subjected to pressure loading using MITC9 elements

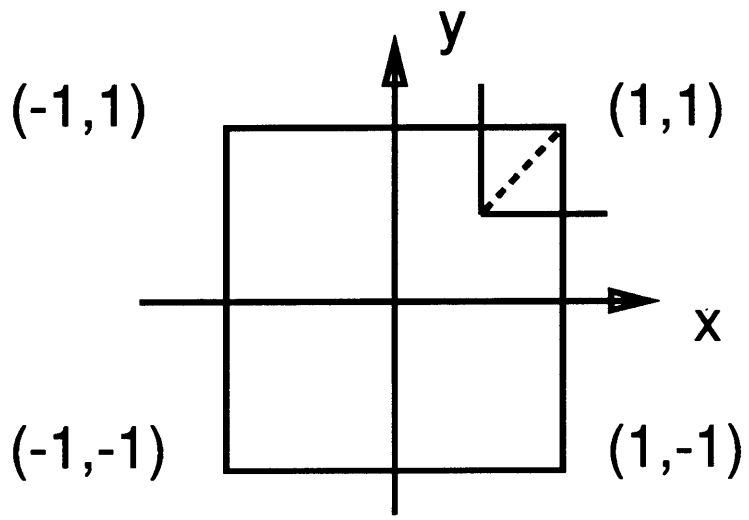

Figure 2-5: Square plate used in analysis of ad-hoc problem. The dashed line indicates the subdivision used for the triangular element meshes.

with $k = 5$. We note that the above equations satisfy the Reissner-Mindlin plate equations for any value of the thickness t, and hence represent the complete (boundary and interior) solution. There is no boundary layer [44; 43], and indeed the transverse shear strains are zero.

Hence this problem is a valuable test problem in that the numerically calculated convergence rates should be close to the theoretically predicted rates.

The plate problem was solved with uniform meshes, where h denotes the side length of each element.

Figures 2-6, 2-7 and 2-8 show the error in the finite element solutions in the Sobolev norms mentioned in Section 2.1, and the convergence of the transverse shear strains, and Table 2-1 gives the average convergence rates. We note that the slopes of the curves in Figures 2-6, 2-7 and 2-8 are in essence constant, and hence the convergence for each element is measured to be quite uniform for each h used.

Tables 2-1 shows that the numerically obtained convergence rates are quite close to the theoretical rates, and that the convergence of the transverse shear strain components

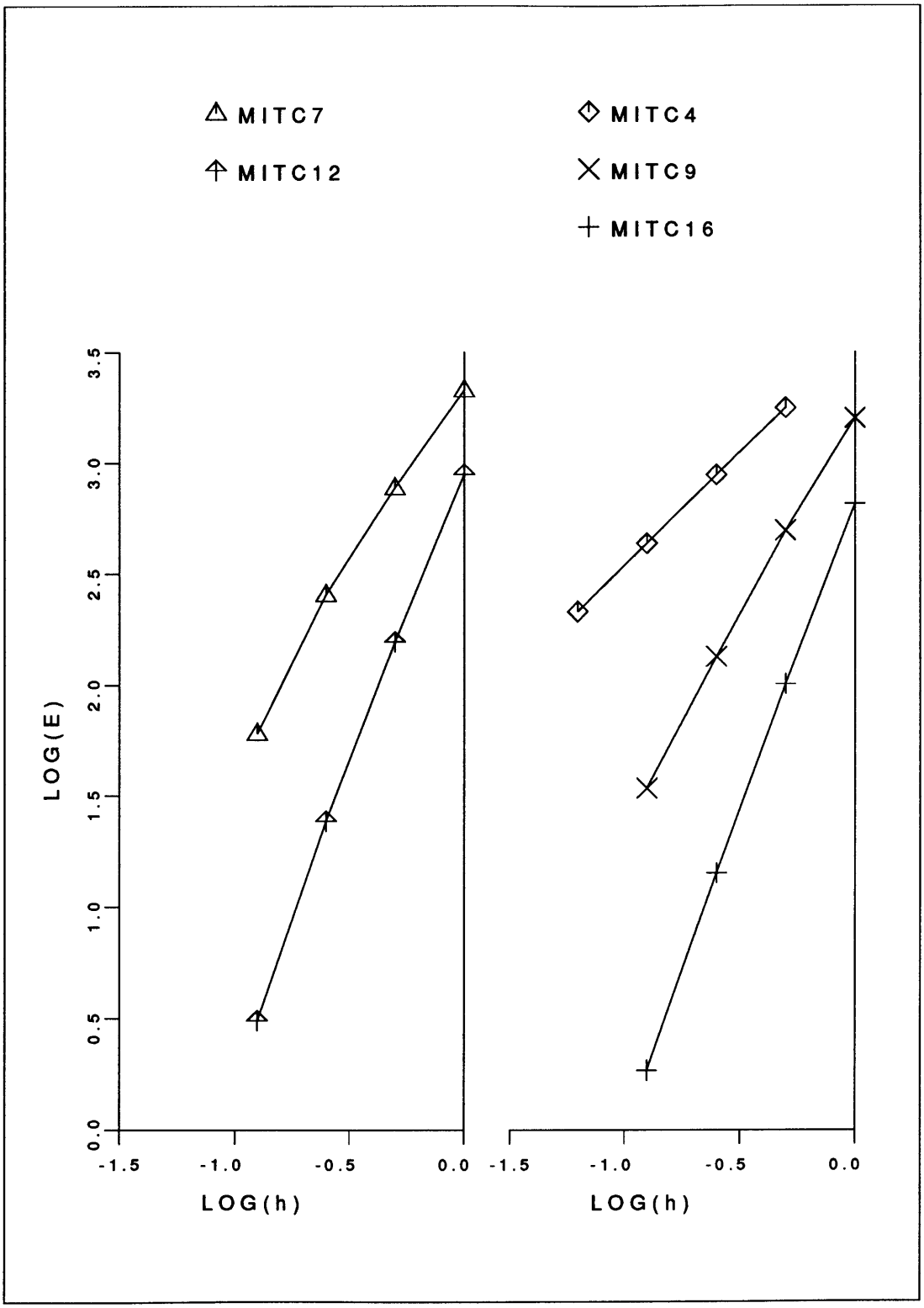

Figure 2-6: Convergence of section rotations in analysis of ad-hoc problem using uniform meshes. The error measure is $E = \|\underline{\theta} - \underline{\theta}_h\|_1$.

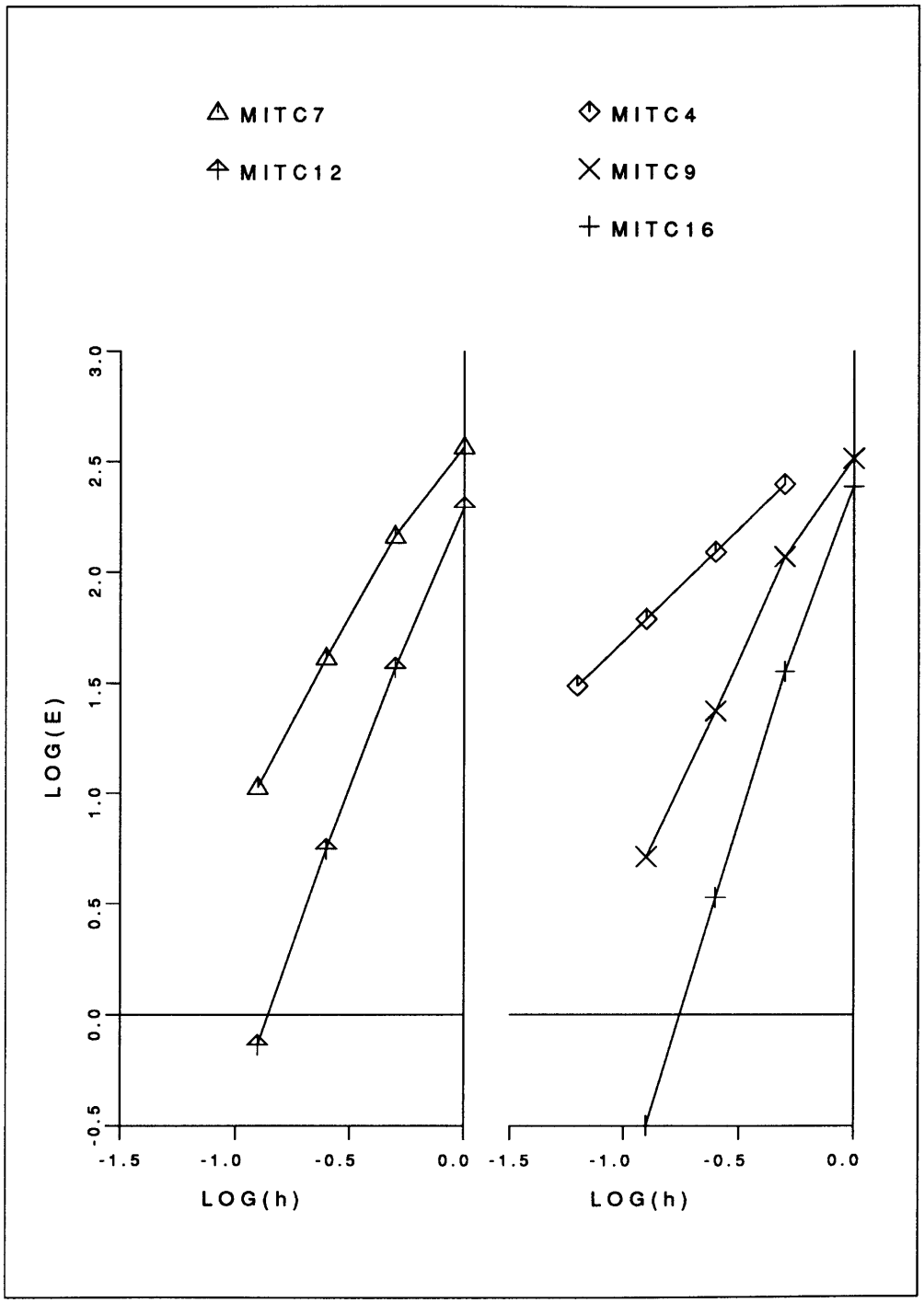

Figure 2-7: Convergence of gradient of vertical displacement in analysis of ad-hoc problem using uniform meshes. The error measure is $E = \|\underline{\nabla} w - \underline{\nabla} w_h\|_0$.

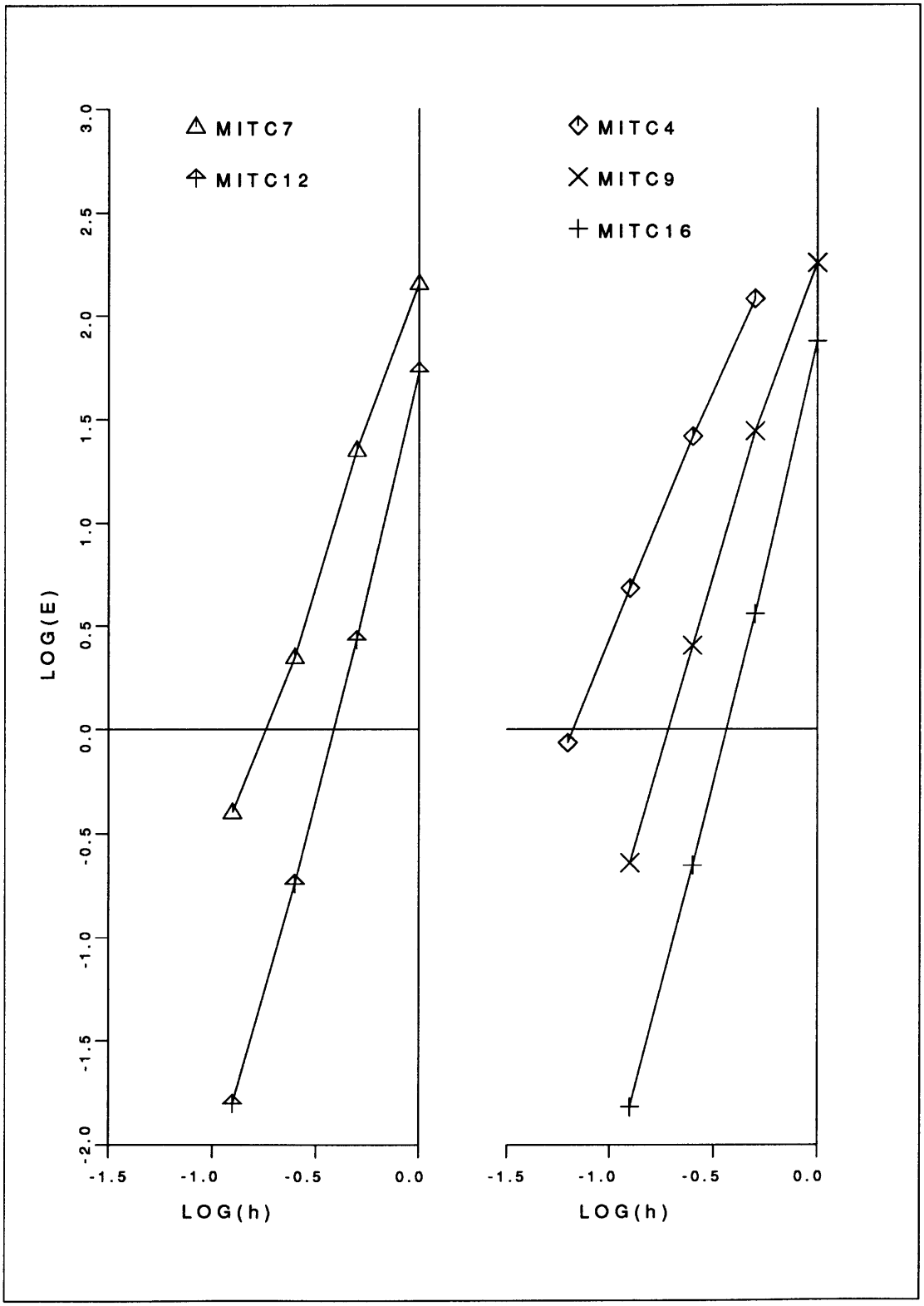

Figure 2-8: Convergence of transverse shear strains in analysis of ad-hoc problem using uniform meshes. The error measure is $E = \|\underline{\gamma} - \underline{\gamma}_h\|_0$.

ELEMENT	$\|\underline{\theta} - \underline{\theta}_h\|_1$		$\|\underline{\theta} - \underline{\theta}_h\|_0$	$\|\underline{\nabla} w - \underline{\nabla} w_h\|_0$		$\|w - w_h\|_0$	$\|\underline{\gamma} - \underline{\gamma}_h\|_0$
	Theory	Numerical		Theory	Numerical		
MITC4	1.0	1.0	2.0	1.0	1.0	2.1	2.4
MITC9	2.0	1.8	2.7	2.0	2.0	3.0	3.2
MITC7	2.0	1.7	2.7	2.0	1.7	2.9	2.8
MITC12	3.0	2.7	3.7	3.0	2.7	3.8	3.9
MITC16	3.0	2.8	3.7	3.0	3.2	4.2	4.1

Table 2-1: Convergence rates obtained in analysis of ad-hoc problem using uniform meshes

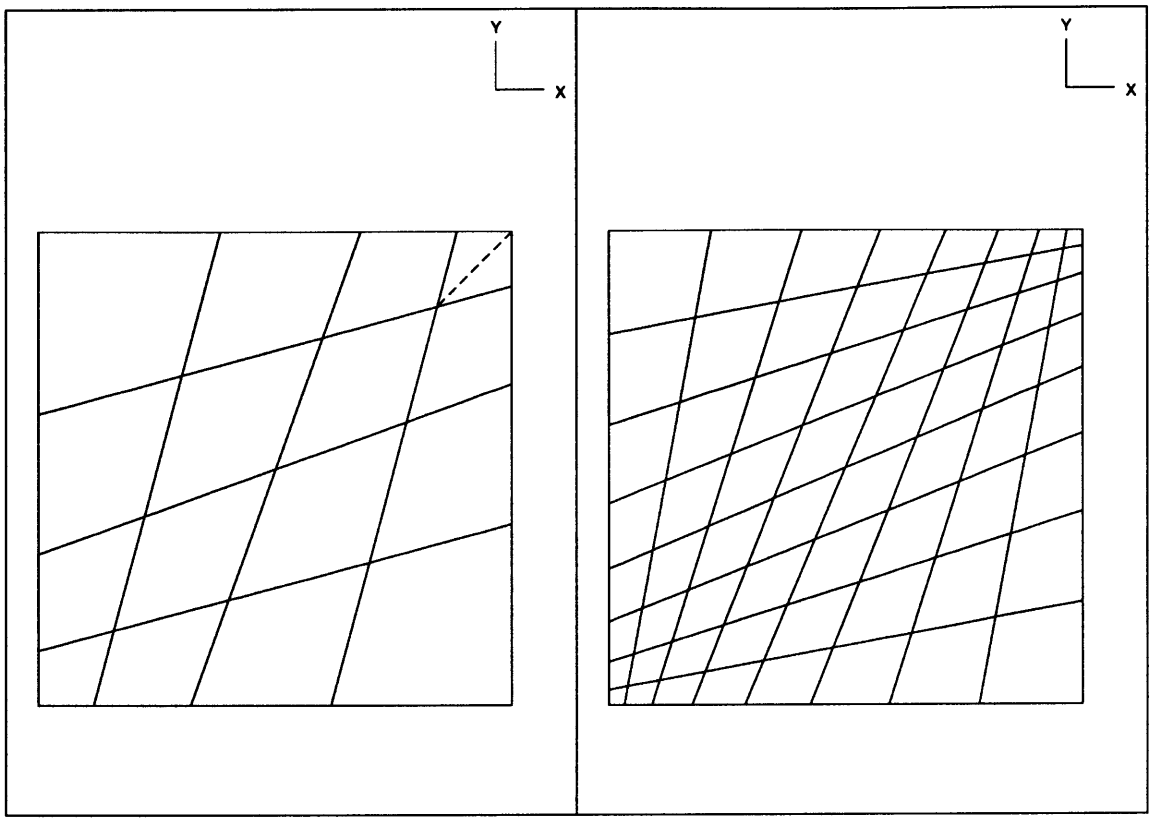

Figure 2-9: Two typical distorted meshes used in analysis of ad-hoc problem. The dashed line indicates the subdivision used for the triangular element meshes.

is surprisingly good.

In the above solutions we used uniform meshes of square elements. In a next study we deliberately distorted the elements in order to identify the effect of element distortions on the convergence rates. Figures 2-9 shows the 4×4 and 8×8 element meshes used. The additional mesh refinements were obtained by similar geometric subdivisions.

Figures 2-10, 2-11 and 2-12 shows the calculated errors in the solutions with the distorted meshes and Table 2-2 summarizes the mean convergence rates. In figures 2-10, 2-11 and 2-12 the element "size" h is the corresponding element "size" of the uniform mesh with the same number of elements.

A comparison of the data given in tables 2-1 and 2-2 shows that the use of distorted

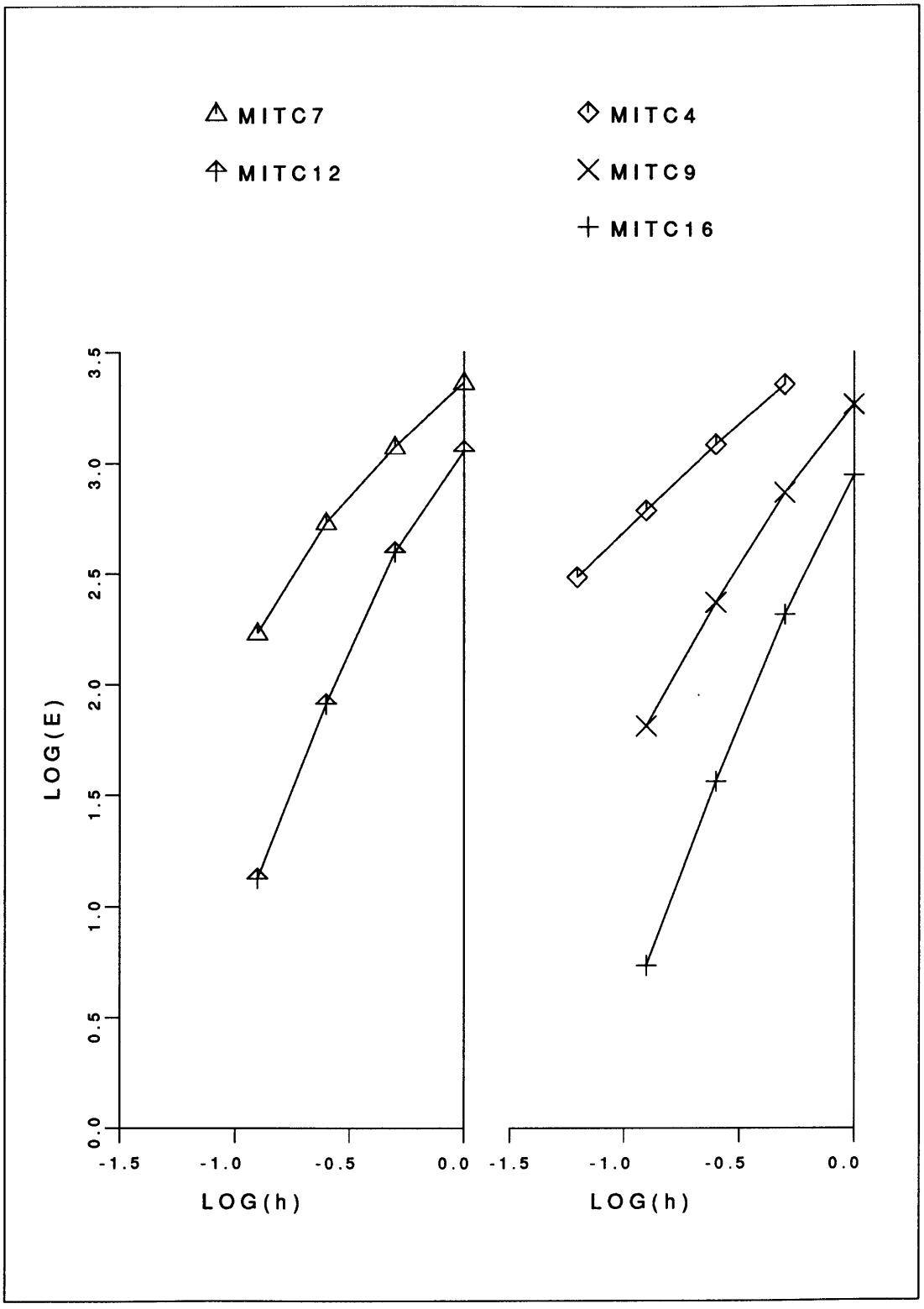

Figure 2-10: Convergence of section rotations in analysis of ad-hoc problem using distorted meshes. The error measure is $E = \|\underline{\theta} - \underline{\theta}_h\|_1$.

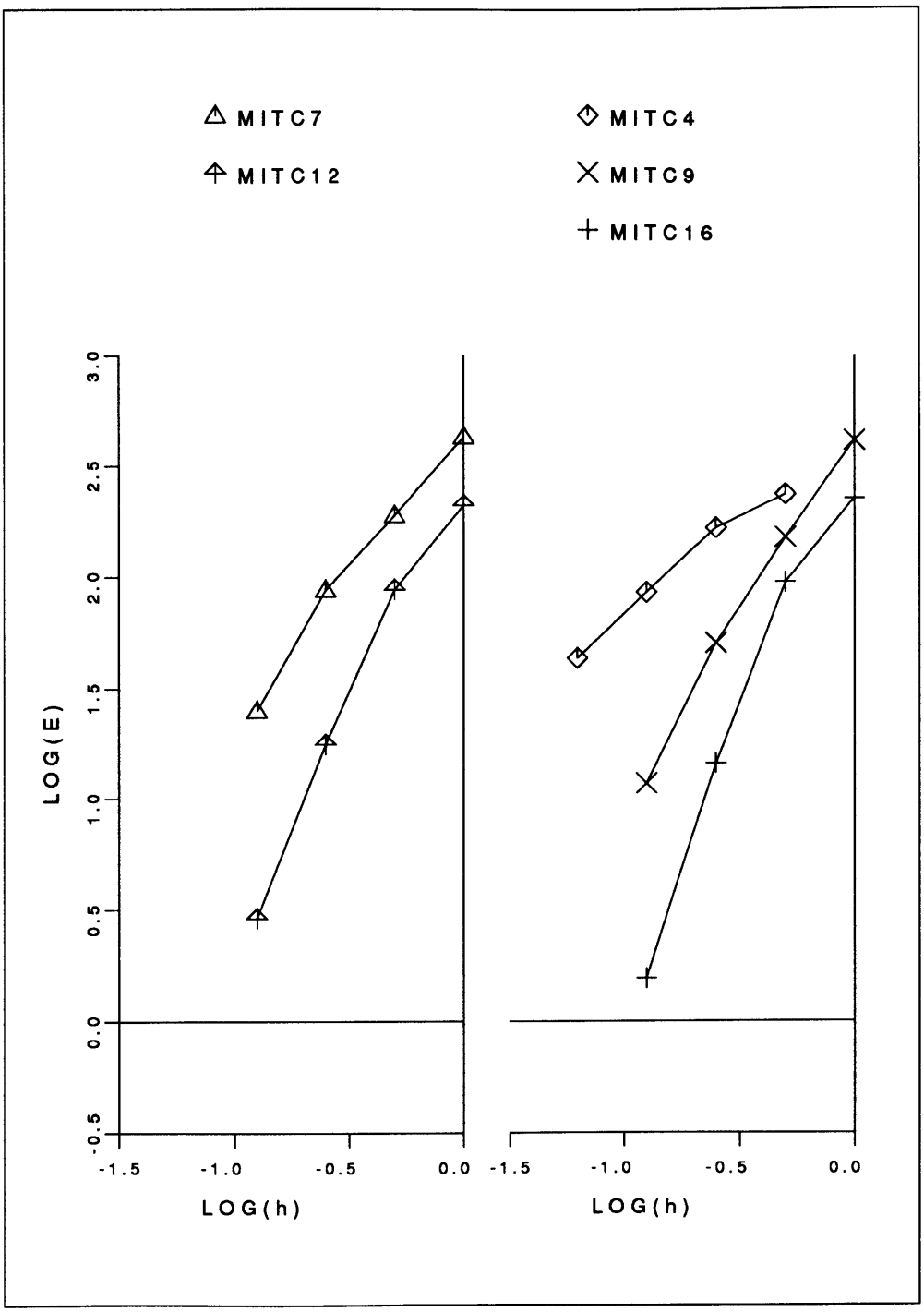

Figure 2-11: Convergence of gradient of vertical displacement in analysis of ad-hoc problem using distorted meshes. The error measure is $E = \|\underline{\nabla} w - \underline{\nabla} w_h\|_0$.

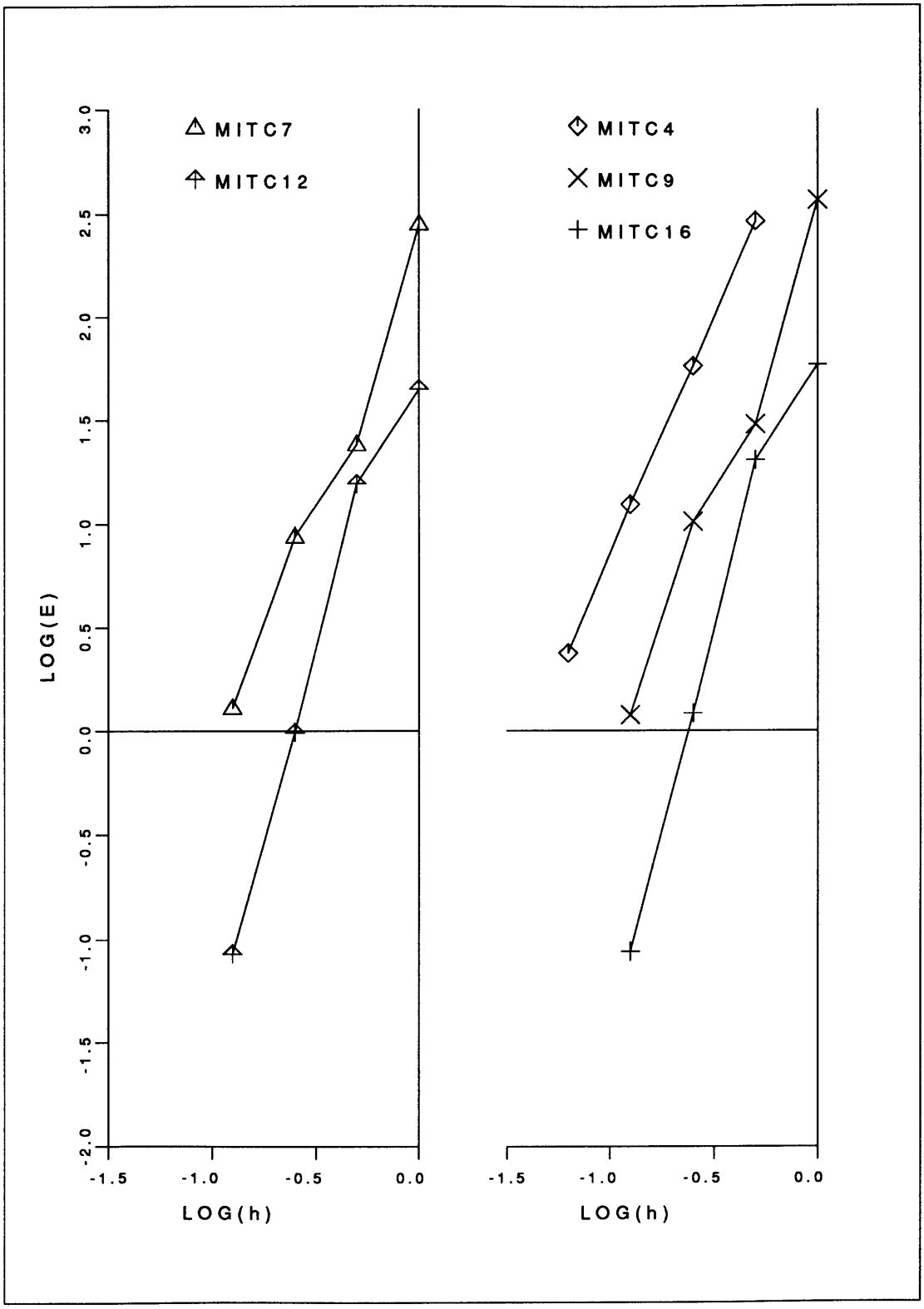

Figure 2-12: Convergence of transverse shear strains in analysis of ad-hoc problem using distorted meshes. The error measure is $E = \|\underline{\gamma} - \underline{\gamma}_h\|_0$.

ELEMENT	$\|\underline{\theta} - \underline{\theta}_h\|_1$		$\|\underline{\theta} - \underline{\theta}_h\|_0$	$\|\underline{\nabla} w - \underline{\nabla} w_h\|_0$		$\|w - w_h\|_0$	$\|\underline{\gamma} - \underline{\gamma}_h\|_0$
	Theory	Numerical		Theory	Numerical		
MITC4	1.0	1.0	1.9	1.0	0.8	1.7	2.3
MITC9	2.0	1.6	2.4	2.0	1.7	2.6	2.8
MITC7	2.0	1.3	2.0	2.0	1.4	2.4	2.6
MITC12	3.0	2.1	2.8	3.0	2.1	2.9	3.0
MITC16	3.0	2.4	3.2	3.0	2.4	3.2	3.1

Table 2-2: Convergence rates obtained in analysis of ad-hoc problem using non-uniform distorted meshes

meshes results generally into a decrease of the convergence rates, but this decrease is not drastic when considering that rather highly distorted meshes were used, and when taking into account that each mesh contained rather large and small elements.

2.3.3 Convergence in the Analysis of a Circular Plate

In this solution we consider a circular plate of thickness t and diameter D. The plate is loaded by a uniform pressure and is simply-supported or clamped along its edge.

Figure 2-13 gives the data of the problem considered and shows the finite element meshes used. Note that the elements are geometrically distorted in a natural way in order to model the plate.

Of particular interest in this analysis is the prediction of the transverse shear stresses. The analytical solution is rather simple (see Figure 2-14) and there is no boundary layer. Figures 2-14, 2-15 and 2-16 show the calculated stresses as obtained for the simply-supported plate using the MITC16 element and the usual 16-node displacement based element. In this figure we show the stresses calculated at those nodal points along line PO where two elements meet. The stresses for an element at a nodal point have been calculated using for that element

$$\underline{\tau} = \underline{C}\,\underline{\hat{B}}\,\underline{u} \tag{2.69}$$

where $\underline{\tau}$ is the vector of the stresses, $\underline{C}$ is the stress-strain matrix, $\underline{\hat{B}}$ is the strain-displacement matrix of the element at the nodal point considered and $\underline{u}$ is the nodal point displacement vector.

Hence there is no stress smoothing and at each nodal points where elements meet two values for each shear stress component are obtained. We note that the solution is quite accurate using the MITC16 element with only three elements. On the other hand, the displacement based element does not give an accurate transverse shear stress prediction

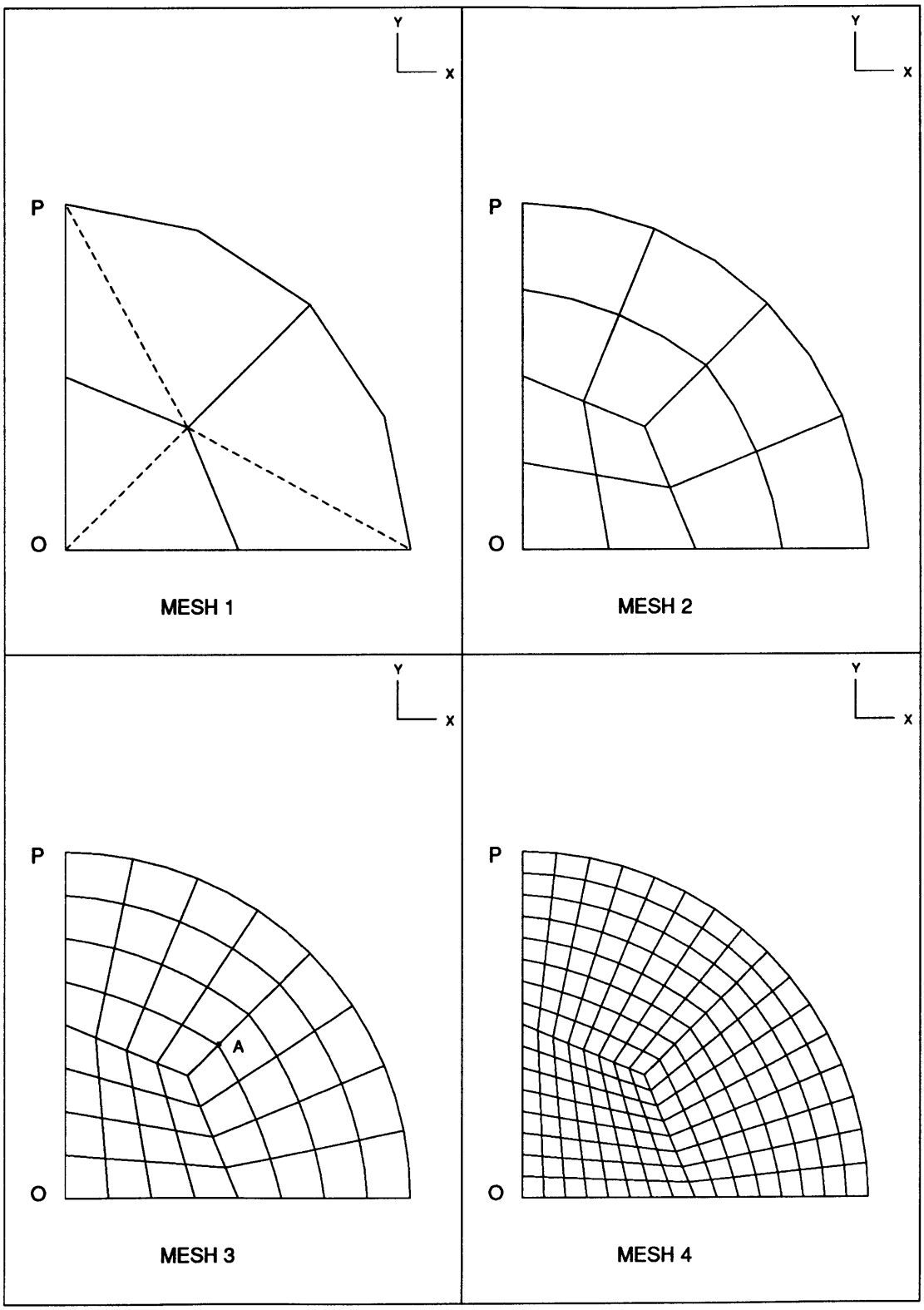

Figure 2-13: Finite element meshes used in analysis of circular plate. The dashed line in mesh 1 indicates the subdivision used to obtain the triangular element meshes. Young's modulus $E = 2.1 \times 10^6$, Poisson's ratio $\nu = 0.3$, pressure $p = 0.03072$, diameter $D = 20.0$

unless a very fine mesh is employed.

In order to identify the effect of a further geometric distortion of a mesh, we also solved the problem with the mesh of Figure 2-17. The results for the transverse shear stress yz for the clamped plate are shown in Figure 2-18. We note that when using the MITC elements, the artificial geometric distortion does not greatly affect the accuracy in the predicted stresses.

For the calculation of the bending stress we can use Mesh 2 of Figure 2-13 that already gives very accurate predictions using the MITC9 and MITC16 elements. The results for the clamped plate are shown in Figure 2-19 for the stresses calculated at all nodal points of each element using Equation (2.69).

Finally we calculated the convergence rates in the solution of the problems when using the various MITC elements. Tables 2-3 and 2-4 summarize the results. We note that in general good convergence is obtained, but the quadrilateral elements perform better than the triangular elements. This is of course not unusual. We may also mention that the slopes of the error curves as h is decreasing from Mesh 1 to Mesh 4 were in most cases quite constant but in a few cases they varied considerably from the average values given in tables 2-3 and 2-4. The tables show a good correlation between the theoretical convergence rates and the numerically calculated rates for the quadrilateral elements, and they show an overall robustness of the MITC4 element in that the rates of convergence of the shear strains are in all cases quite close to 1.

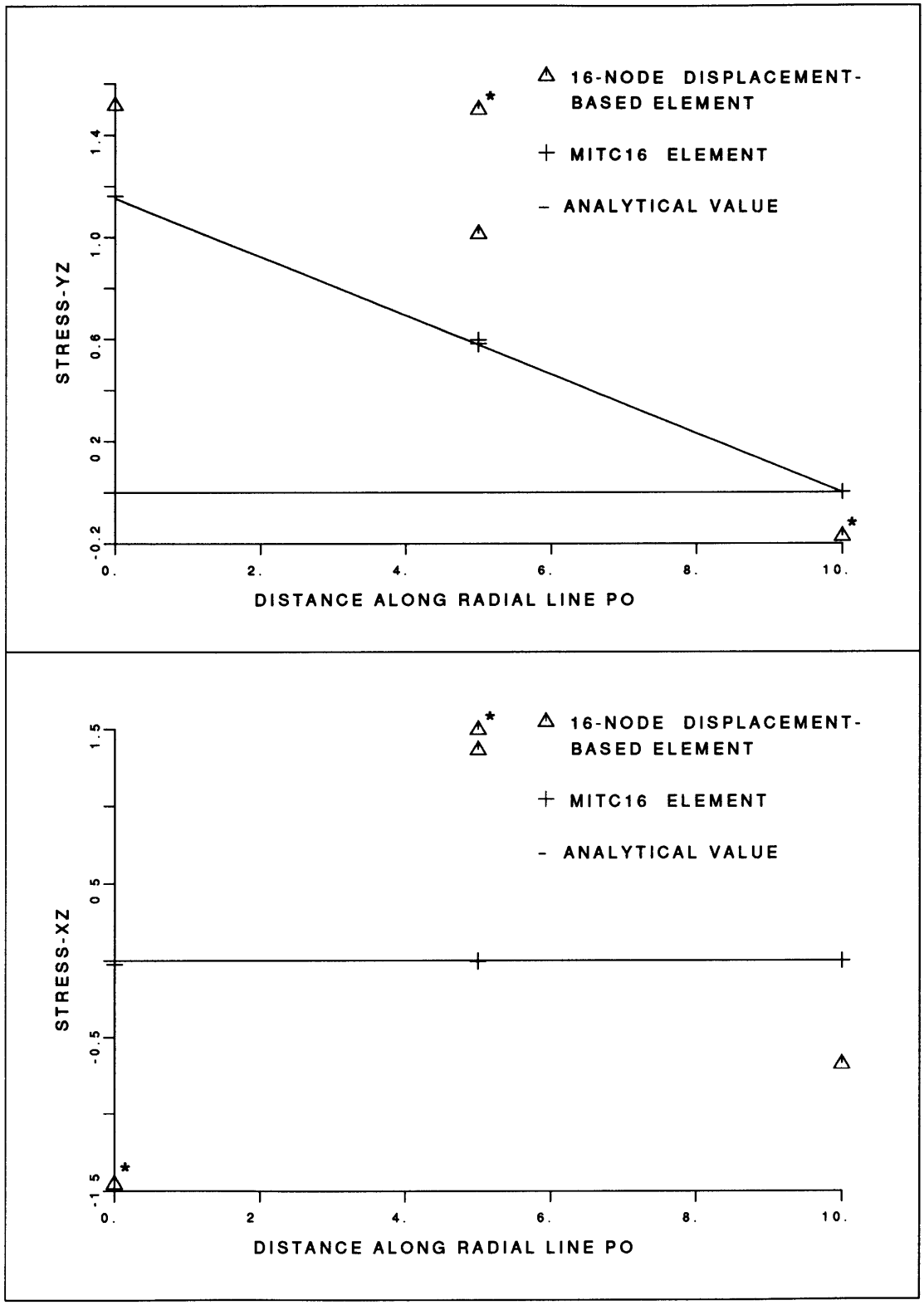

Figure 2-14: Transverse shear stress predictions for simply supported circular plate, $t/D = 1/100$. Mesh 1 with three quadrilateral elements. For the 16–node displacement–based element the results shown with a star (*) are actually outside the figure.

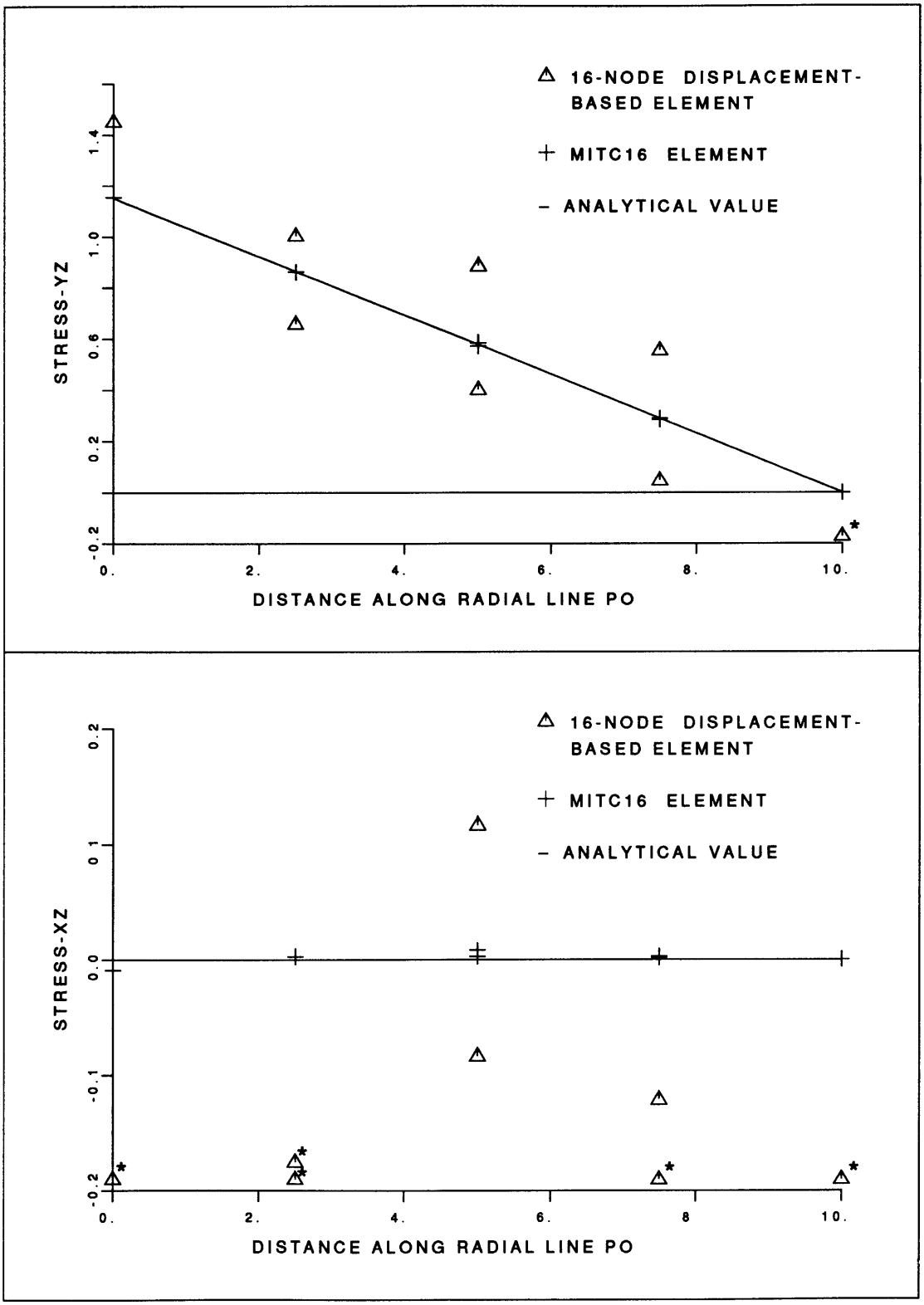

Figure 2-15: Transverse shear stress predictions for simply supported circular plate, $t/D = 1/100$. Mesh 2 with twelve quadrilateral elements. For the 16–node displacement–based element the results shown with a star (*) are actually outside the figure.

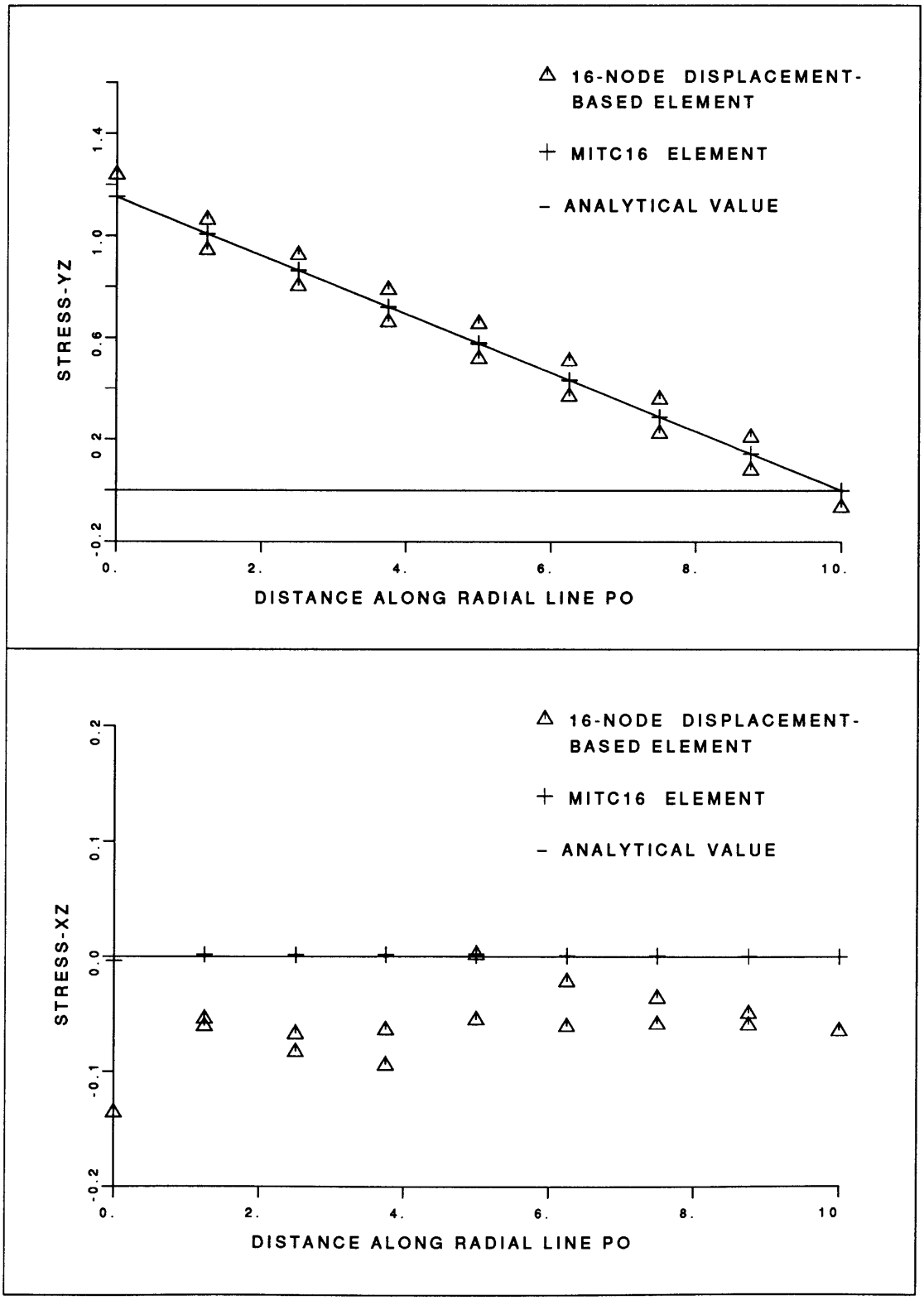

Figure 2-16: Transverse shear stress predictions for simply supported circular plate, $t/D = 1/100$. Mesh 3 with forty–eight quadrilateral elements.

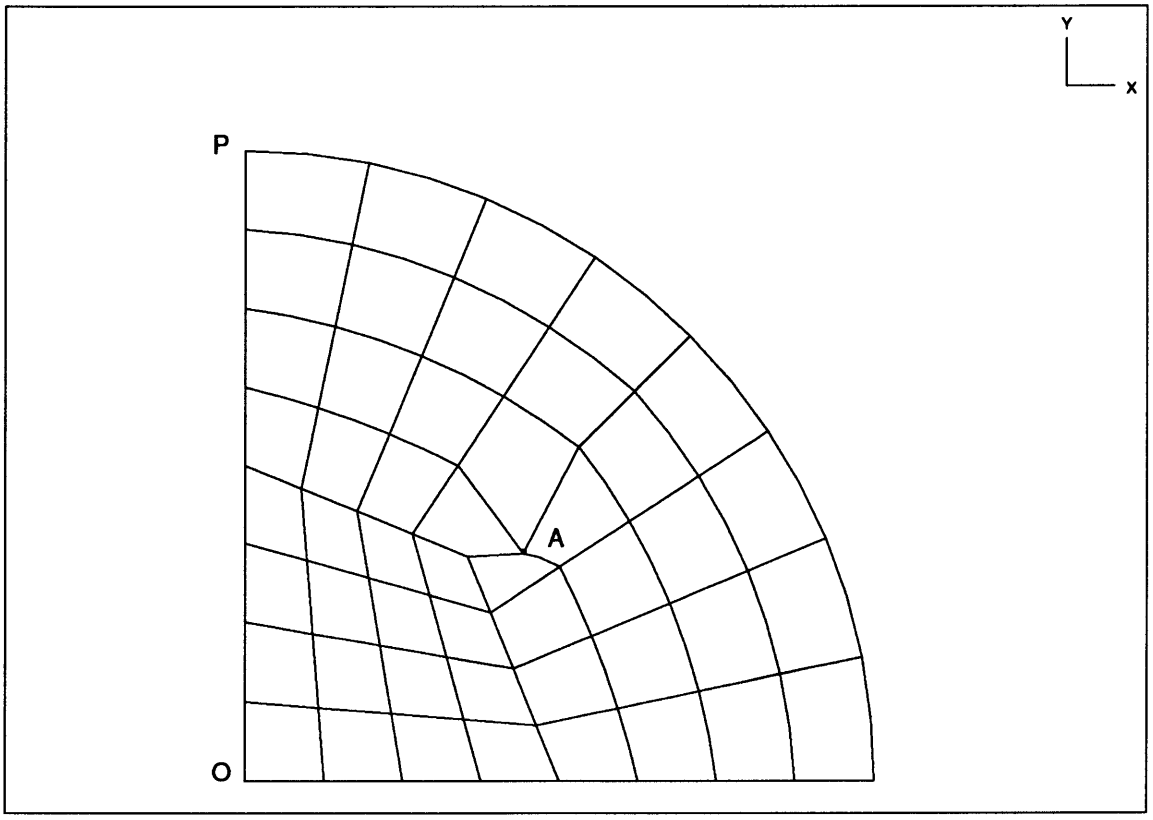

Figure 2-17: Artificially distorted mesh (of Mesh 3) used in analysis of circular plate.

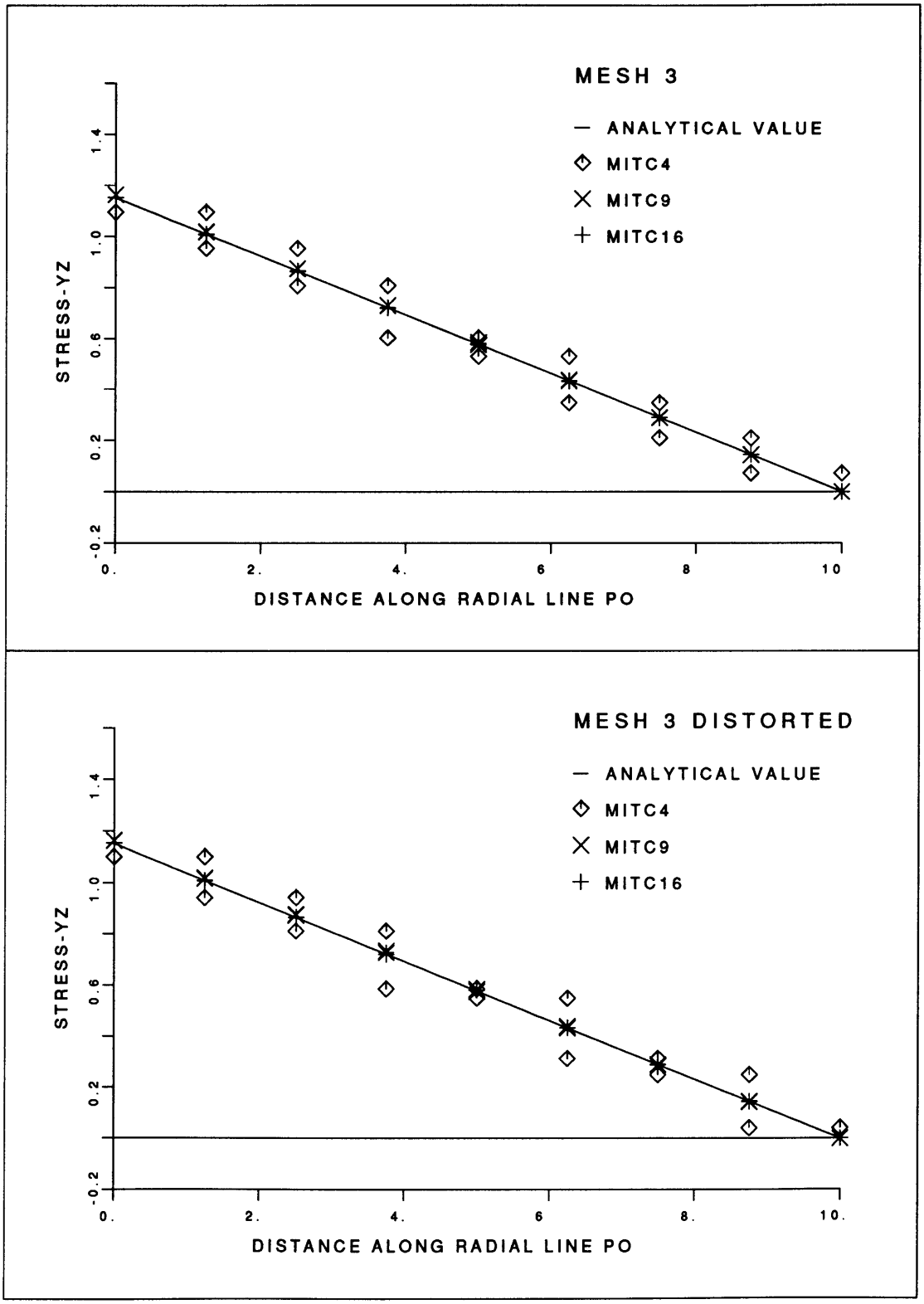

Figure 2-18: Transverse shear stress predictions for clamped circular plate, $t/D = 1/100$.

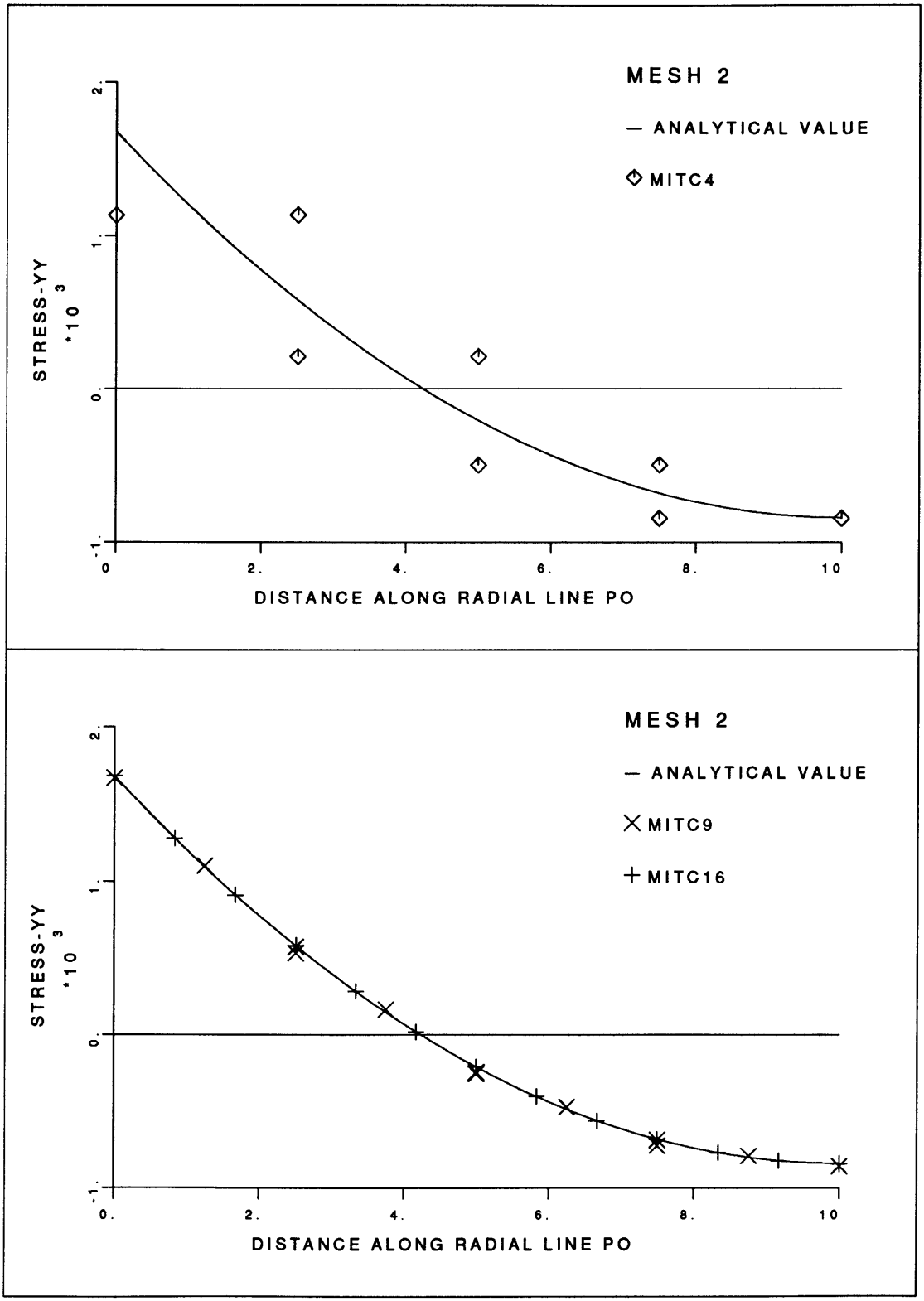

Figure 2-19: Radial bending stress predictions for clamped circular plate, $t/D = 1/100$. The stresses calculated at all nodal points along line PO are shown.

ELEMENT	$\|\underline{\theta} - \underline{\theta}_h\|_1$		$\|\underline{\theta} - \underline{\theta}_h\|_0$	$\|\underline{\nabla} w - \underline{\nabla} w_h\|_0$		$\|w - w_h\|_0$	$\|\underline{\gamma} - \underline{\gamma}_h\|_0$	$\|\underline{\gamma} - \underline{\gamma}_h\|_0$
	Theory	Numerical		Theory	Numerical		t/D=1/1000	t/D=1/100
MITC4	1.0	1.4	1.9	1.0	1.0	1.9	0.95	0.96
MITC9	2.0	2.0	2.9	2.0	2.0	3.1	0.7	1.8
MITC7	2.0	1.4	2.0	2.0	1.1	2.1	0.3	1.1
MITC12	3.0	2.1	2.9	3.0	2.1	3.2	1.5	1.6
MITC16	3.0	2.8	3.7	3.0	3.3	4.5	1.2	2.0

Table 2-3: Convergence rates obtained in analysis of simply supported circular plate, $t/D = 1000$

ELEMENT	$\|\underline{\theta} - \underline{\theta}_h\|_1$		$\|\underline{\theta} - \underline{\theta}_h\|_0$	$\|\underline{\nabla} w - \underline{\nabla} w_h\|_0$		$\|w - w_h\|_0$	$\|\underline{\gamma} - \underline{\gamma}_h\|_0$	$\|\underline{\gamma} - \underline{\gamma}_h\|_0$
	Theory	Numerical		Theory	Numerical		t/D=1/1000	t/D=1/100
MITC4	1.0	1.2	1.9	1.0	0.8	1.9	0.94	0.95
MITC9	2.0	2.2	3.1	2.0	2.0	3.0	1.4	1.6
MITC7	2.0	1.9	2.7	2.0	1.4	2.5	0.5	1.2
MITC12	3.0	2.2	3.1	3.0	2.1	3.1	1.1	1.4
MITC16	3.0	2.9	3.8	3.0	3.4	4.5	1.6	1.9

Table 2-4: Convergence rates obtained in analysis of clamped circular plate, $t/D = 1000$

Chapter 3

Locking Study for the Isoparametric Beam Elements

Membrane locking is an additional phenomenon, besides shear locking, that should not arise in shell elements. In this section, rather than facing directly the issue of membrane locking in shell elements, we plan to study this phenomenon in the context of an isobeam element, which is the one dimensional analogue of displacement based degenerated shell elements.

The purpose of going through this step is to gain a deeper understanding of and insight into the essence of the locking behavior without getting involved into the complexity of the problem directly in the context of shell elements.

3.1 The 3-node Isobeam Element

The particular problem that we select to study is described in Figure 3-1. We consider a circular arch subjected to self equilibrating bending moments at its ends. The finite element model is shown in Figure 3-2. The circular arch is discretized with only one 3-node isobeam element having its midnode clamped. Due to symmetry conditions only three degrees of freedom, u, v and θ, are required to solve the problem.

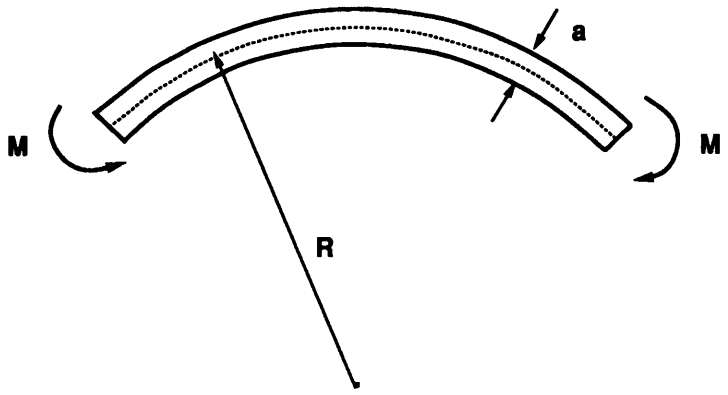

Figure 3-1: Physical model for beam study

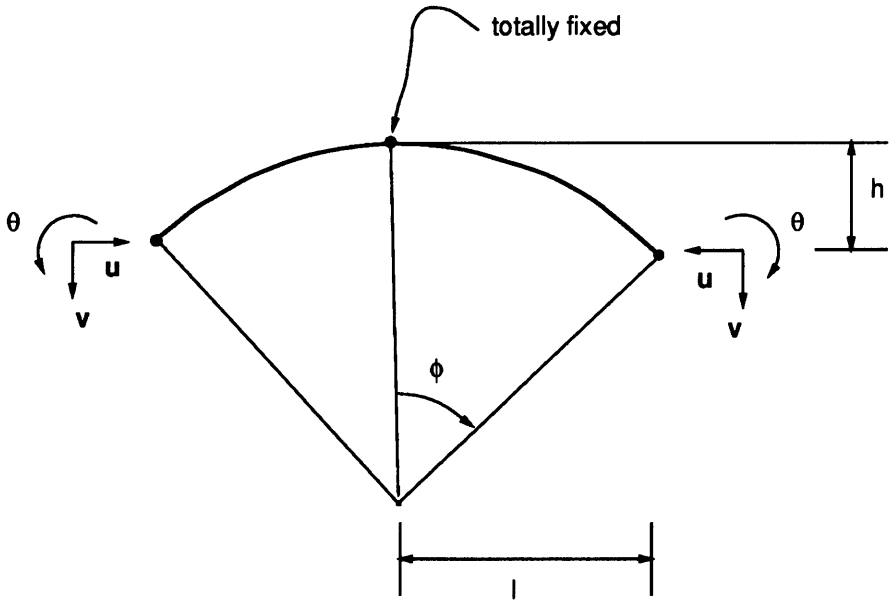

Figure 3-2: Finite element model for 3-node isobeam study

In Table 3-1 we show results obtained for the case where $l = 50$, $h = 20$ and $a = 1$. We see that when 3-point integration in the r direction is used, the element shows a severe locking behavior, whereas for 2-point integration, we obtain an accurate prediction of the rotation θ and reasonable predictions of u and v, considering that just one element is used. The natural question that we want to explore in some detail is "why does the element work using 2-point integration and why does it not work using 3-point integration ?".

Table 3-1: Comparison between 2 and 3 integration points for 3-node isobeam, $a/2l = 1/100$.

$\frac{\text{fe sol.}}{\text{analytical sol.}}$	2-point int. r-direction	3-point int. r-direction
u	0.886	0.0003
v	0.926	0.0007
θ	1.014	0.0008

We analytically derived how the strains vary along the beam as a function of u, v, θ and the geometric parameters of the arch. We use the finite element assumptions both for the interpolation of the geometry and for the interpolation of the displacement variables. The functional dependency of the covariant strain component ε_{rr} is given by

$$\begin{aligned} \varepsilon_{rr} &= e_m(u, v, r^2, \text{geometry}) + \\ &\quad a\, t\, e_b(u, v, \theta, r^2, \text{geometry}) + \end{aligned} \tag{3.1}$$

$$a^2\, t^2\, e_q(\theta, r^2, \text{geometry})$$

where r and t are the natural coordinates along the beam and the thickness. The variable "geometry" in Equation (3.1) indicates dependency on the geometrical parameters of the arch (thickness excluded). As the thickness a decreases the term proportional to $a^2 t^2$ becomes increasingly less important and is neglected hereafter. Considering $a << R$ the strain energy of the beam can be written as

$$W = aW_{membrane} + aW_{shear} + a^3 W_{bending} \tag{3.2}$$

where $aW_{membrane}$ is defined as the membrane energy and $W_{membrane}$ is the part of the membrane energy that does not depend on a. Analogous definitions are used for the shear and bending energies. Specifically,

$$W_{membrane} = C_m \int_{-1}^{+1} e_m^2 dr \tag{3.3}$$

$$W_{bending} = C_b \int_{-1}^{+1} e_b^2 dr \tag{3.4}$$

and W_{shear} depends on the component ε_{rt} and will be dealt with later when we address the issue of shear locking. In equations (3.3) and (3.4), C_m and C_b are constants depending on the geometric parameters of the arch but not on its thickness.

The solution of our finite element problem is given by the minimization of the following functional

$$\Pi = W - P \tag{3.5}$$

where W is the strain energy and P is the total potential of the applied loads both defined for the discrete problem.

Let us consider a sequence of problems, each problem associated with a particular thickness a, and with loading depending on the thickness. In our sequence of problems

the concentrated moment associated with thickness a, denoted by M_a, is defined as

$$M_a = a^3 M \tag{3.6}$$

where M is fixed. Then the total potential for a problem in our sequence reads

$$\Pi_a = aW_{membrane} + aW_{shear} + a^3 W_{bending} - a^3 2M\theta. \tag{3.7}$$

We can also define a scaled potential, Π_a^s, associated with each thickness a in the sequence given as

$$\Pi_a^s = \frac{\Pi_a}{a^3}. \tag{3.8}$$

It is easy to see that to find the minimizer of Π_a or Π_a^s yields equivalent problems. Therefore our sequence of problems P_a can be written as

$$P_a: \quad \min\left\{\frac{W_{membrane} + W_{shear}}{a^2} + W_{bending} - 2M\theta\right\}. \tag{3.9}$$

It is possible to show that as $a \to 0$, $W_{membrane} \to 0$ and $W_{shear} \to 0$. It is not difficult to see that the terms corresponding to the membrane and shear energy in Equation (3.9) would tend to infinity otherwise. Therefore Equation (3.3) implies that as $W_{membrane} \to 0$, $e_m \to 0$. Our analytical study shows that

$$e_m = 4avr^2 - \frac{l}{4h}u. \tag{3.10}$$

We show schematically in Figure 3-3 the parabolic variation of e_m with the element coordinate r.

Now it is very easy to see that if 3-point integration is used the only way to enforce $W_{membrane} \to 0$ is to have $u \to 0$ and $v \to 0$. Therefore, as the thickness of the beam decreases, u and v become smaller and smaller due to the particular functional variation of e_m. However, if we use 2-point integration we can always find u and v such that

$e_m(r) = 0$. In fact, we can set ζ, defined in Figure 3-3, to be equal to the Gauss point coordinate. Let

$$\zeta = \sqrt{\frac{l}{4h}\frac{u}{v}} = \frac{1}{\sqrt{3}} \tag{3.11}$$

then

$$\frac{u}{v} = \frac{4h}{3l}. \tag{3.12}$$

Therefore, as the thickness a of the beam decreases, Equation (3.12) is gradually enforced. Although in this case we are free from locking in the sense that the displacements do not tend to zero as the thickness decreases, as occurs in the 3-point integration scheme, Equation (3.12) works as a constraint on the degrees of freedom u and v that is totally enforced in the limit.

In order to numerically check the results just obtained, we analyzed the problem shown in Figure 3-2 with $l = 50$, $h = 20$ for various thicknesses and looked at how the ratio u/v obtained from the finite element solution compares with the constraint given by Equation (3.12). The results are shown in Table 3-2.

It is interesting to see in Table 3-2 that the constraint is indeed enforced and for $h/2l = 1/100$, which is not a value unusual in practice, it is already close to the limit.

The idea of reducing the order of integration can be viewed in this case as an application of mixed interpolation of tensorial components that we have studied for the plate elements. Here we plan to introduce it in the particular context of the beam elements.

An assumed covariant strain field for the component ε_{rr} can be defined by

$$\varepsilon_{rr}^{AS}(r,t) = \sum_{k=1}^{n_{rr}} h_k(r)\varepsilon_{rr}^{DI}(r|^k,t) \tag{3.13}$$

Where ε_{rr}^{DI} is the direct interpolated strain since it is obtained from the nodal displace-

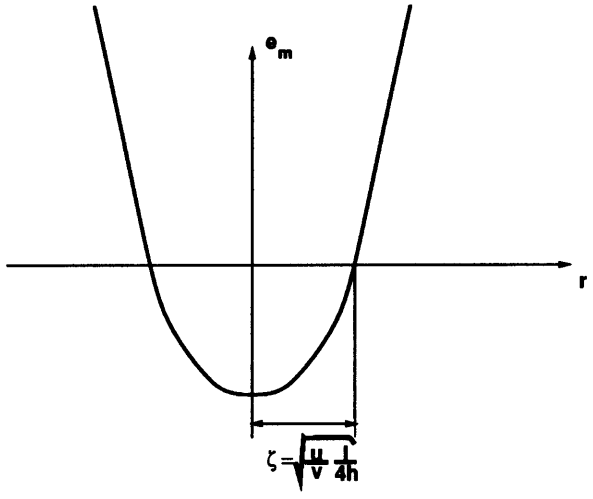

Figure 3-3: Variation of e_m along r

Table 3-2: Comparison between the ratio u/v predicted for the limit case and finite element solutions for various thicknesses

$\frac{a}{2l}$	u/v	
	finite element	analytical
1/100	0.533282	0.533333
1/1000	0.533332	0.533333
1/10000	0.533333	0.533333

ments by applying the finite element interpolations. Also a set of points $k = 1, \ldots, n_{rr}$, along the element coordinate r, called tying points is defined. As can be read from Equation (3.13) the strain ε_{rr}^{DI} is evaluated at each of the tying points and then interpolated by the functions $h_k(r)$ to obtain the assumed strain field ε_{rr}^{AS}. We study here the choice of two tying points symmetrically placed in the coordinate line r as shown in Figure 3-4.

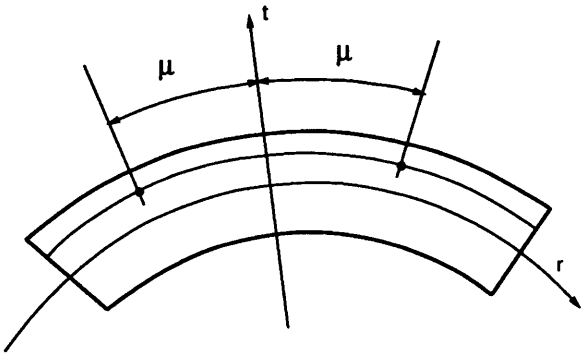

Figure 3-4: Isobeam with two tying points

Therefore,

$$\varepsilon_{rr}^{AS} = h_1 \varepsilon_{rr}^{DI}(r|^1, t) + h_2 \varepsilon_{rr}^{DI}(r|^2, t) \tag{3.14}$$

with

$$h_1 = \frac{1}{2\mu}(\mu - r) \quad ; \quad h_2 = \frac{1}{2\mu}(\mu + r) \qquad -1.0 \leq \mu \leq +1.0 \tag{3.15}$$

and it follows

$$e_m^{AS} = h_1 e_m^{DI}(r|^1) + h_2 e_m^{DI}(r|^2). \tag{3.16}$$

Using the same type of energy argument as before we can assert that as $a \to 0$, u and v will be such as to make

$$\zeta = \mu \tag{3.17}$$

or

$$\zeta = \sqrt{\frac{l}{4h}\frac{u}{v}} = \mu \tag{3.18}$$

what leads to the constraint

$$\frac{u}{v} = \frac{4h}{l}\mu^2. \tag{3.19}$$

Note that the choice of $\mu = 1/\sqrt{3}$ leads to the same constraint as obtained for 2-point integration. The question that arises here is "what is the best choice of μ in order to minimize the deleterious effect of the constraint ?". One approach to select the "ideal" tying point is to choose μ such that the ratio $\frac{u}{v}$ given by the constraint is the ratio $(\frac{u}{v})^{\text{analytical}}$ that we obtain when solving analytically the mathematical model of the problem for u and v. Therefore using Equation (3.19) we obtain,

$$\mu = \sqrt{\frac{4h}{l}(\frac{u}{v})^{\text{analytical}}}. \tag{3.20}$$

We have used this approach and found, as expected, that μ, as given by Equation (3.20), depends on the geometrical parameters of the arch. Therefore, for each element with different geometrical properties, we would find a different point tying. We denote by μ^v, for variable point tying, the μ given by Equation (3.20). If we want to find a point tying that is independent of the geometry of the element, we can take into account that, as the finite element model is refined, each element tends to a shallow situation. Therefore, we could use for $(\frac{u}{v})^{\text{analytical}}$, the value obtained using a shallow arch mathematical model,

$$(\frac{u}{v})^{\text{analytical}} = (\frac{u}{v})^{\text{shallow}} = \frac{4h}{3l} \tag{3.21}$$

what would lead to the tying point given by

$$\mu^f = \frac{1}{\sqrt{3}} \tag{3.22}$$

where μ^f stands for fixed point tying. It is interesting to note that the value obtained for μ^f is exactly the value corresponding to 2-point integration.

The same type of study that we presented for membrane locking was also performed for shear locking. Although we do not plan to show in the same detail the shear locking study, we do want to go through the basic steps.

For the shear locking problem the relevant strain component is ε_{rt}. Proceeding in analogous fashion, we could find analytically the covariant component ε_{rt} which has the following functional dependency

$$\varepsilon_{rt} = a\, e_s(u, v, \theta, r, r^3, \text{geometry}). \tag{3.23}$$

In the above expressions, the terms that depend on t were not included, since they are not important for thin beams. The quantity W_{shear} has the following form

$$W_{shear} = C_s \int_{-1}^{+1} e_s^2 dr. \tag{3.24}$$

Using an energy argument it can be shown that as $a \to 0$, $W_{shear} \to 0$. Analogously, we assumed that

$$\varepsilon_{rt}^{AS} = h_1 \varepsilon_{rt}^{DI}(r|^1, t) + h_2 \varepsilon_{rt}^{DI}(r|^2, t) \tag{3.25}$$

with

$$h_1 = \frac{1}{2\varrho}(\varrho - r) \qquad ; \qquad h_2 = \frac{1}{2\varrho}(\varrho + r) \qquad -1.0 \leq \varrho \leq +1.0 \tag{3.26}$$

and it follows

$$e_s^{AS} = h_1 e_s^{DI}(r|^1) + h_2 e_s^{DI}(r|^2). \tag{3.27}$$

As we impose that $e_s^{AS} = 0$, we are lead to a constraint equation of the type

$$f(u, v, \theta, \varrho, \text{geometry}) = 0 \tag{3.28}$$

Although in this case the algebraic expressions are much more complicated (the algebraic manipulations were performed using the program MACSYMA [45]) than those of the membrane locking case, we were able to derive a variable point tying denoted by ϱ^v and a fixed point tying ϱ^f for the shear strain component ε_{rt}. It is worth noting that we obtained for the fixed point tying

$$\varrho^f = \frac{\sqrt{5}}{3} \tag{3.29}$$

which has a different value from that of the component ε_{rr}.

We have implemented the isobeam element allowing for independent choice of tying points for the membrane and shear components. Therefore we could perform numerical experiments to assess the validity of our conclusions. The problem studied is described in Figure 3-2 with $l = 50$, $h = 20$ and $a = 0.1$. We summarize in Table 3-3 the tying schemes that are used in the numerical examples.

In Table 3-4 we compare the results obtained when the variable tying scheme (μ^v for the membrane tying and ϱ^v for the shear tying) and the scheme with 2-point integration (current point tying) are employed. The overall improvement of the results confirms our predictions.

Next, we want to compare the fixed point tying scheme that was derived using shallow arch assumptions and the current tying scheme. We recall that the only difference between these two schemes is the tying used for the shear component for which $\varrho^f = \sqrt{5}/3 \neq 1/\sqrt{3}$. Although we do not expect a large difference between these two

Table 3-3: Summary of tying schemes

Tying Scheme Name	Membrane tying point μ	Shear tying point ϱ
Current	$1/\sqrt{3}$	$1/\sqrt{3}$
Fixed	$1/\sqrt{3}$	$\sqrt{5}/3$
Variable	function of geometry	function of geometry
Artificial	1.0	$\sqrt{5}/3$

Table 3-4: Predictions for nodal variables using the variable point tying scheme and the current one.

	ERROR (%)		
	u	v	θ
Variable Point Tying	1.35	1.29	1.31
Current Point Tying	11.42	7.51	1.26

schemes, we would like to see a better convergence for the fixed point tying scheme since the individual elements go from a deep arch situation to a shallow one as the mesh is refined. The results obtained are shown in Table 3-5 and we notice that the convergence is very fast in both cases but the fixed tying scheme displays the expected behavior.

Table 3-5: Convergence of nodal variables using the fixed point tying scheme and the current one

MESH # of elements along complete arch	ERROR (%)					
	u		v		θ	
	current tying	fixed tying	current tying	fixed tying	current tying	fixed tying
1	11.42	3.36	7.51	7.93	1.26	1.06
2	0.91	0.17	0.37	0.12	0.13	0.12
3	0.10	0.03	0.04	0.02	0.01	0.01
8	0.047	0.043	0.017	0.016	0.0006	0.0006
16	0.044	0.044	0.015	0.015	0.00004	0.00004

As a last example, we chose arbitrarily a tying point, $\mu^f = 1.0$, for the membrane component and kept $\varrho^f = \sqrt{5}/3$ for the shear. The results are presented in Table 3-6 where the above tying scheme is referred as artificial. We note that, although convergence

still occurs, the predictions for coarse meshes become very inaccurate.

Table 3-6: Convergence of nodal variables using the fixed point tying scheme and the artificial point tying scheme

MESH # of elements along complete arch	ERROR (%)					
	u		v		θ	
	current tying	artificial tying	current tying	artificial tying	current tying	artificial tying
1	19.23	3.36	71.88	7.93	59.84	1.06
2	0.84	0.17	34.17	0.12	27.80	0.12
3	1.56	0.03	11.10	0.02	8.80	0.01
8	0.490	0.043	2.980	0.016	2.3500	0.0006
16	0.090	0.044	0.740	0.015	0.59000	0.00004

3.2 The 4-node Isobeam Element

We performed for the 4–node isobeam element a similar study as for the 3–node isobeam. The problem analyzed is described in Figure 3-5 and in this case we need 6 d.o.f. to characterize our problem. We analytically obtained the following equations:

$$e_m = \quad e_m(u_b, v_b, u_m, v_m, r^2, r^4, \text{geometry}) \tag{3.30}$$

$$e_s = \quad e_s(u_b, v_b, u_m, v_m, \theta_b, \theta_m, r, r^3, r^5, \text{geometry}) \tag{3.31}$$

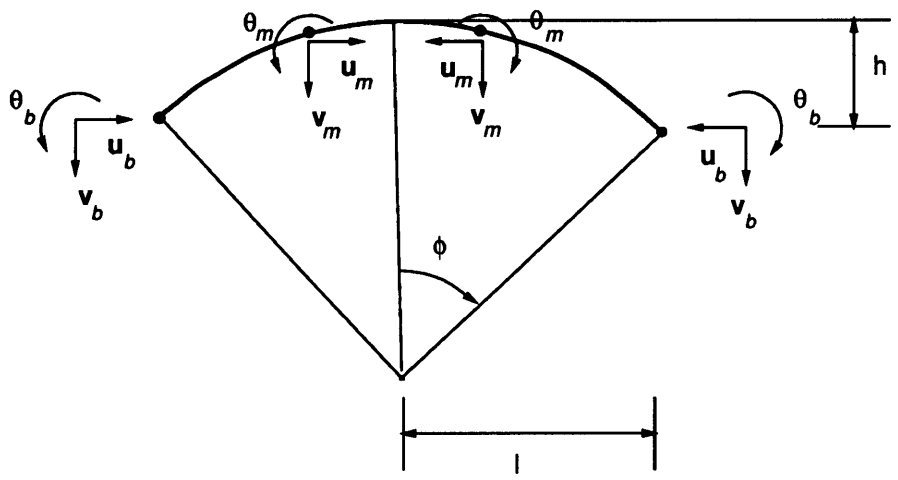

Figure 3-5: Finite element model for 4-node isobeam study

As argued before, as $a \to 0$, $e_m \to 0$ and $e_s \to 0$ which leads to constraints for the d.o.f. $u_b, v_b, u_m, v_m, \theta_b$ and θ_m. We checked that for both 3 and 4-point integration in the r direction there are nontrivial $u_b, v_b, u_m, v_m, \theta_b$ and θ_m, such that the constraints are satisfied, as expected, due to the particular functional dependency of e_m and e_s on the variable r. Although obvious at this point, we remark that less constraints arise when 3–point integration is used.

In this study we also searched for tying points that would lead to constraint equations according to the shallow arch solutions for the nodal degrees of freedom. We obtained that the choice of two tying points, at $r = \sqrt{3}/9$ and $r = -\sqrt{3}/9$, for both membrane and shear leads to the desired result. However, just two tying points for a 4-node beam element yield spurious zero energy modes rendering the element not adequate for practical applications.

In summary for the 4–node isobeam study, we conclude that locking, in the sense that the displacements variables go to zero as the thickness decreases, does not occur. Also a 3-point integration scheme leads to less constraints than a 4-point scheme as the thickness tends to zero.

We recall that the purpose of the study was to get insight in the locking behavior, therefore we chose a particular problem *i.e.*, a specific geometry (circular arch) and a particular loading (pure bending moment). Although we consider this case important, care should be exercised when generalizing our conclusions.

Chapter 4

Mixed–Interpolated General Shell Elements

Although some of the issues that we discuss in this introduction have already been addressed to some extend in Chapter 1, we feel that to convey the motivations and ideas behind the developments presented in this chapter we need to reinforce them.

Our approach towards the development of finite elements for the analysis of plate and shell structures has been guided by the following requirements:

1. The elements should be reliable.
2. The elements should be computationally effective.
3. The element formulation should be general *i.e.*, the elements should be applicable to:
   - nonlinear analysis (geometric and material nonlinear solutions)
   - thick and thin plate/shell situations
   - any shell geometry.
4. The formulation of the element should be mechanistically clear and sufficiently simple to render the elements suitable for engineering analysis.

The continuum based degenerated shell elements originally proposed by Ahmad, Irons and Zienkiewicz [7] and extended for nonlinear analysis by Ramm [8] and Bathe and Bolourchi [9] satisfy requirements 3 and 4, but the lower-order elements do not satisfy requirements 1 and 2, and the higher–order 16-node element does not satisfy requirement 2 due to the effects of membrane and shear locking.

Ideally, considering requirements 1 and 2, the element formulation would lead to finite element discretizations that could be shown mathematically to be convergent, stable and to have optimal error bounds. In plate analysis much progress has been made in this regard, see specifically, the MITC family of Reissner-Mindlin plate bending elements that we have discussed in Chapter 2.

In general shell analysis, as stated in requirement 3, the situation is quite different. A mathematical analysis of the type just mentioned is not available. However, a very valuable contribution in this direction, although restricted in its applicability, has been published by Pitkäranta [46]. We refer again to his work later in this introduction.

Since a complete mathematical theory is lacking, the following conditions should be strictly enforced to satisfy requirement 1:

- The elements should not have any spurious zero energy mode.
- The elements should not membrane or shear lock, when used in, of course, undistorted and reasonably distorted meshes.
- The predictive capability of the elements should be high and relatively insensitive to geometric distortions.

Of course, insight into element behavior and the use of numerical experiments will be important in the design of elements to satisfy the above conditions. It is our view that an element which fails any one of these conditions should not be used in engineering practice.

The MITC approach has been used successfully to propose shell elements that satisfy the above conditions and requirement 2. Also, the formulation of the MITC elements

preserves the essential and appealing characteristics of the continuum based degenerated shell elements, therefore satisfying requirements 3 and 4.

The approach of mixed interpolation of tensorial components for shell elements finds its roots in the work of Dvorkin and Bathe [18], where the MITC4 element was developed and assumed covariant strain component fields were first introduced.

Subsequently Bathe and Dvorkin [2] developed an eight node element in which not only the transverse shear strains were mixed interpolated to avoid shear locking but also the in–layer strains, to avoid membrane locking. In this work, the strain tensor was decomposed in a transverse shear strain part and an in–layer strain part and the two resulting tensors were interpolated in different ways.

Nine node shell elements were developed by Huang and Hinton [19], Park and Stanley [20], Jang and Pinsky [21] and Cho. Huang and Hinton used a local cartesian system to separate bending and membrane strains and mixed interpolated just the membrane part. The transverse shear strains were evaluated and mixed interpolated in the natural coordinate system. Park and Stanley used assumed physical strain component fields that were derived from special assumptions on the strains along selected coordinate lines. A second version of their element was presented in Reference [47]. Jang and Pinsky assumed the covariant strain components in natural coordinates for both the in–layer strains and transverse shear strains. Cho used for the in–layer strains the assumptions of the MITC8 element and for the shear strains the field and tying scheme of the MITC9 plate bending element [31] in which the integral tying condition is replaced by point tying conditions. This requires that the internal node only has rotational degrees of freedom.

Recently, as mentioned above, Pitkäranta [46] mathematically analyzed the membrane locking problem of a clamped hemicylindrical shell subjected to varying distributed pressure. He was able to conclude that the displacement based elements would require order greater or equal to 4 in the local polynomial expansion for the displacement variables to be free of locking for rectangular grids, whereas for quadrilateral grids the elements would not be in general free of locking for any order of polynomial expansions.

Pitkäranta, motivated by the high predictive capability of the MITC8 element of Bathe and Dvorkin, analyzed mathematically a family of mixed interpolated schemes very close to the scheme of Bathe and Dvorkin. Although his analysis is only valid for rectangular grids and is based on additional restrictive assumptions, he was able to prove that these schemes avoid membrane and shear locking and converge with an optimal rate.

It is interesting to note that the conclusions of Pitkäranta regarding displacement based elements suggest that the 16–node isoparametric displacement based shell element widely used in engineering practice is not entirely free of locking even for rectangular grids. Our numerical experiences show that in some cases this element presents a very low convergence rate and when curved and geometrically distorted can display a locking behavior.

In this chapter we present a 16-node mixed–interpolated element which we call the MITC16 element. Numerical experiments show that this new element is free of locking and presents a significant improvement with respect to its displacement based counterpart.

Our motivations to develop the 16-node element were reinforced by our observations that higher–order Lagrangian elements predict stresses accurately and efficiently. For two–dimensional analysis Kato and Bathe [22] found that the 16–node isoparametric element was more efficient than the lower–order elements for problems with high stress gradients, and together with the 25-node Lagrangian isoparametric element were the most efficient in a study of these elements versus p-type elements up to order 10. Moreover, in shell analysis the higher–order Lagrangian elements have the additional advantage of describing more accurately the geometry of the shell.

Encouraged by the performance of the MITC16 element, we formulated with the same approach a 9-node mixed interpolated shell element, that we also present in this chapter.

In the following section we give the formulations of the MITC9 and MITC16 elements.

4.1 Formulation of the Mixed–Interpolated Shell Elements

In this section we formulate mixed interpolated shell elements. First, we introduce, in a general framework, how elements based on assumed covariant strain fields can be proposed and subsequently we discuss the specific elements that we have developed.

4.1.1 Shell Elements Based on Assumed Covariant Strain Fields

Let us use a total Lagrangian formulation to derive the governing equations of our finite element shell model. The starting point is the statement of the principle of virtual work written at time step $t + \Delta t$ [10]

$$\int_{{}^0V} {}^{t+\Delta t}_{0}\tilde{S}^{ij} \; \delta\, {}^{t+\Delta t}_{0}\tilde{\varepsilon}_{ij} \; d^0V = {}^{t+\Delta t}\mathcal{R} \tag{4.1}$$

where ${}^{t+\Delta t}_{0}\tilde{S}^{ij}$ is the contravariant component of the 2nd Piola–Kirchhoff stress tensor, ${}^{t+\Delta t}_{0}\tilde{\varepsilon}_{ij}$ is the covariant component of the Green–Lagrange strain tensor and ${}^{t+\Delta t}\mathcal{R}$ is the virtual work of the applied loads. All quantities are defined at time step $t + \Delta t$.

The governing equations of the isoparametric displacement based elements are obtained from Equation (4.1) by using the finite element interpolation assumptions both for the geometry and for the displacement variables to evaluate the strain ${}^{t+\Delta t}_{0}\tilde{\varepsilon}_{ij}$, more precisely denoted by ${}^{t+\Delta t}_{0}\tilde{\varepsilon}^{DI}_{ij}$. Here the superscript DI indicates that the strains are obtained by "direct" interpolation using the finite element displacement assumptions. The mixed interpolated elements are constructed using ${}^{t+\Delta t}_{0}\tilde{\varepsilon}^{AS}_{ij}$ in place of ${}^{t+\Delta t}_{0}\tilde{\varepsilon}^{DI}_{ij}$, where the superscript AS indicates that it is an assumed field.

The next step is to show how the assumed strain fields, ${}^{t+\Delta t}_{0}\tilde{\varepsilon}^{AS}_{ij}$, are constructed from the direct interpolated strain fields, ${}^{t+\Delta t}_{0}\tilde{\varepsilon}^{DI}_{ij}$. We omit temporarily, merely for ease of notation, the sub- and superscripts relating to time $(0, t+\Delta t)$ in the strain expressions.

In order to define the assumed covariant strain fields, Equation (4.1) has to be written

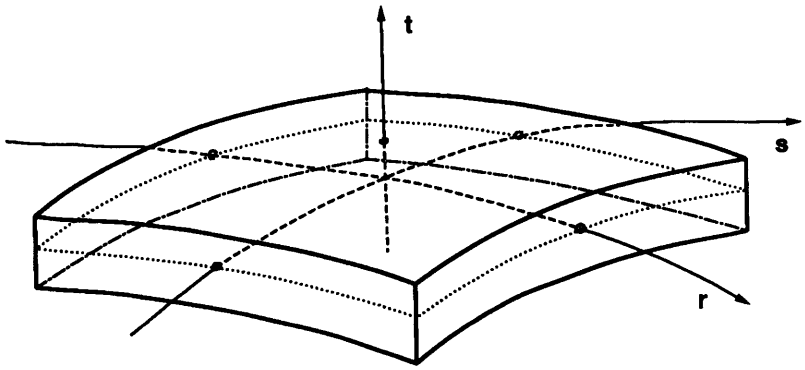

Figure 4-1: Local coordinates for a shell element

in a particular convected coordinate system. This coordinate system is defined element-wise by the element isoparametric coordinates r, s and t as shown in Figure 4-1 with the following convention for indicial notation: $r_1 \equiv r$, $r_2 \equiv s$ and $r_3 \equiv t$.

Associated with each strain component $\tilde{\varepsilon}_{ij}$ we define a set of points, $k = 1, \ldots, n_{ij}$, by specifying for each point k its natural coordinates $r = r_k$, $s = s_k$ and t. These points are called tying points.

Now the assumed covariant strain component $\tilde{\varepsilon}_{ij}^{AS}$ is defined as

$$\tilde{\varepsilon}_{ij}^{AS}(r,s,t) = \sum_{k=1}^{n_{ij}} h_k^{ij}(r,s)\tilde{\varepsilon}_{ij}^{DI}(r_k,s_k,t) \tag{4.2}$$

where $h_k^{ij}(r,s)$ are interpolation functions (polynomials in r and s) associated with the strain component $\tilde{\varepsilon}_{ij}$ such that

$$h_k^{ij}|^l := h_k^{ij}(r_l,s_l) = \delta_{kl}, \quad l = 1, \ldots, n_{ij} \tag{4.3}$$

and denoting

$$\tilde{\varepsilon}_{ij}^{DI}|^k := \tilde{\varepsilon}_{ij}^{DI}(r_k,s_k,t) \quad \text{and} \quad \tilde{\varepsilon}_{ij}^{AS}|^k := \tilde{\varepsilon}_{ij}^{AS}(r_k,s_k,t) \tag{4.4}$$

it follows

$$\tilde{\varepsilon}_{ij}^{AS}|^k = \tilde{\varepsilon}_{ij}^{DI}|^k, \quad k = 1, \ldots, n_{ij} \tag{4.5}$$

Of course, this selection is the reason why the n_{ij} points are called tying points.

4.2 The Proposed Elements

The formulation described in the previous section is quite general and, of course, allows us to propose a number of elements. However, an element is only useful if the conditions for reliability and effectiveness stated in the introduction are satisfied.

The choice of tying points for the 9–node element is given in Figure 4-2 and the choice for the 16–node element is presented in Figure 4-3.

We remark that using the tying points of Figure 4-2 it is also possible to propose an 8-node element. We did implement and test such element, but the element was not sufficiently effective and reliable. Although it performed quite effectively in some cases, in a few cases the element presented a very stiff behavior rendering it not useful.

We assumed for the transverse shear strain components that

$$\tilde{\varepsilon}_{rt}(r,s,t) = \tilde{\varepsilon}_{rt}(r,s,0) \tag{4.6}$$

$$\tilde{\varepsilon}_{st}(r,s,t) = \tilde{\varepsilon}_{st}(r,s,0). \tag{4.7}$$

Both proposed elements do not have any spurious zero energy mode and their stiffness matrices are evaluated with "full" numerical integration *i.e.*, 3×3 Gauss integration, in the rs plane for the MITC9 element, and 4×4 for the MITC16 element. As the numerical results will show, the proposed elements are free of locking and perform quite effectively.

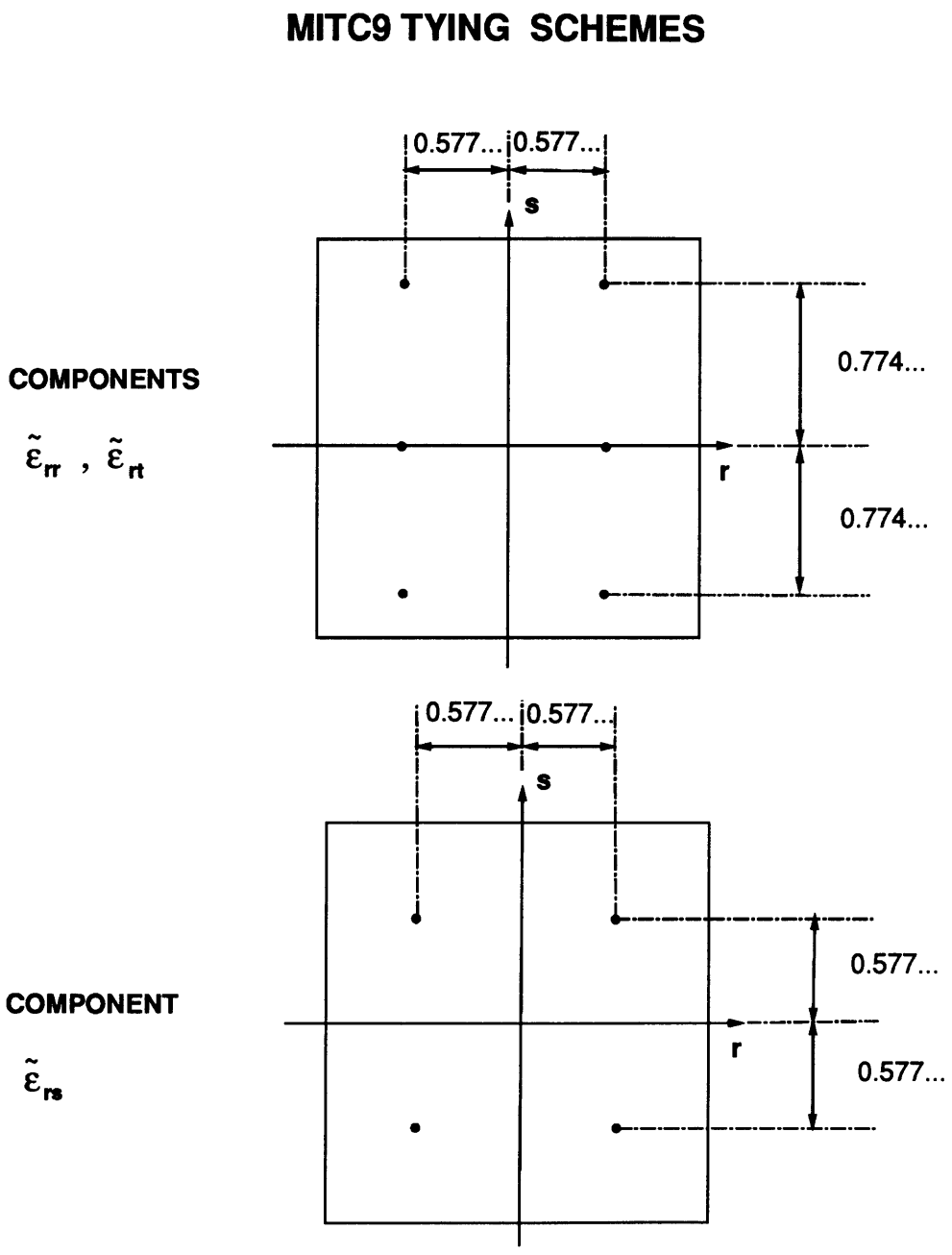

Figure 4-2: Tying schemes used for the strain components of the MITC9 element. Tying schemes for the components ε_{ss} and ε_{st} are implied by symmetry. Coordinates of tying points always coincide with one–dimensional Gauss point coordinates, *e.g.*, $(1/3)^{1/2} = 0.577...$

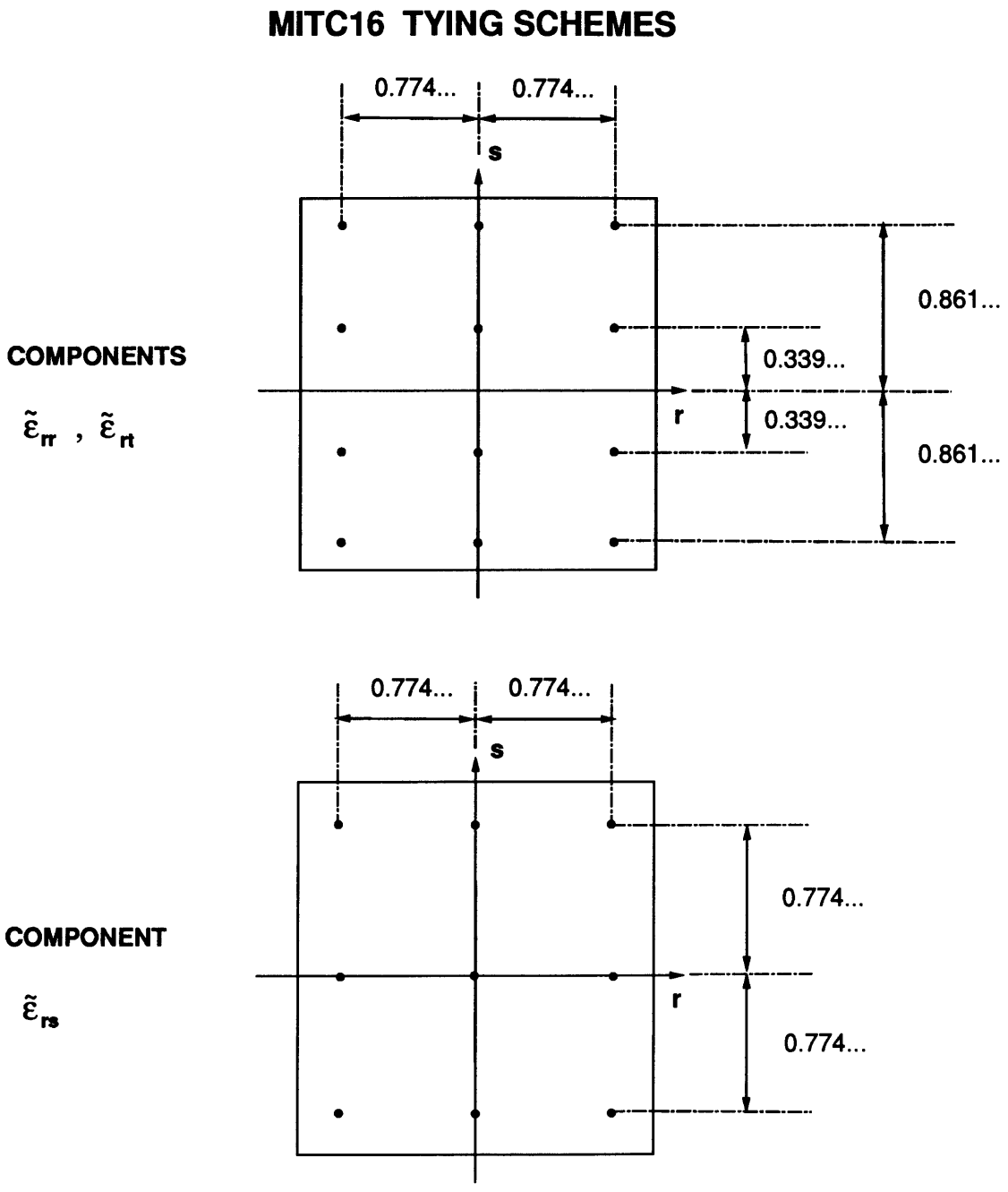

Figure 4-3: Tying schemes used for the strain components of the MITC16 element. Tying schemes for the components ε_{ss} and ε_{st} are implied by symmetry. Coordinates of tying points always coincide with one–dimensional Gauss point coordinates, *e.g.*, $(3/5)^{1/2} = 0.774...$

4.3 Construction of the Element Stiffness Matrices

We present very briefly in this section how the stiffness matrices of these elements can be constructed. Although the stiffness matrix for linear analysis is obtained directly from the general nonlinear element formulation, we present here, just for clarity of exposition, first the construction of the stiffness matrices for linear analysis and then for nonlinear analysis. We note that the kinematic assumptions are the same as for the isoparametric displacement based elements [10] and will not be repeated here.

The covariant component $\tilde{\varepsilon}_{ij}$ of the Green–Lagrange strain tensor can be written as

$$ {}^{t}_{0}\tilde{\varepsilon}^{DI}_{ij} = \frac{1}{2}({}^{t}\mathbf{g}_i.{}^{t}\mathbf{g}_j - {}^{0}\mathbf{g}_i.{}^{0}\mathbf{g}_j) \tag{4.8} $$

where ${}^{0}\mathbf{g}_i$ and ${}^{t}\mathbf{g}_i$ are the covariant base vectors associated with coordinate r_i at times 0 and t, respectively. If ${}^{t}\mathbf{x}$ and ${}^{t}\mathbf{u}$ are the position and displacement vectors at time t of any point in our shell model then,

$$ {}^{0}\mathbf{g}_i = \frac{\partial {}^{0}\mathbf{x}}{\partial r_i} \tag{4.9} $$

$$ {}^{t}\mathbf{g}_i = \frac{\partial {}^{t}\mathbf{x}}{\partial r_i} = \frac{\partial({}^{0}\mathbf{x} + {}^{t}\mathbf{u})}{\partial r_i} = {}^{0}\mathbf{g}_i + \frac{\partial {}^{t}\mathbf{u}}{\partial r_i} \tag{4.10} $$

4.3.1 Linear Analysis

Substituting Equation (4.10) into Equation (4.8) we obtain

$$ {}^{t}_{0}\tilde{\varepsilon}^{DI}_{ij} = \frac{1}{2}(\frac{\partial {}^{t}\mathbf{u}}{\partial r_i}.{}^{0}\mathbf{g}_j + \frac{\partial {}^{t}\mathbf{u}}{\partial r_j}.{}^{0}\mathbf{g}_i + \frac{\partial {}^{t}\mathbf{u}}{\partial r_i}.\frac{\partial {}^{t}\mathbf{u}}{\partial r_j}). \tag{4.11} $$

The quadratic term $\frac{\partial {}^{t}\mathbf{u}}{\partial r_i}.\frac{\partial {}^{t}\mathbf{u}}{\partial r_j}$ is neglected in linear analysis yielding

$$ {}^{t}_{0}\tilde{\varepsilon}^{DI}_{ij} = \frac{1}{2}(\frac{\partial {}^{t}\mathbf{u}}{\partial r_i}.{}^{0}\mathbf{g}_j + \frac{\partial {}^{t}\mathbf{u}}{\partial r_j}.{}^{0}\mathbf{g}_i) \tag{4.12} $$

where in this case the superscript t just indicates the deformed configuration. From Equation (4.12) we can write

$$ {}^{t}_{0}\tilde{\varepsilon}^{DI}_{ij} = \mathbf{B}^{DI}_{ij}\hat{\mathbf{u}} \tag{4.13} $$

where $\mathbf{B}^{DI}_{ij}$ is the strain–displacement matrix corresponding to the covariant strain component ${}^{t}_{0}\tilde{\varepsilon}^{DI}_{ij}$ and $\hat{\mathbf{u}}$ is the nodal point displacement vector. Using Equation (4.2) we obtain the assumed strain components as

$$ {}^{t}_{0}\tilde{\varepsilon}^{AS}_{ij} = \sum_{k=1}^{n_{ij}} h^{ij}_{k}\mathbf{B}^{DI}_{ij}|^{k}\hat{\mathbf{u}} \tag{4.14} $$

where

$$ \mathbf{B}^{DI}_{ij}|^{k} := \mathbf{B}^{DI}_{ij}(r_k, s_k, t). \tag{4.15} $$

We can also define $\mathbf{B}^{AS}_{ij}$, the strain–displacement matrix for the assumed strain, as

$$ \mathbf{B}^{AS}_{ij} = \sum_{k=1}^{n_{ij}} h^{ij}_{k}\mathbf{B}^{DI}_{ij}|^{k} \tag{4.16} $$

Using Equation (4.14) it is now straight forward to obtain the stiffness matrix of the element, either by using the constitutive law written in the convected coordinate system or by transforming the strains and the constitutive law to the global system.

4.3.2 Nonlinear Analysis

Equation (4.1) can be rewritten in the following form

$$ \int_{{}_0V} {}_0\tilde{S}^{ij}\,\delta_0\tilde{\varepsilon}_{ij}\,d\,{}^0V + \int_{{}_0V} {}^{t}_{0}\tilde{S}^{ij}\,\delta_0\tilde{\eta}_{ij}\,d\,{}^0V + \int_{{}_0V} {}^{t}_{0}\tilde{S}^{ij}\,\delta_0\tilde{e}_{ij}\,d\,{}^0V = {}^{t+\Delta t}\mathcal{R} \tag{4.17} $$

where

$$
\begin{aligned}
{}^{t+\Delta t}_{0}\tilde{S}^{ij} &= {}^{t}_{0}\tilde{S}^{ij} + {}_{0}\tilde{S}^{ij} && (4.18)\\
{}^{t+\Delta t}_{0}\tilde{\varepsilon}_{ij} &= {}^{t}_{0}\tilde{\varepsilon}_{ij} + {}_{0}\tilde{\varepsilon}_{ij} && (4.19)\\
{}_{0}\tilde{\varepsilon}_{ij} &= {}_{0}\tilde{e}_{ij} + {}_{0}\tilde{\eta}_{ij}. && (4.20)
\end{aligned}
$$

Here ${}_{0}\tilde{e}_{ij}$ and ${}_{0}\tilde{\eta}_{ij}$ are the linear and nonlinear parts of the incremental strain ${}_{0}\tilde{\varepsilon}_{ij}$. Note that Equation (4.17) corresponds to a complete linearization of the governing continuum mechanics equations provided the incremental displacements are expressed in terms of the nodal point incremental displacements, rotations and rotation–squared [10].

Using equations (4.11) and (4.19) and defining $\mathbf{u} = {}^{t+\Delta t}\mathbf{u} - {}^{t}\mathbf{u}$ we obtain

$$
{}_{0}\tilde{\varepsilon}^{DI}_{ij} = \frac{1}{2}\left(\frac{\partial \mathbf{u}}{\partial r_i}\cdot {}^{t}\mathbf{g}_j + \frac{\partial \mathbf{u}}{\partial r_j}\cdot {}^{t}\mathbf{g}_i + \frac{\partial \mathbf{u}}{\partial r_i}\cdot\frac{\partial \mathbf{u}}{\partial r_j}\right). \tag{4.21}
$$

The above equation can be rewritten as

$$
{}_{0}\tilde{\varepsilon}^{DI}_{ij} = {}_{0}\tilde{e}^{DI}_{ij} + {}_{0}\hat{\eta}^{DI}_{ij} \tag{4.22}
$$

where ${}_{0}\tilde{e}^{DI}_{ij}$ involves only terms that are linear in the nodal variables and ${}_{0}\hat{\eta}^{DI}_{ij}$ contains all the quadratic terms including those arising from the rotations at the nodal points.

We can write

$$
{}_{0}\tilde{e}^{DI}_{ij} = \mathbf{L}^{DI}_{ij}\hat{\mathbf{u}} \tag{4.23}
$$

where $\mathbf{L}^{DI}_{ij}$, implicitly defined in the above equation, is the strain–displacement matrix associated with the incremental strain component ${}_{0}\tilde{e}_{ij}$. The above equation leads to

$$
\delta\,{}_{0}\tilde{e}^{DI}_{ij} = \delta\hat{\mathbf{u}}^{T}\mathbf{L}^{DI}_{ij}. \tag{4.24}
$$

We can also write

$$\delta_0\hat{\eta}_{ij}^{DI} = \delta\hat{\mathbf{u}}^T\mathbf{N}_{ij}^{DI}\hat{\mathbf{u}}. \tag{4.25}$$

which defines the square matrix $\mathbf{N}_{ij}^{DI}$.

The assumed incremental strains can now be defined as

$$_0\tilde{e}_{ij}^{AS} = \sum_{k=1}^{n_{ij}} h_k^{ij}\mathbf{L}_{ij}^{DI}|^k\hat{\mathbf{u}} \tag{4.26}$$

and

$$\delta_0\hat{\eta}_{ij}^{AS} = \delta\hat{\mathbf{u}}^T\sum_{k=1}^{n_{ij}} h_k^{ij}\mathbf{N}_{ij}^{DI}|^k\hat{\mathbf{u}}. \tag{4.27}$$

Therefore,

$$\mathbf{L}_{ij}^{AS} = \sum_{k=1}^{n_{ij}} h_k^{ij}\mathbf{L}_{ij}^{DI}|^k \tag{4.28}$$

and

$$\mathbf{N}_{ij}^{AS} = \sum_{k=1}^{n_{ij}} h_k^{ij}\mathbf{N}_{ij}^{DI}|^k. \tag{4.29}$$

The stiffness matrices $\mathbf{K}_L$ and $\mathbf{K}_{NL}$ can be derived as for the standard isoparametric elements by replacing the direct interpolated incremental strains by the assumed incremental strains defined in the above equations.

Chapter 5

Numerical Evaluation of the Elements

In this chapter we present some numerical results obtained with the proposed shell elements. The MITC9 and MITC16 have been implemented in an experimental manner in the general purpose finite element program ADINA [48].

The problems studied have been selected to display the predictive capabilities of the elements for a range of situations and to show that the elements do satisfy our criteria for reliability and effectiveness.

5.1 The Patch Test

The patch test has been widely used as a test for element convergence, despite of its limitations for mixed formulations. We use the test here to assess the sensitivity of our elements to geometric distortions.

In Figure 2-1 of Chapter 2 we show the mesh used for the patch test. The minimum number of degrees of freedom are constrained to prevent rigid body motion, and we study the stresses along arbitrarily selected lines passing through Gauss integration points as shown schematically in Figure 5-1. In figures 5-2 and 5-3 we show the stresses along

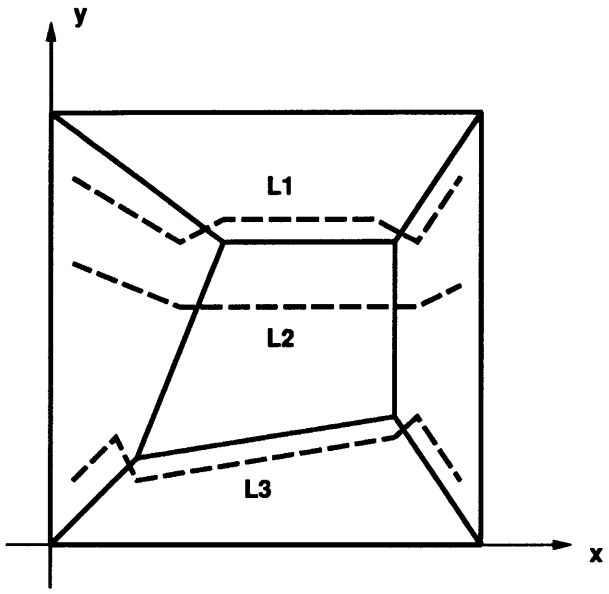

Figure 5-1: Lines through element Gauss points for stress evaluation

lines L1 and L2 obtained with the MITC16 element for the membrane and bending tests respectively. Although there are slight deviations from the analytical values, the constant stress state is closely represented indicating a low sensitivity to element geometric distortions. For the MITC9 element very similar results are obtained.

5.2 Analysis of a Curved Cantilever

We consider the curved cantilever problem described in Figure 5-4. In Table 5-1 we show the results obtained for various meshes using the 16-node displacement based element and the MITC16 element. The ratio between the finite element and the analytical predictions for the tip rotation, at point A, are shown for several values of the thickness. We notice that the predictions are excellent for most discretizations even for extremely thin situations ($h/R = 1/10^5$) and also for the two element case with the side common to the two elements parallel to the axis of the cylindrical surface. However, when this side is skewed the results significantly deteriorate for the 16-node displacement based

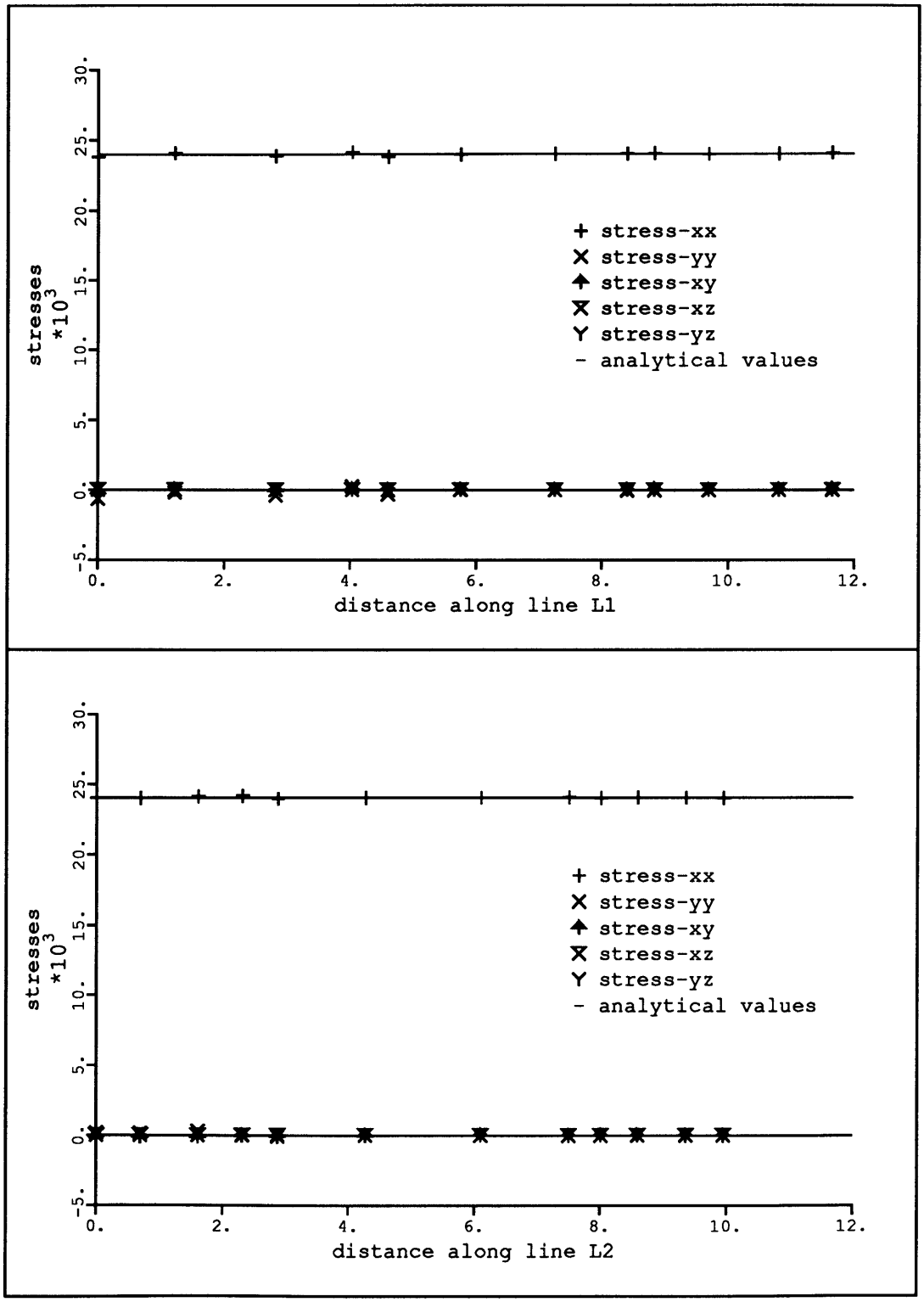

Figure 5-2: Stresses along lines L1 and L2 for membrane patch test

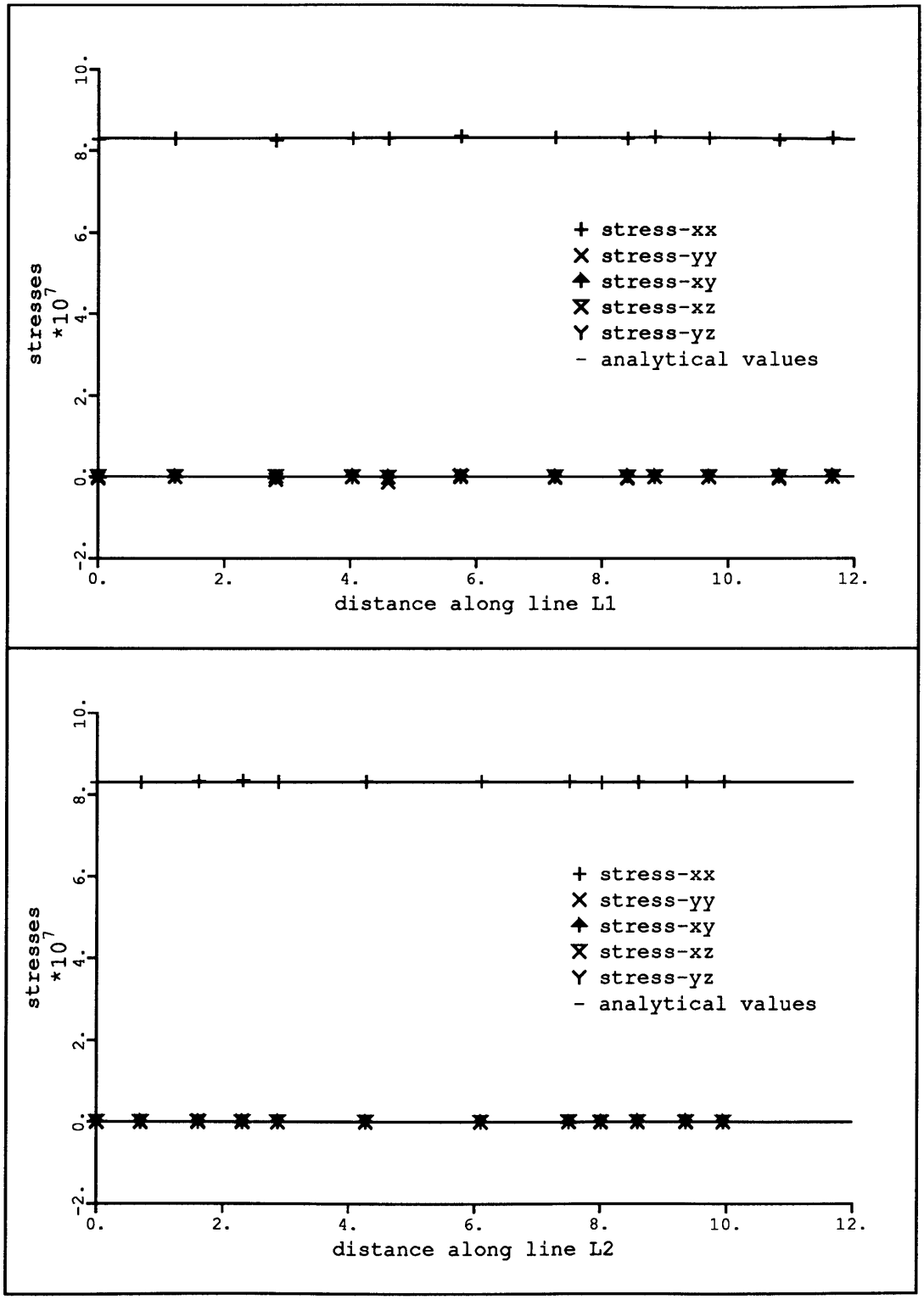

Figure 5-3: Stresses along lines L1 and L2 for bending patch test

element displaying a locking behavior. This type of behavior was theoretically predicted by Pitkäranta [46].

Table 5-1: Summary of results for the curved cantilever problem using 16-node elements. Point A always coincides with an element node.

MESH	h/R	$\theta_{FE} / \theta_{AN}$	
		16 node disp. based	MITC16
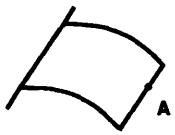	1/100 1/1000 1/100000	0.9995 0.9995 0.9995	1.0001 1.0001 1.0001
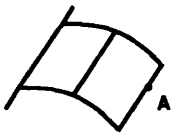	1/100 1/1000 1/100000	0.9996 0.9996 0.9994	1.0000 1.0000 0.9999
	1/100 1/1000 1/100000	0.9868 0.9277 0.0029	0.9975 0.9796 0.9318
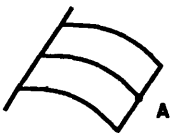	1/100 1/1000 1/100000	0.9995 0.9995 0.9994	1.0001 1.0001 1.0001
	1/100 1/1000 1/100000	0.9993 0.9995 0.9994	1.0000 1.0001 1.0001

In Table 5-2 we show analogous results for the MITC8 [2] and the MITC9 elements. Using the MITC8 element, which is a good element in general, the same type of result deterioration that appeared for the 16-node displacement based element is observed. We notice that the MITC9 does not display such a behavior.

In the results presented we used $\nu = 0.0$ but when using $\nu \neq 0.0$ *i.e.* , $\nu = 0.3$, the

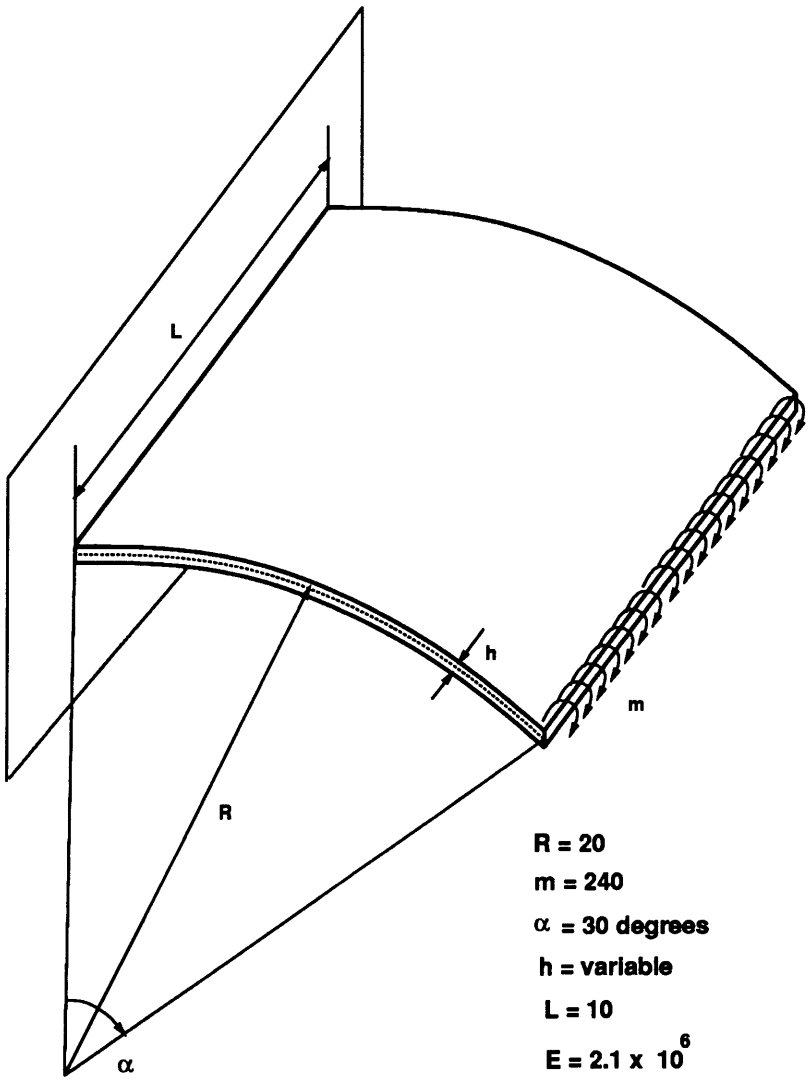

Figure 5-4: Physical model used for curved cantilever

Table 5-2: Summary of results for the curved cantilever problem using 8 and 9 node mixed-interpolated elements. Point A always coincides with an element node.

MESH	h/R	$\theta_{FE} / \theta_{AN}$	
		MITC8	MITC9
	1/100 1/1000 1/100000	0.9998 0.9995 0.9995	0.9995 0.9995 0.9995
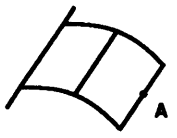	1/100 1/1000 1/100000	1.0001 1.0000 1.0000	1.0000 1.0000 1.0000
	1/100 1/1000 1/100000	0.8958 0.7230 0.0626	0.9956 0.9913 0.9883
	1/100 1/1000 1/100000	0.9996 0.9995 0.9995	0.9995 0.9995 0.9995
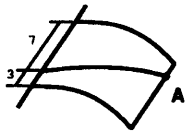	1/100 1/1000 1/100000	0.9999 0.9997 0.9997	0.9995 0.9995 0.9995

same kind of solution accuracy is displayed.

5.3 Analysis of a Pinched Cylinder

The pinched cylinder problem has been widely used to test shell elements. The physical problem is presented in Figure 5-5. Due to symmetry conditions only one octant of the cylinder needs to be considered. In Figure 5-6 we compare the convergence of the vertical displacement under the load for the 16-node displacement based element and the MITC16 element. Uniform meshes have been used and the results are normalized with respect to the analytical solution for this problem reported by Lindberg *et. al.* [49]. We note the poor performance of the 16-node displacement based element with coarse meshes.In Figure 5-7 we show the performance of the MITC elements of various orders and also the performance of elements that have been proposed by other authors. In order to make the comparison more appropriate, we used as the index of mesh refinement the number of nodes per side of the region discretized. Both the heterosis element [50] and the 9-node SRI element (selective reduced integrated element with 2×2 Gauss integration for the shear energy) are shown just for completeness purposes since they do not satisfy our criteria for reliability. The results shown in Figure 5-7 for the heterosis and the 9-node SRI elements were taken from Reference [21]. We notice the excellent performance of the higher–order MITC elements.

As a general comment regarding element comparisons we note that when the difference in predicted response between two elements is small, a conclusive evaluation about the relative predictive capability of the elements is often difficult to make, since usually there are not enough results available for an adequate range of situations. Moreover, when considering mixed–interpolated elements, a particular choice of tying points can be constructed to yield very accurate solutions for a specific problem as discussed in Chapter 3 for the isobeam elements. Therefore individual results should be interpreted with care. However, differences in performance as shown in Figure 5-6 for the 16–node elements

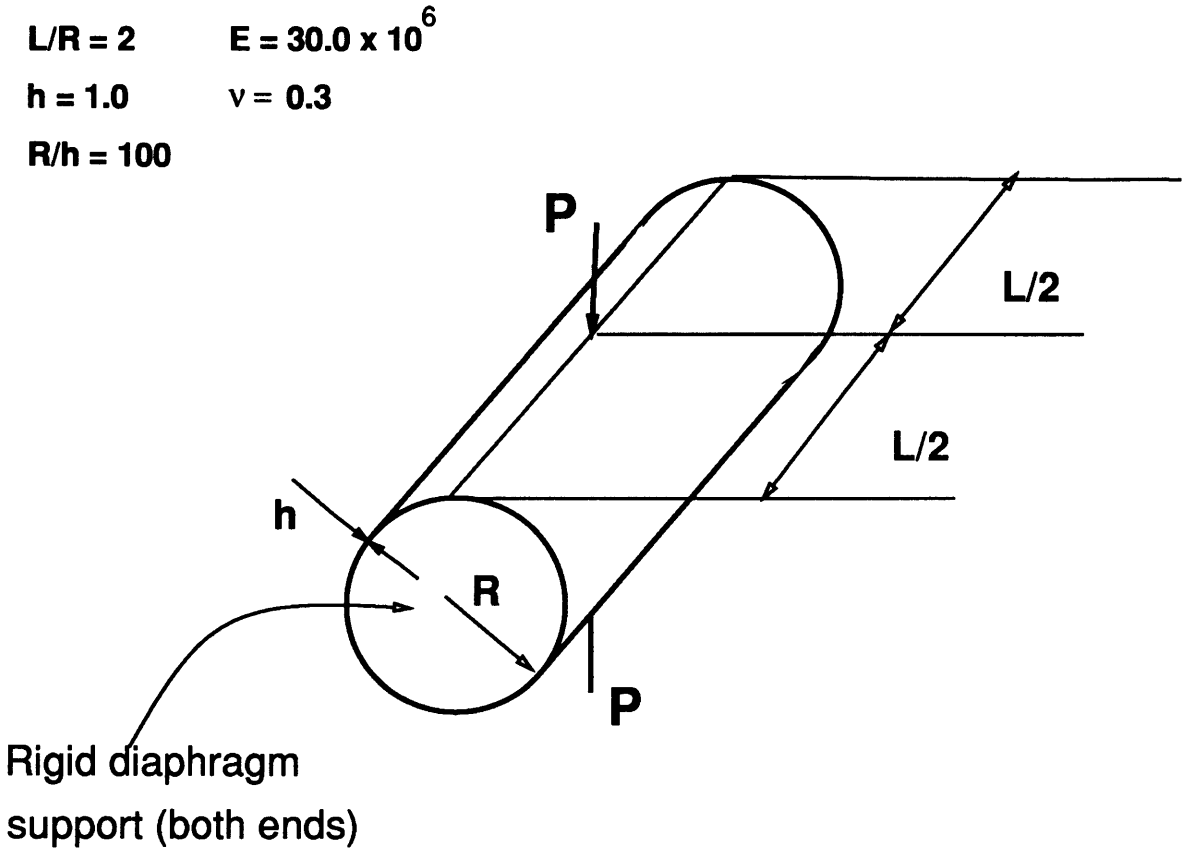

Figure 5-5: Pinched cylinder problem

clearly reveal different behavior due to locking effects and can not be overlooked. This is the kind of improvement in element performance that we have been aiming for in our research.

Another consideration regarding element performance is that the comparative efficiency between elements of different orders depends on the type of response sought. For example, higher–order elements are in general more efficient to predict stresses for problems in which high stress gradients occur. Therefore it is more adequate to compare elements of the same order.

The "Sussman–Bathe" pressure band plots [51] were used to compare stress predictions for the 16-node elements. In figures 5-8 through 5-11 we show pressure band plots

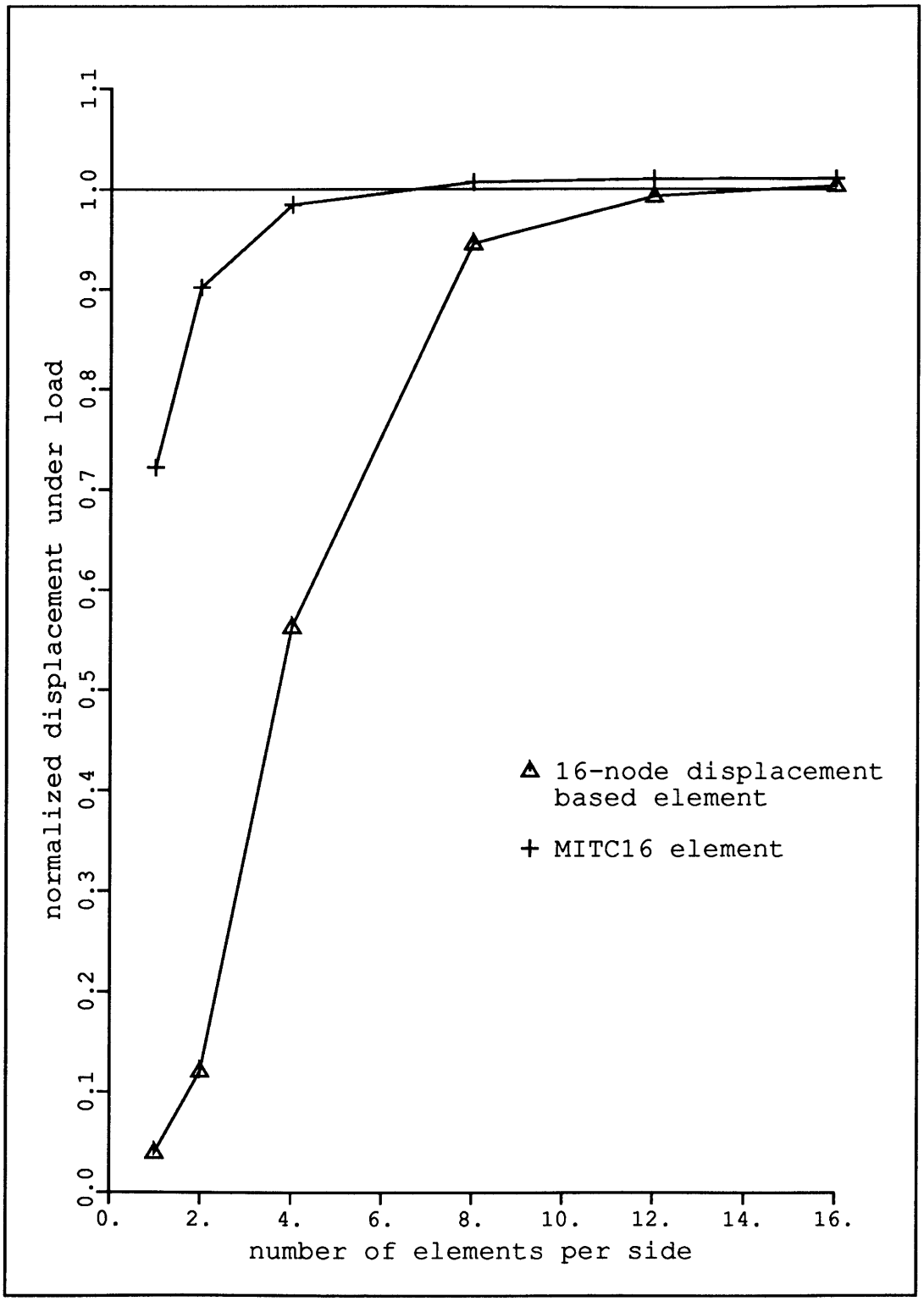

Figure 5-6: Convergence of 16-node shell elements in pinched cylinder problem

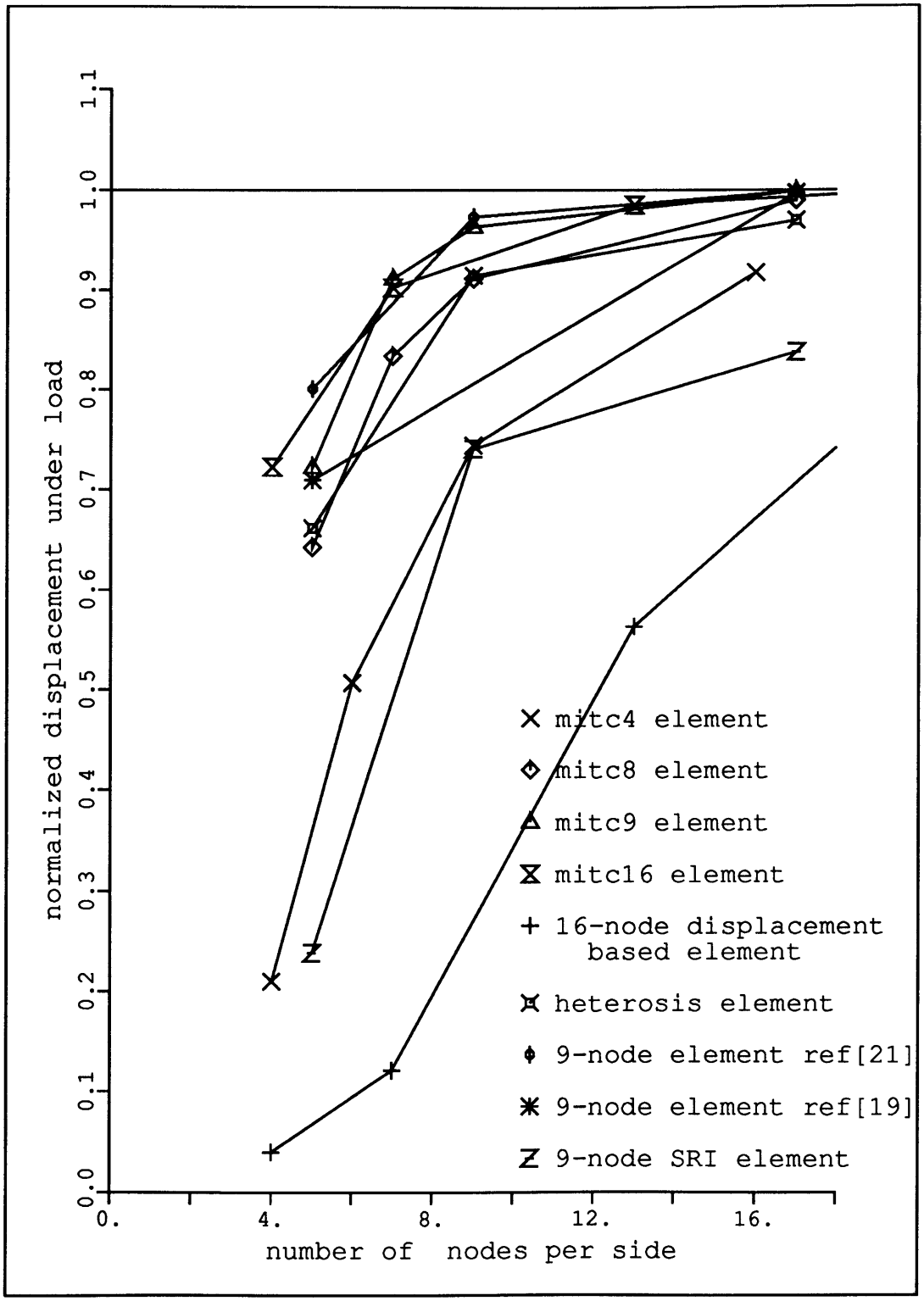

Figure 5-7: Convergence of various shell elements in pinched cylinder problem using uniform meshes.

on the top surface of the cylinder for 4x4 and 8x8 meshes. We can see that using the MITC16 element, the 4x4 mesh already captures most of the stress behavior, whereas for the 16-node displacement based element the 4x4 mesh is unable to show a distinguishable band pattern displaying large regions of discontinuity. Using this element the 8x8 mesh is required to obtain a reasonably accurate prediction of stresses.

5.4 Analysis of a Hemispherical Shell

The hemispherical shell subjected to self–equilibrating concentrated loads has been used as a benchmark problem for the analysis of doubly curved shells. The hemispherical shell that we analyzed has an 18–degree cut–out on its top and it is free on both bottom and top edges. Only one quarter of the shell needs to be considered and a particular discretization is shown in Figure 5-12.

The convergence for the displacement under the load is shown in Figure 5-13 for the cubic elements. Again the superior performance of the MITC16 element over its displacement based counterpart is noted. In Figure 5-14 we show the performance of the MITC9 element compared with the 9-node element proposed by Huang and Hinton [19]. We notice the excellent performance of the MITC9 element.

A theoretical lower bound for the displacements under the load was derived by Morley and Morris [52] for the hemispherical shell without the cut–out and it is equal to 0.0924. We used for the normalization of our results the value 0.09355 which corresponds to the converged solution when using the MITC16 element.

5.5 Plate Bending Analysis with the MITC Shell Elements

The MITC9 and MITC16 elements that we have formulated for general shell analysis do not degenerate to the corresponding MITC plate bending elements of Chapter 2, when

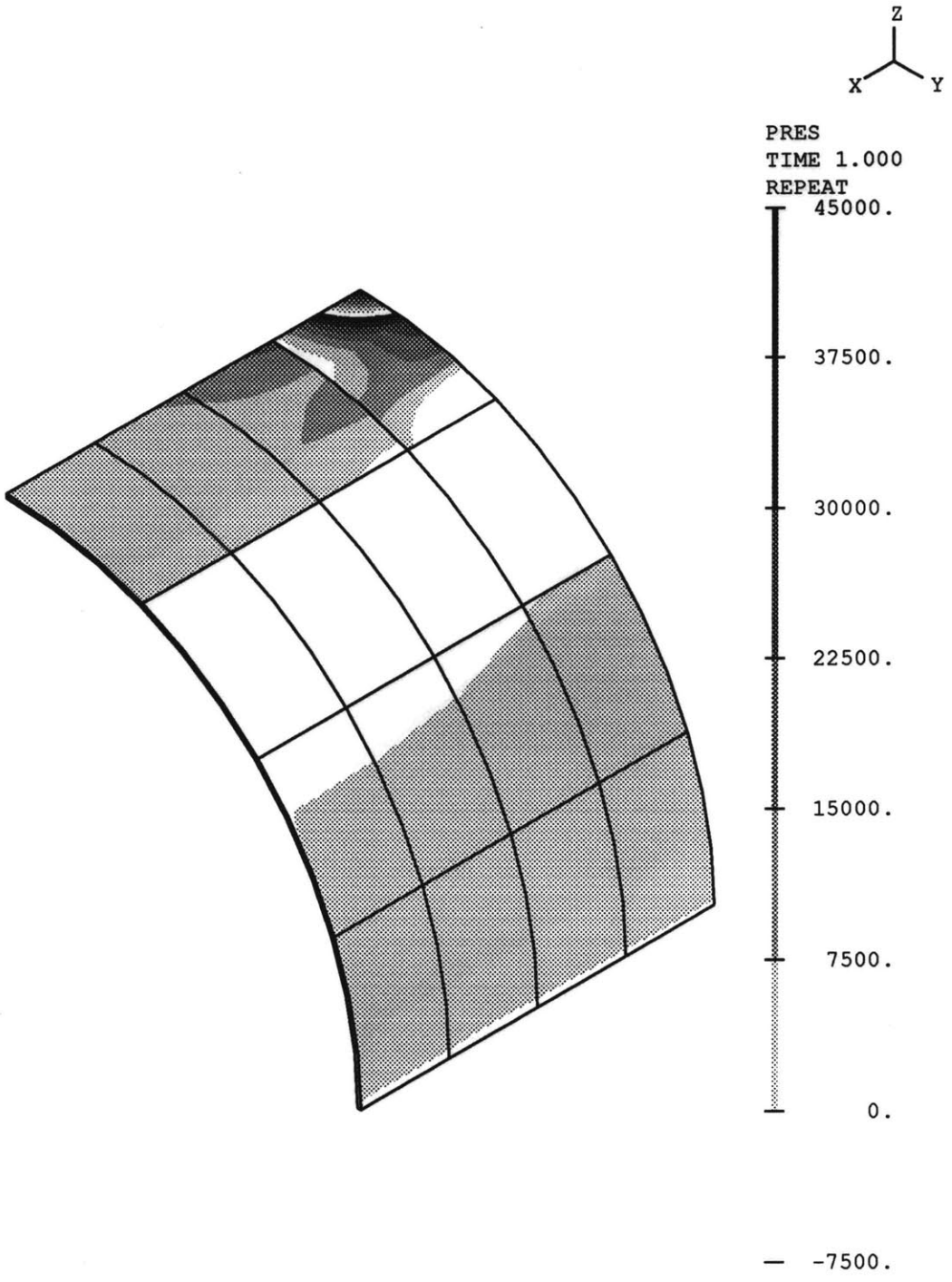

Figure 5-8: Pressure band plot in analysis of pinched cylinder problem. Uniform 4×4 mesh of 16-node displacement based elements

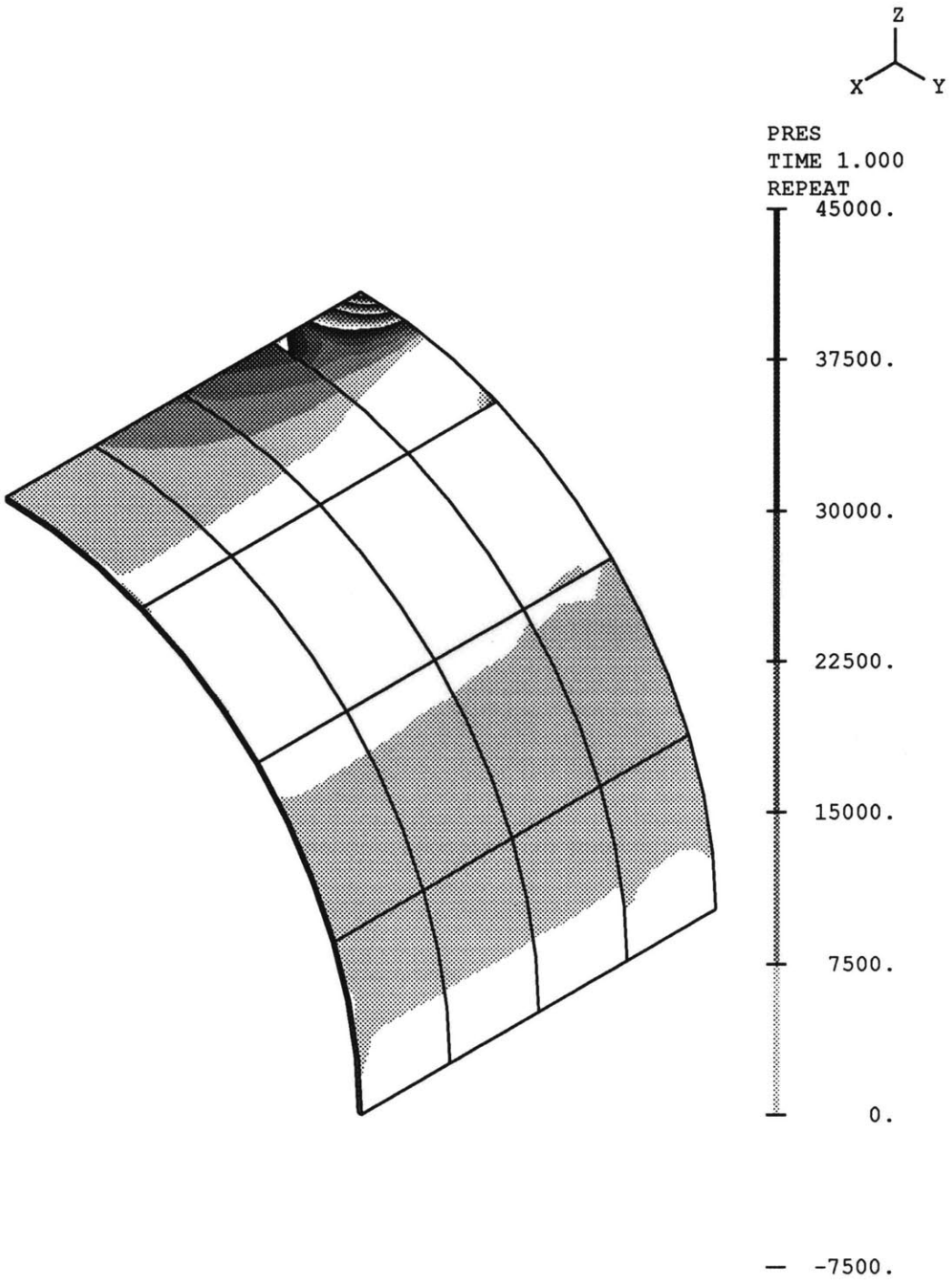

Figure 5-9: Pressure band plot in analysis of pinched cylinder problem. Uniform 4×4 mesh of MITC16 elements

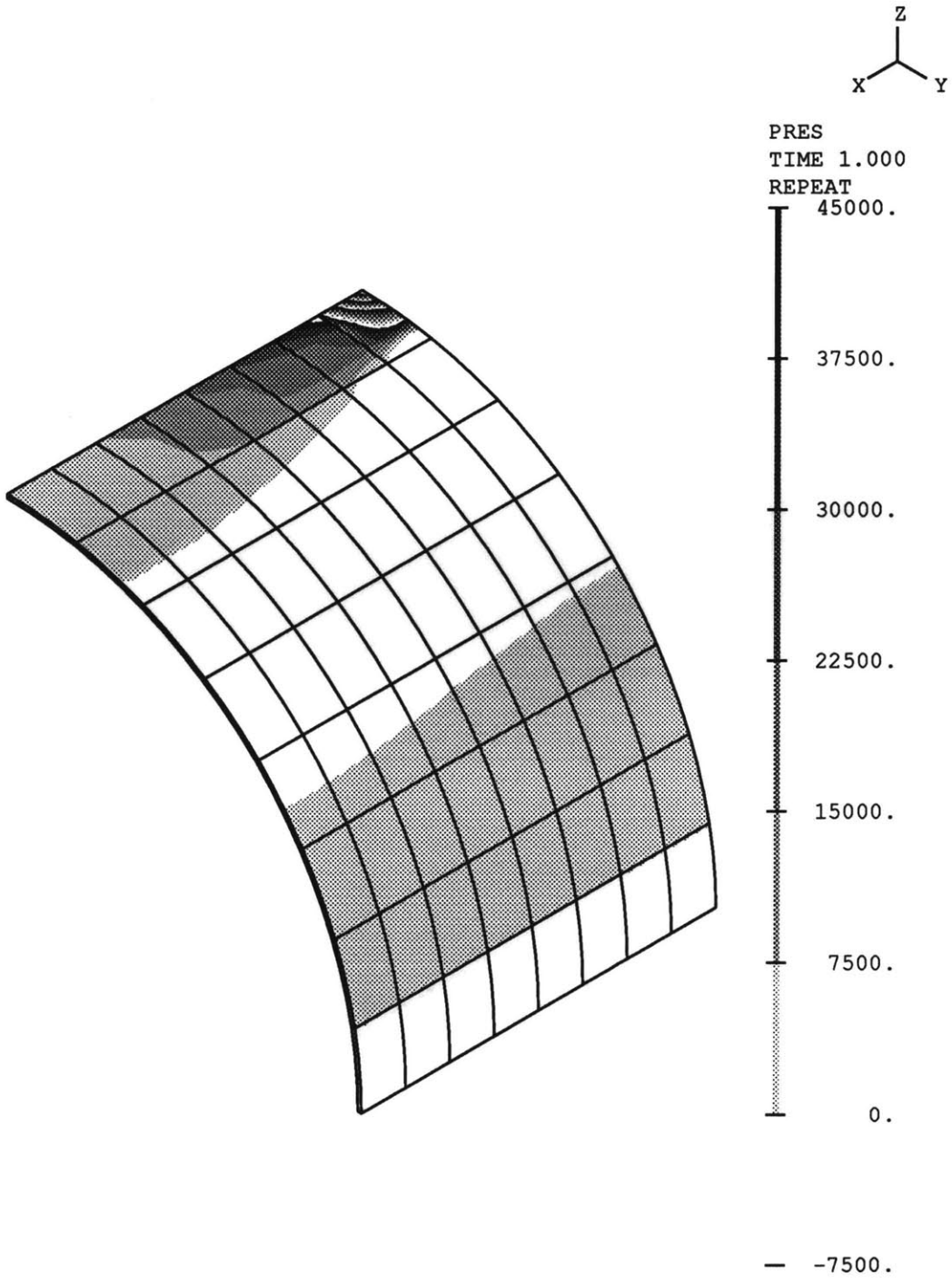

Figure 5-10: Pressure band plot in analysis of pinched cylinder problem. Uniform 8×8 mesh of 16-node displacement based elements

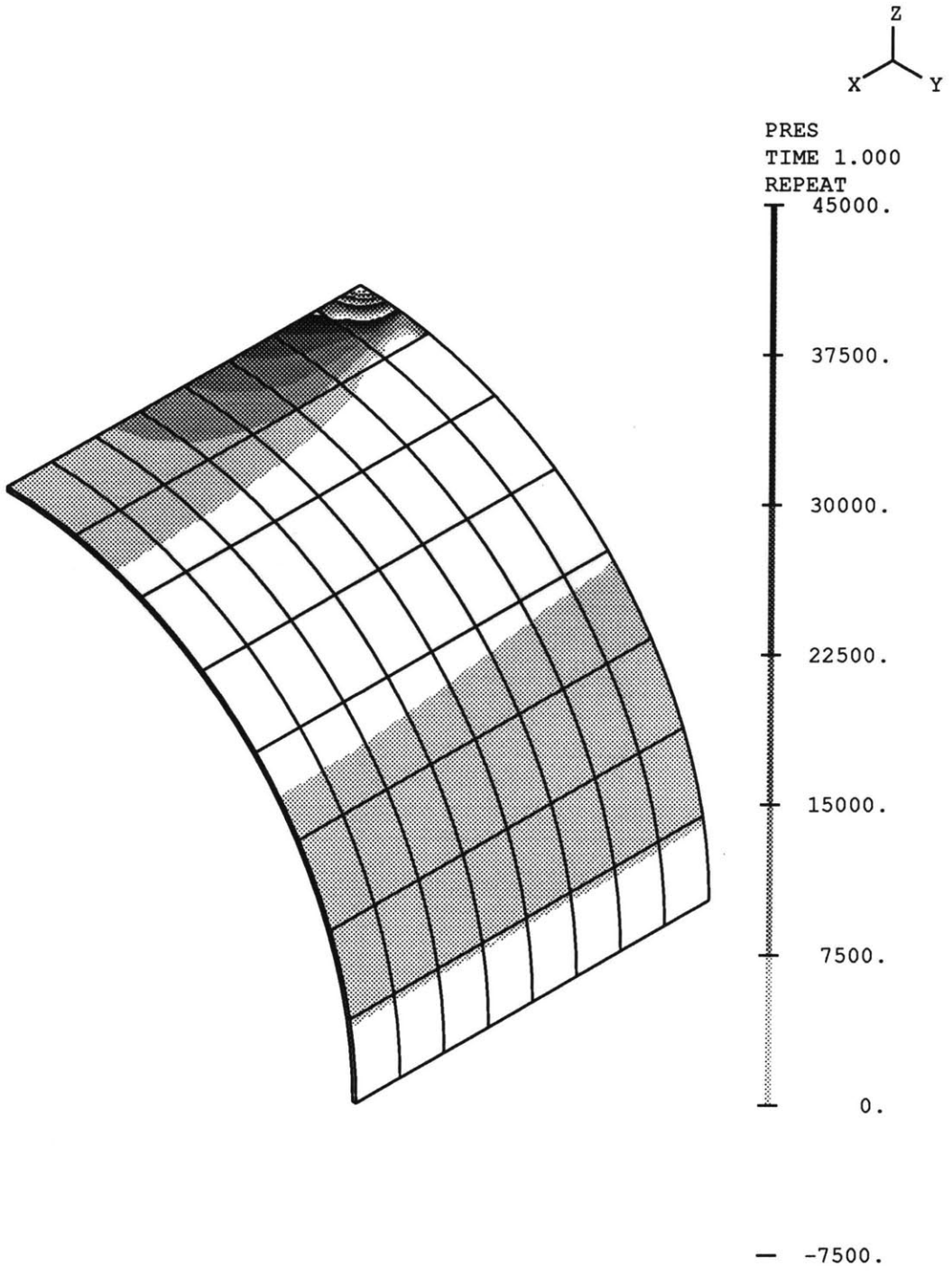

Figure 5-11: Pressure band plot in analysis of pinched cylinder problem. Uniform 8×8 mesh of MITC16 elements

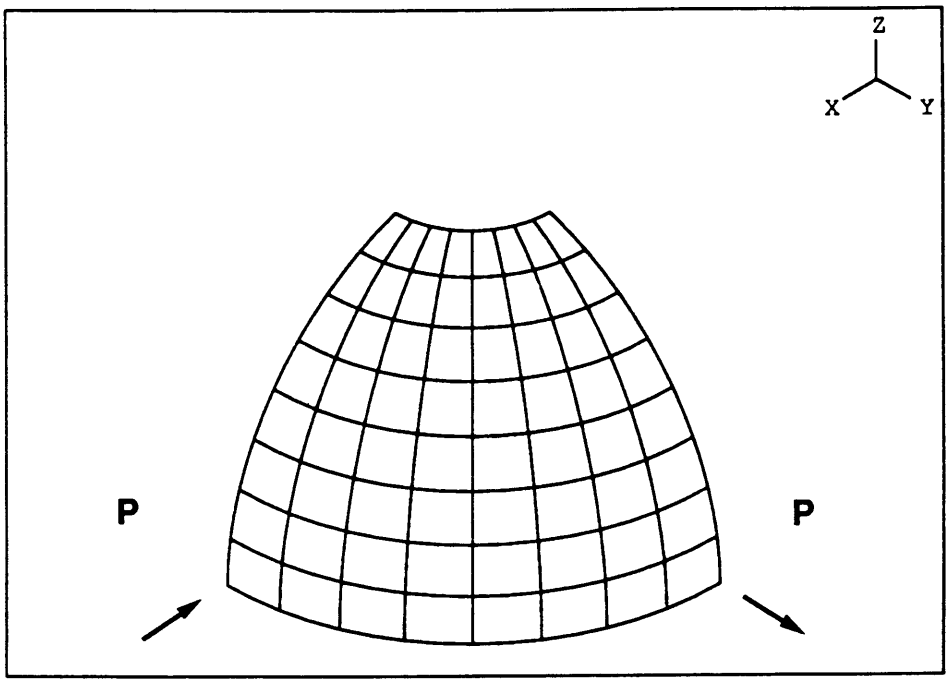

Figure 5-12: Typical finite element discretization for analysis of hemispherical shell (8×8 mesh). Radius=10.0, thickness=0.04, $E = 6.825 \times 10^7$, $\nu = 0.3$ and $P = 1.0$

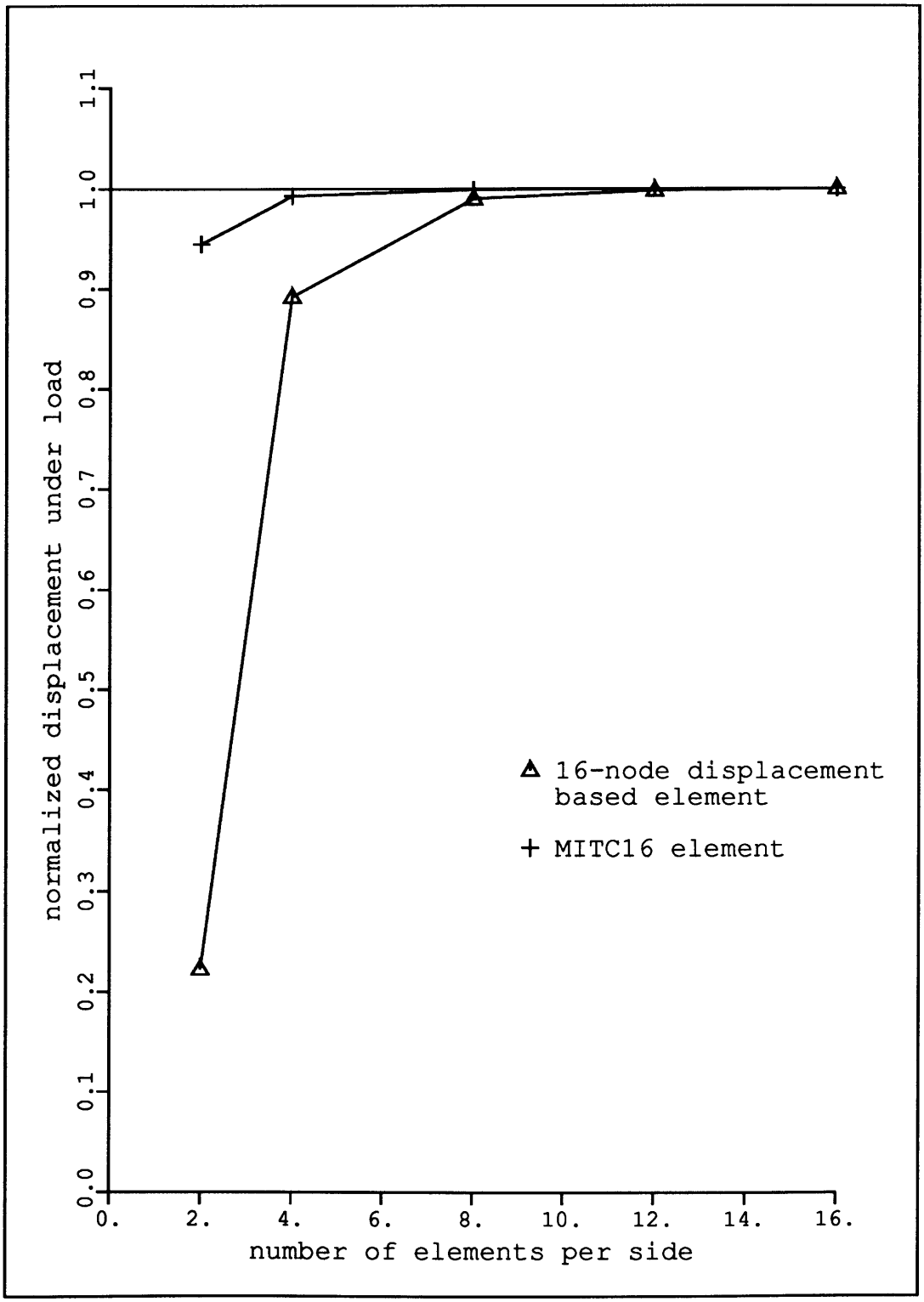

Figure 5-13: Convergence in analysis of hemispherical shell, cubic elements

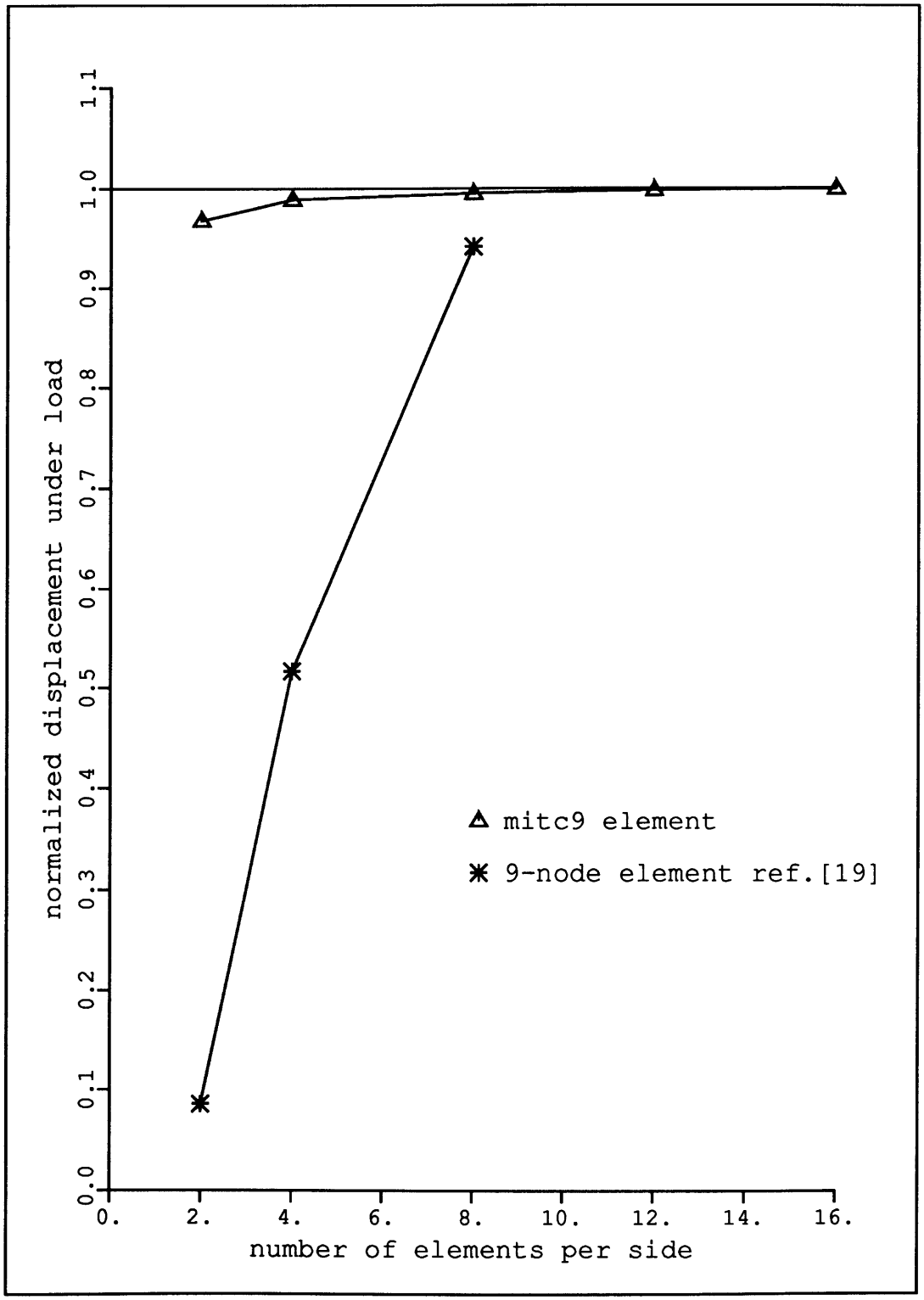

Figure 5-14: Convergence in analysis of hemispherical shell, 9-node elements

the shell is flat, the analysis is linear and the plate is subjected to transverse loading only.

The first reason is the fact that for the plate bending elements the in–layer strains (in this case just the bending strains) are not mixed–interpolated.

The other two reasons are:

1. For the plate bending elements different interpolation fields are used for the section rotations and the section transverse displacement. This requires different sets of nodal degrees of freedom for the rotations and the transverse displacement.

2. The assumed transverse shear strain fields for the plate bending elements involved not only point tying conditions but also integral tying conditions.

The construction of shell elements that degenerate to the plate bending elements would, therefore, involve different sets of nodal degrees of freedom for rotations and displacements. Such elements, however, are not as easy to use in engineering practice. Another requirement would be the enforcement of integral tying conditions for the assumed transverse shear strain fields. Integral tying conditions are expensive, in terms of computational effort, and tend to make an element inefficient.

Our choice, in formulating shell elements, was to use the same set of nodal degrees of freedom for both rotations and displacements. Also, integral tying conditions were not used for the transverse shear strain fields.

One additional consideration that supports our choice is that the MITC plate bending elements are designed to take into account the known nature of the Reissner–Mindlin plate bending mathematical model. When considering general curved shells the mathematical model is quite different, and it is not likely that the optimal choice of assumed transverse shear strain fields would be the same as for the plate model.

The idea of replacing the integral tying conditions by additional point tying conditions such that the integral tying requirements are approximately satisfied was first explored in the context of plate analysis for the MITC9 plate element by Bathe *et. al.* [38]. This

approach, of course, reduces the cost and complexity of the element at the expense of losing some accuracy [33].

It turned out that, if we use for the transverse shear strain assumptions of the MITC9 shell element the simplified scheme of the MITC9 plate element abovementioned, we would have to delete the degrees of freedom for displacements at the center node, as in the plate bending element, otherwise a spurious zero energy mode would arise.

For the MITC16 element, an attempt to formulate point tying schemes that would replace the integral tying conditions and preserve the functional form of the assumed transverse shear strain fields was unsuccessful.

In the following we present the solutions of sample problems in which the MITC9 and the MITC16 shell elements are used to model plate bending situations. Of course, we do not expect that the mixed–interpolated shell elements would behave as well as the MITC plate bending elements in these particular analyses, but we do expect and require that shear locking is not present and that the elements display a good predictive capability.

In the numerical solutions of the circular plate and the skew plate we distinguish between two "types" of MITC9/MITC16 elements. We refer to the "MITC9/MITC16 plate" elements as the ones that have been formulated for plate analysis and fully comply with the mathematical theory of the MITC plate bending elements (see Chapter 2) and we refer to the elements presented in Section 4.2 as the "MITC9/MITC16 shell" elements.

5.5.1 Analysis of a Circular Plate

We consider the transverse shear stress predictions for simply supported and clamped circular plates subjected to uniform pressure. The transverse shear stresses are often the most difficult stress components to predict with Reissner–Mindlin plate elements. The circular plate problems that we consider are very suitable to assess the element performance regarding transverse shear stresses because the analytical solution is known, there is no boundary layer and the elements are naturally distorted to model the problem geometry (see Figure 2-13).

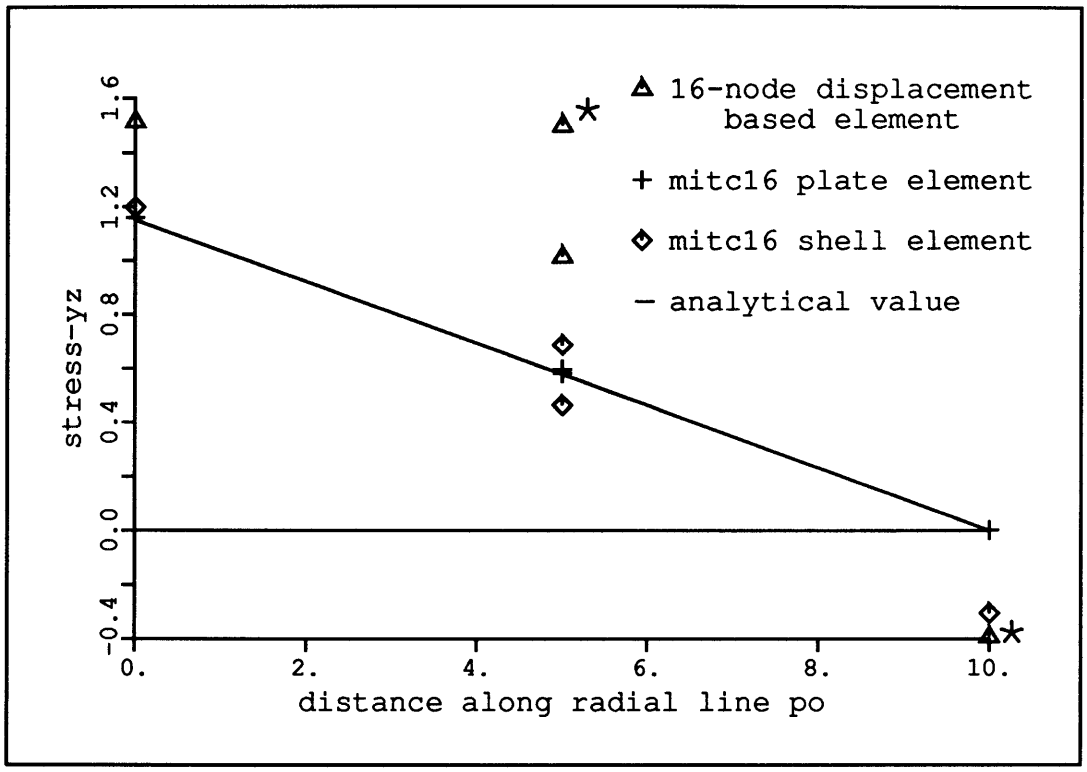

Figure 5-15: Shear stress predictions for analysis of simply supported circular plate, diameter/thickness = 100. The results marked with a star (*) are actually outside the figure.

Actually we considered these problems in Chapter 2 and the finite element models used are described in Figure 2-13. The stresses are calculated in the same way and at the same locations as described in details in Section 2.3.

Figure 5-15 shows the calculated stresses as obtained for Mesh 1 of Figure 2-13 using the MITC16 plate and shell elements and the usual 16-node displacement based element.

We note that the solution is very accurate using the MITC16 plate element with only three elements. On the other hand, the displacement based element does not give an accurate transverse shear stress prediction unless a very fine mesh is employed (see Section 2.3). The MITC16 shell element is not as accurate as the MITC16 plate element, as expected, but it provides good stress predictions considering that the mesh used is quite coarse.

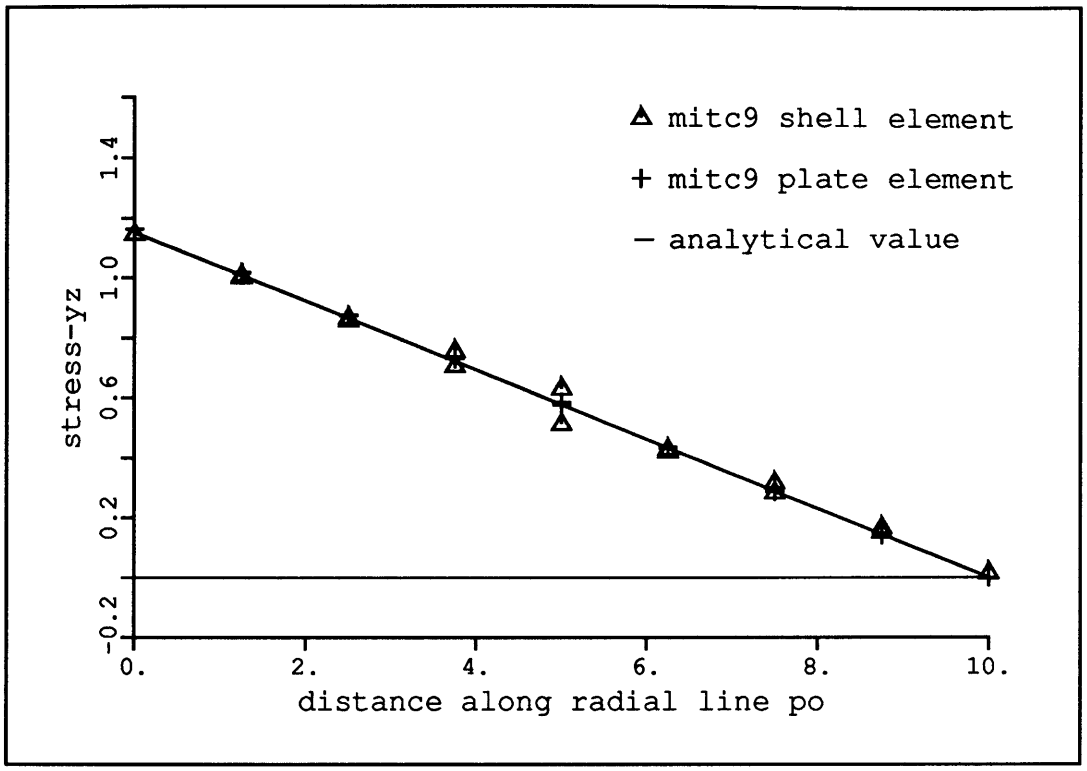

Figure 5-16: Shear stress predictions for analysis of clamped circular plate, diameter/thickness = 100.

Figure 5-16 presents the same type of shear stress results using Mesh 3 of Figure 2-13 and the MITC9 plate and shell elements. A similar behavior as noted for the 16–node elements is encountered.

5.5.2 Analysis of a Skew Plate

The Morley skew plate problem has also been used as a test problem for plate/shell elements. The problem is described in Figure 5-17. The simply supported edges are modeled using the appropriate soft boundary conditions *i.e.*, just the vertical displacement is constrained [43]. The convergence of the vertical displacement at point E is shown in Figure 5-18 for the cubic elements and in Figure 5-19 for the quadratic elements. A uniform skew mesh topology has been used (the 2x2 mesh is shown in Figure 5-17). The

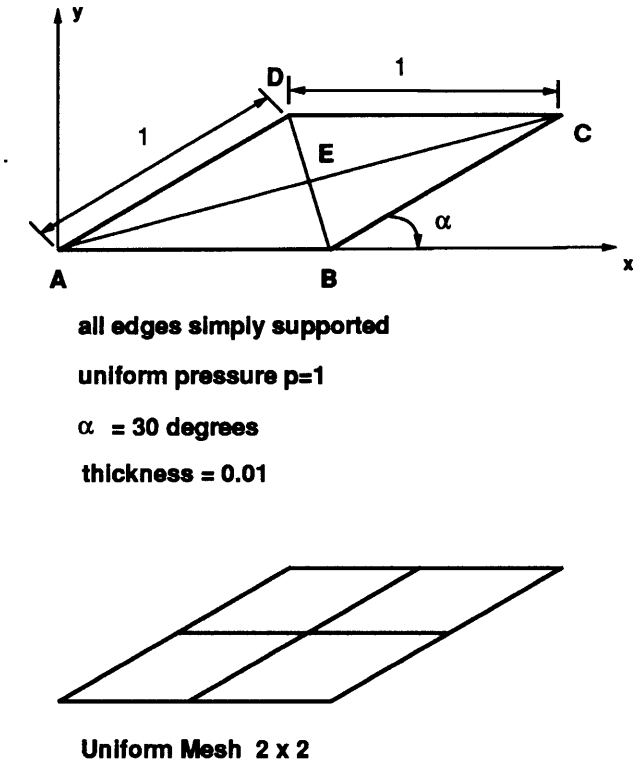

Figure 5-17: Morley skew plate problem and typical finite element mesh used

results are normalized with respect to the analytical solution derived by Morley [53]. It is noted that a rather large number of elements need to be used to obtain an accurate solution. However, in the analysis uniform meshes were employed, much less elements could be used with graded meshes.

The same trend as observed in the analysis of the circular plate is displayed for the skew plate. The MITC plate elements perform best but the shell elements also behave well. The MITC16 shell element shows a considerable improvement in response prediction when compared to the displacement based element and the MITC9 shell element shows better results than the MITC8 element which is a reasonable performer for this case.

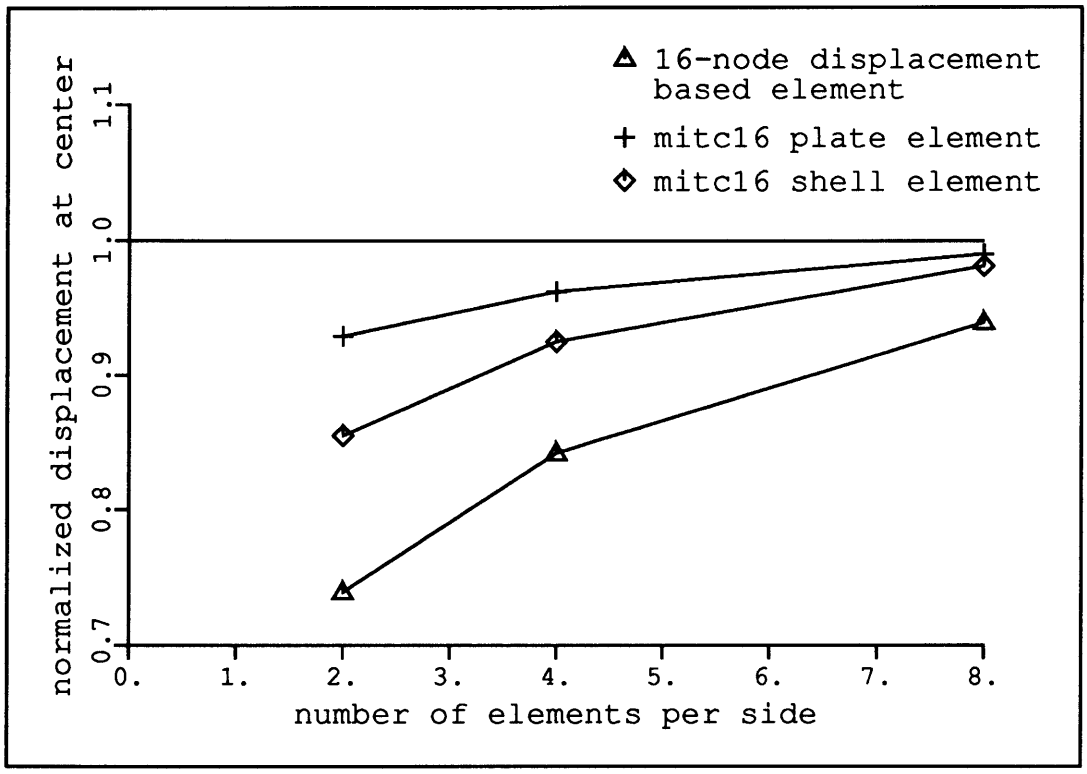

Figure 5-18: Convergence of center displacement for cubic elements in analysis of the Morley skew plate

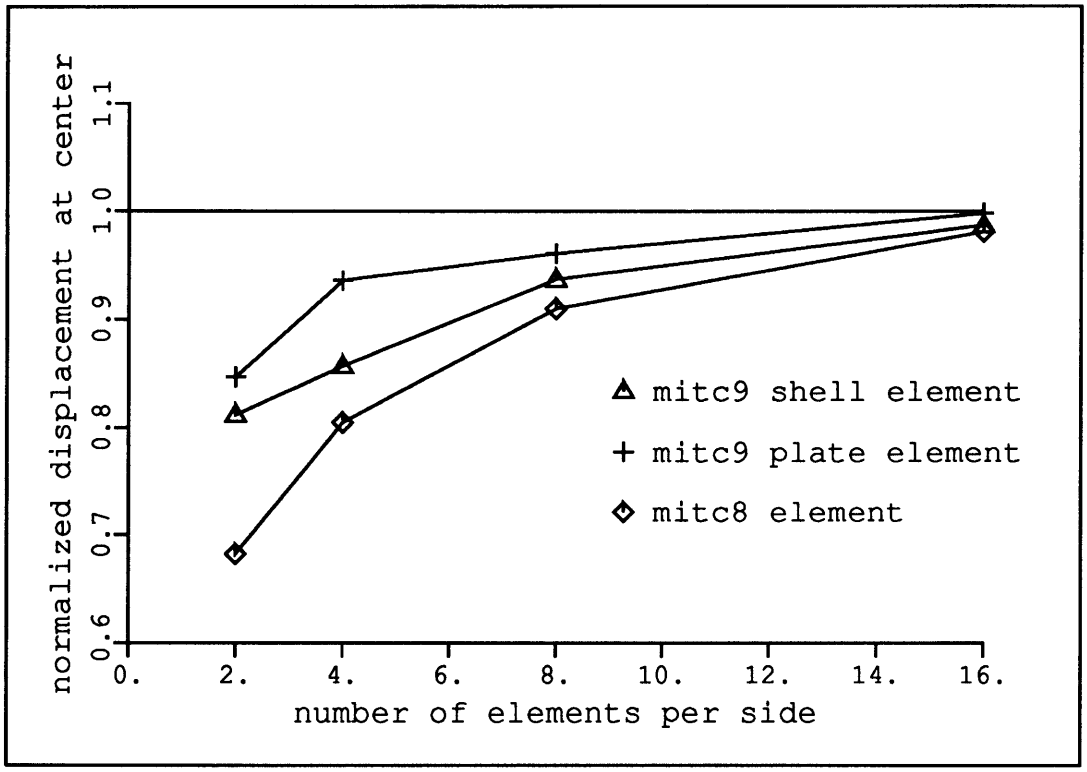

Figure 5-19: Convergence of center displacement for quadratic elements in analysis of the Morley skew plate

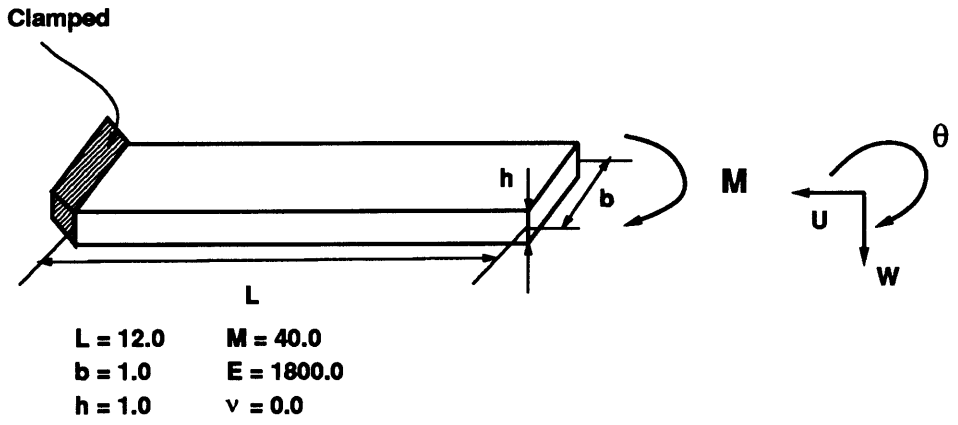

Figure 5-20: Physical model used for nonlinear analysis of a cantilever

5.6 Large Displacement Analysis of a Cantilever

We consider the large displacement analysis of the cantilever described in Figure 5-20. Only one 16-node element is used to model the cantilever and in Figure 5-21 the deformed configurations corresponding to an intermediate and final time steps are shown for the solution obtained with the MITC16 element. In Figure 5-22 the displacement and rotation ratios at the tip of the cantilever are compared with the analytical solutions for the 16-node displacement based element and analogously, in Figure 5-23, for the MITC16 element. We note that the 16-node displacement based element is not able to predict all the nonlinear response of the cantilever since after time step 18 (a total of 20 equally spaced time steps were used) convergence could not be reached. The MITC16 is able to describe all the response and we notice that for the last few time steps it presented a much smaller deviation from the analytical solution than its displacement based counterpart.

5.7 Snap-Through of a Shallow Spherical Cap

We analyzed a shallow spherical cap subjected to a concentrated loading. The physical model considered is shown in Figure 5-24. Using a load displacement control method [54] we obtained the complete nonlinear response of the shell including the snap-through

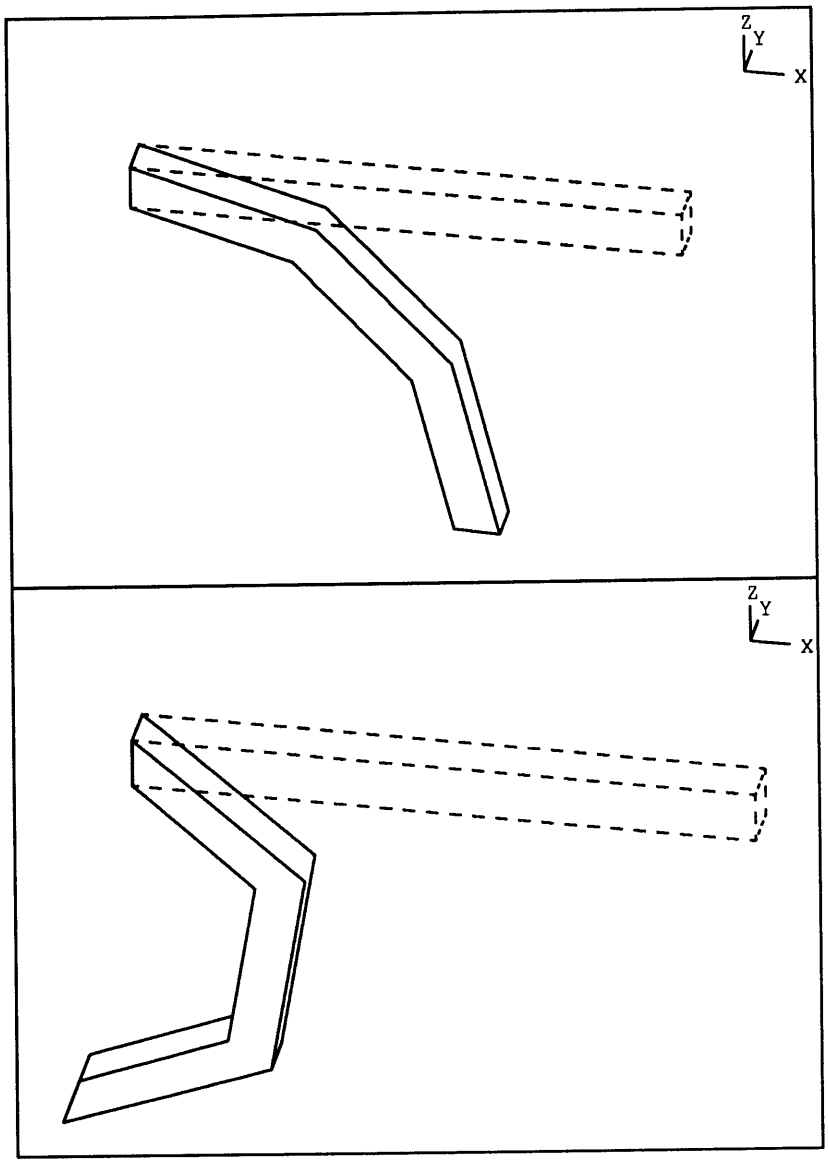

Figure 5-21: Deformed and undeformed meshes for half and total loading in nonlinear analysis of cantilever. The "kinks" in the geometry of the deformed beam is due only to the plotting program used

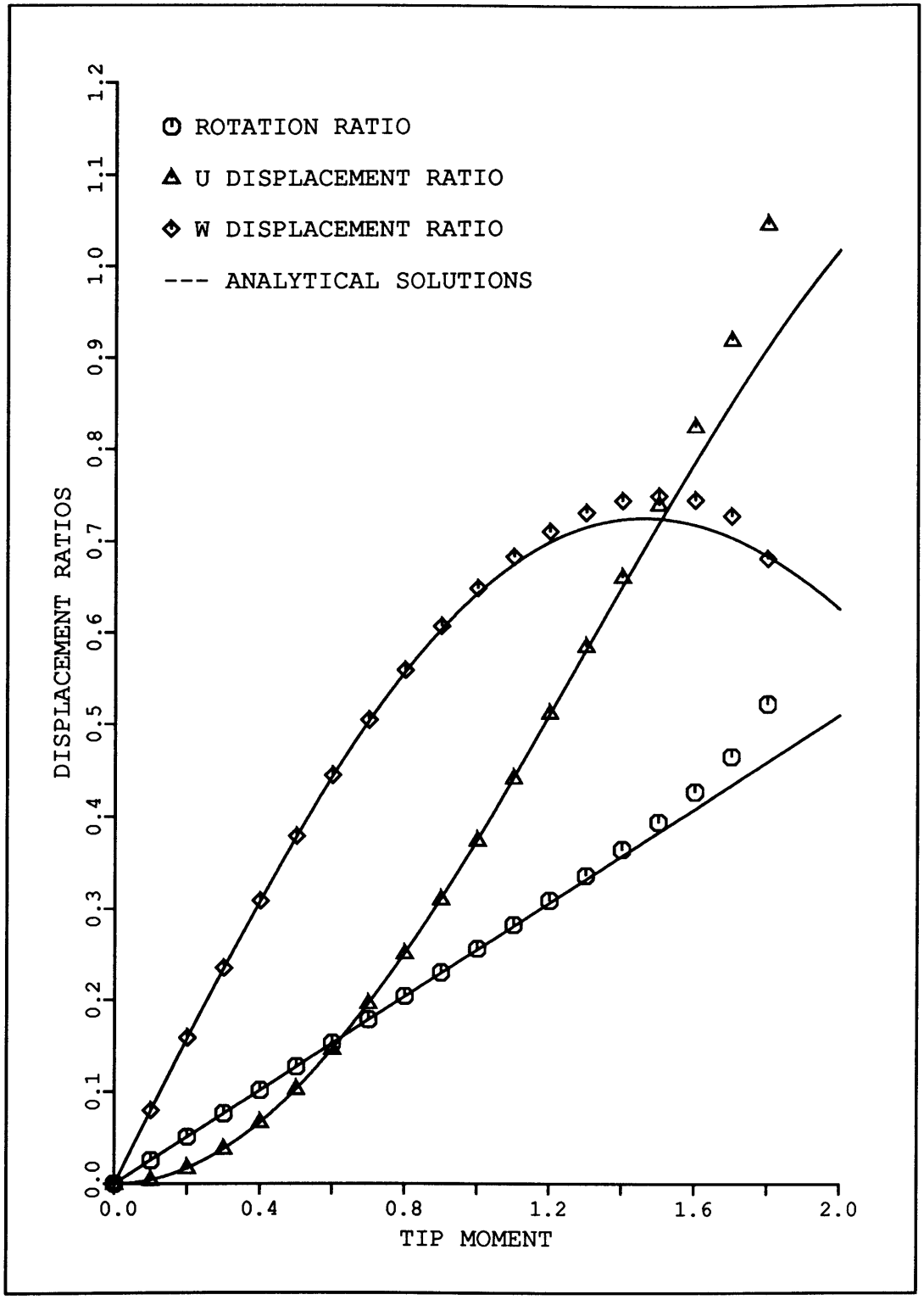

Figure 5-22: Nonlinear response of a cantilever subjected to pure bending moment using one 16-node displacement based element. The displacement ratios are defined as: U displacement ratio $= U/L$, W displacement ratio $= W/L$ and rotation ratio $= \theta/2\pi$

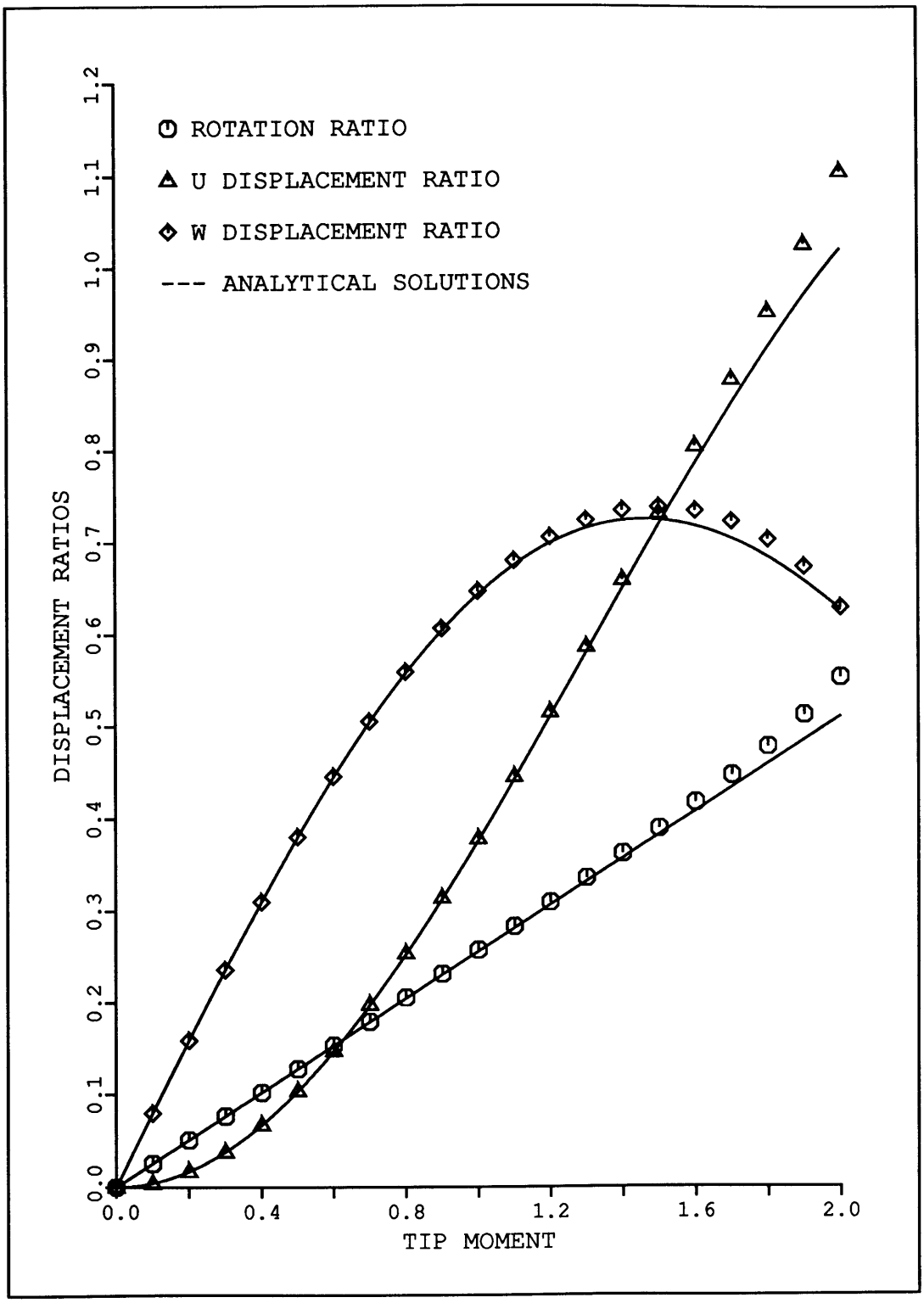

Figure 5-23: Nonlinear response of a cantilever subjected to pure bending moment using one MITC16 element. The displacement ratios are defined as: U displacement ratio $= U/L$, W displacement ratio $= W/L$ and rotation ratio $= \theta/2\pi$

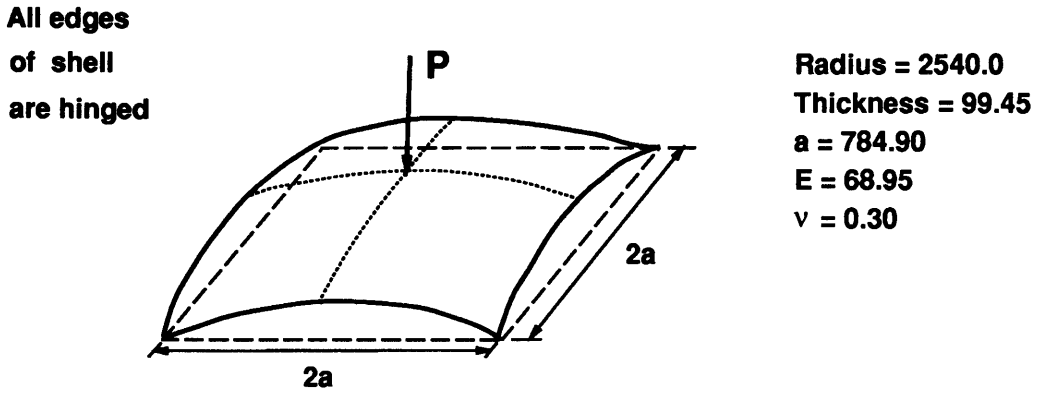

Figure 5-24: Physical model used for analysis of spherical cap. One quarter of the shell is discretized.

response. Due to symmetry conditions only one quarter of the shell needs to be discretized and we used meshes of one and four 16-node elements.

Figures 5-25 and 5-26 show the central deflection plotted against the load for the results obtained with the 16-node displacement based element and with the MITC16 element. The solution reported by Leicester [55] using a semi-analytical approach is also shown, just as an additional solution, since it has approximations of its own and should not be regarded as the solution of the mathematical model of the problem in consideration.

We note that the solutions obtained with the MITC16 element using the one and four element meshes are quite close to each other in contrast to the solutions obtained with the 16-node displacement based element (Figure 5-25). We also note that the 16-node displacement based solution with four elements is close to the solutions obtained with the MITC16 element. Hence, we can conclude that for the 16-node displacement based element at least a four element mesh is required whereas with the MITC16 element a good response prediction is already obtained with using just one element for a quarter of the structure.

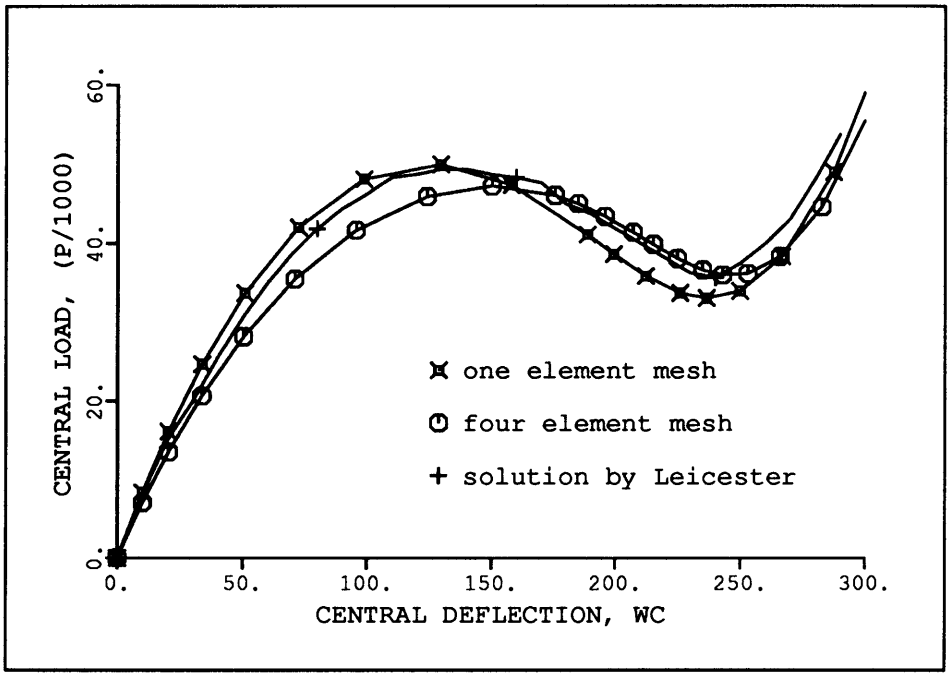

Figure 5-25: Nonlinear response of a shallow spherical cap subjected to concentrated load using the 16-node displacement based element

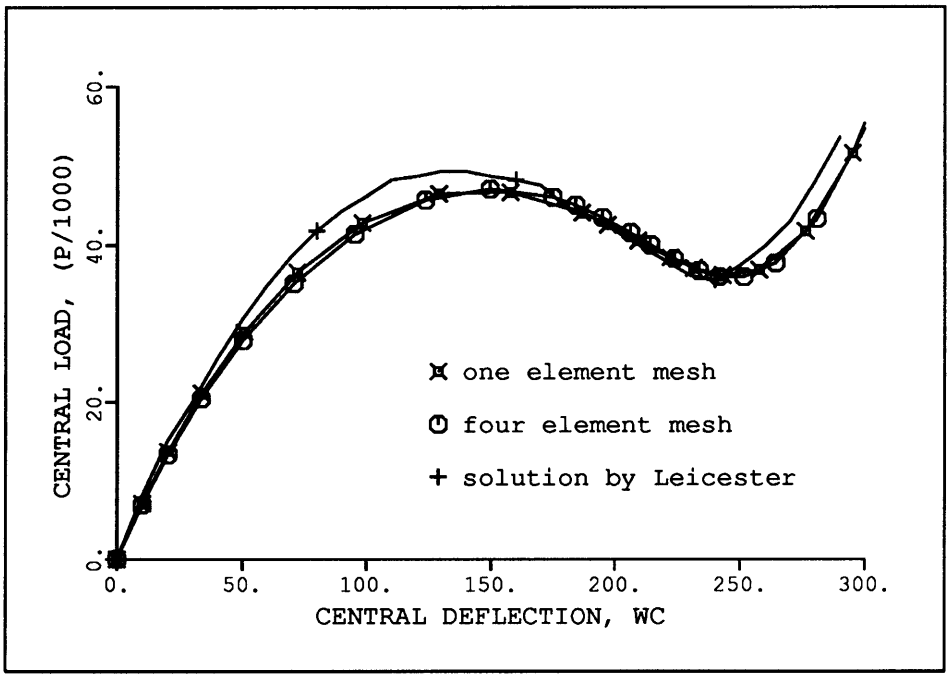

Figure 5-26: Nonlinear response of a shallow spherical cap subjected to concentrated load using the MITC16 element

Chapter 6

Concluding Remarks

In the next section we briefly summarize what has been accomplished in this thesis and in Section 6.2 we mention two interesting research topics that would complement this work.

6.1 Conclusions

We presented in this thesis the development of higher–order plate bending and general nonlinear shell finite elements. The motivations behind these developments, as discussed earlier in this work, are to formulate reliable and effective plate/shell finite elements that can be used confidently in engineering practice.

The starting point of our work was the study, development and numerical assessment of a family of Reissner–Mindlin mixed-interpolated plate bending elements. These elements have a distinctive feature that separates them from the other plate bending elements that appeared in the literature. They possess a mathematical theory that guarantees the convergence of the discretizations with optimal error bounds even in the limit case when the thickness tends to zero.

Although the mathematical analysis is very important, the numerical assessment of the behavior of the elements is also of interest. We numerically studied the convergence

properties of the elements not only for special problems in which most of the requirements of the mathematical theory are fulfilled, but also for more practical engineering problems. The theoretical predictions were confirmed and the elements displayed high predictive capabilities. The behavior of the elements for mesh topologies that included distorted elements was truly good.

The transverse shear stress predictions were very accurate for all problems considered. This is an important asset for the plate elements since these stress components are difficult to predict and their optimality is still not assured by the mathematical analysis.

In summary, the MITC plate bending elements are reliable and effective and their use is recommended for practical applications.

Membrane and shear locking of curved elements were studied in the context of isoparametric beam elements. Using a particular problem, a series of analytical and numerical studies were performed. In this setting the nature of the locking phenomenon was identified and insight was gained on how the mixed interpolation of tensorial components approach prevents locking.

A mathematical theory as the one for the plate bending problem is not available for the discretizations of general shells. Therefore a set of requirements to ensure reliability of the element formulations was discussed.

Two new higher–order mixed–interpolated general shell elements for nonlinear analysis were proposed. An interpolation scheme for the covariant strain components both for shear and membrane actions was developed and used to formulate the elements. The newly developed elements do not exhibit either shear or membrane locking and were tested in a number of important problems displaying a very good performance. The objective, set in the early stages of this research, of developing a 16–node mixed element that would replace the usual displacement based element was fully accomplished. The MITC16 element presents a substantial improvement in performance when compared with the 16-node displacement based element.

Both the MITC9 and MITC16 elements do satisfy our criteria for reliability and

together with the MITC4 and MITC8 elements that have been previously developed form a family of general nonlinear shell elements that can be recommended for use in engineering practice.

6.2 Suggestions for Future Research

As mentioned before a mathematical analysis as the one discussed for the MITC plate bending elements is not available for the general mixed interpolated shell elements. The development of such mathematical theory would be very valuable and could enlighten how optimal assumed strain fields should be constructed.

Mixed–interpolated triangular general shell elements have not yet been proposed. Their development would constitute an interesting research area. However, we remark that the MITC plate bending triangular elements were not as efficient as the quadrilateral elements. This is not unusual and we might expect that the same would occur in shell analysis. Nevertheless, it is convenient as a modelling option to have reliable triangular elements available.

References

[1] A. Noor et al., editors. *Analytical and Computational Models of Shells.* ASME Special Publication, 1989. CED–3.

[2] K. J. Bathe and E. Dvorkin. A formulation of general shell elements — the use of mixed interpolation of tensorial components. *International Journal for Numerical Methods in Engineering*, 22:697–722, 1986.

[3] A. E. H. Love. The small free vibrations and deformation of a thin elastic shell. *Phil. Trans. Roy. Soc. London*, (Ser. A 179):491–546, 1888.

[4] W. T. Koiter. A consistent first approximation in general theory of thin elastic shells. In *Proc. IUTAM Symposium on the theory of thin elastic shells*, pages 12–33, Delft, 1959.

[5] Sanders, J. L. Jr. An improved first approximation theory for thin shells. Tech. Report R-24, Nasa, 1959.

[6] H. Kardestuncer, editor. *Finite Element Handbook.* MacGraw-Hill, 1987.

[7] S. Ahmad, B. M. Irons, and O. C. Zienkiewicz. Analysis of thick and thin shell structures by curved finite elements. *International Journal for Numerical Methods in Engineering*, 2:419–451, 1970.

[8] E. Ramm. A plate/shell element for large deflections and rotations. In K. J. Bathe, editor, *Formulations and Computational Algorithms in Finite Element Analysis.* M.I.T. press, 1977.

[9] K. J. Bathe and S. Bolourchi. A geometric and material nonlinear plate and shell element. *Computers & Structures*, 11:23–48, 1979.

[10] K. J. Bathe. *Finite Element Procedures in Engineering Analysis.* Prentice-Hall, Inc., Englewood Cliffs, 1982. 2nd edition 1993.

[11] O. C. Zienkiewicz, R. L. Taylor, and J. M. Too. Reduced integration techniques in general analysis of plates and shells. *International Journal for Numerical Methods in Engineering*, 3:275–290, 1971.

[12] E. Onate, E. Hinton, and N. Glover. Techniques for improving the performance of the Ahmad shell elements. In E. Alarcon and C. A. Brebbia, editors, *Procceedings of the 2nd International Conference on Applied Numerical Modelling*, pages 389–399, Madrid, 1978. Pentech Press.

[13] T. J. R. Hughes, M. Cohen, and M. Haroun. Reduced and selective integration techniques in the finite element analysis of plates. *Nuclear Engineering Design*, 46:203–222, 1978.

[14] D. S. Malkus and T. J. Hughes. Mixed finite element methods. reduced and selective integration techniques: a unification of concepts. *Computer Methods in Applied Mechanics and Engineering*, 15:63–81, 1978.

[15] M. Bercovier. Perturbation of a mixed variational problems, applications to mixed finite element methods. *R.A.I.R.O. Anal. Numer.*, 12:211–236, 1978.

[16] T. Belytschko, W.-K. Liu, S.-J. Ong, and D. Lam. Implementation and application of a 9-node Lagrange shell element with spurious mode control. *Computers & Structures*, 20(1-3):121–128, 1985.

[17] T. Belytschko, S. J. Ong, and W. K. Liu. A consistent control of spurious singular modes in the 9-node Lagrangian element for the Laplace and Mindlin plate equations. *Computer Methods in Applied Mechanics and Engineering*, 44:269–295, 1985.

[18] E. Dvorkin and K. J. Bathe. A continuum mechanics based four-node shell element for general nonlinear analysis. *Engineering Computations*, 1:77–88, 1984.

[19] H. C. Huang and E. Hinton. A new nine node degenerated shell element with enhanced membrane and shear interpolation. *International Journal for Numerical Methods in Engineering*, 22:73–92, 1986.

[20] K. C. Park and G. M. Stanley. A curved C^0 shell element based on assumed natural-coordinate strains. *Journal of Applied Mechanics, Transactions of ASME*, 53:278–290, 1986.

[21] J. Jang and P. M. Pinsky. An assumed covariant strain based 9-node shell element. *International Journal for Numerical Methods in Engineering*, 24:2389–2411, 1987.

[22] Kato, K. and Bathe, K. J. . On the use of higher-order finite elements in structural mechanics. Report 89–4, Finite Element Research Group, Massachusetts Institute of Technology, Cambridge, MA., 1989.

[23] M. M. Hrabok and T. J. Hrudey. A review and catalogue of plate bending elements. *Computers & Structures*, 19(3):479–495, 1984.

[24] E. Reissner. The effect of transverse shear deformations on the bending of elastic plates. *Journal of Applied Mechanics, Transactions of ASME*, 12:69–76, 1945.

[25] R. D. Mindlin. Influence of rotatory inertia and shear in flexural motions of isotropic, elastic plates. *Journal of Applied Mechanics, Transactions of ASME*, 18:1031–1036, 1951.

[26] K. J. Bathe and E. Dvorkin. A four-node plate bending element based on Mindlin /Reissner plate theory and a mixed interpolation. *International Journal for Numerical Methods in Engineering*, 21:367–383, 1985.

[27] K. J. Bathe and F. Brezzi. On the convergence of a four-node plate bending element based on Mindlin/Reissner plate theory and a mixed interpolation. In J. R. Whiteman, editor, *Proceedings of the Conference on Mathematics of Finite Elements and Applications V*, pages 491–503. Academic Press, 1985.

[28] R. H. MacNeal. Derivation of element stiffness matrices by assumed strain distributions. *Nuclear Engineering Design*, 70:3–12, 1982.

[29] T. J. R. Hughes and T. E. Tezduyar. Finite elements based upon mindlin plate theory with particular reference to the four-node bilinear isoparametric element. *Journal of Applied Mechanics, Transactions of ASME*, 48:587–596, 1981.

[30] E. Hinton and H. C. Huang. A family of quadrilateral mindlin plate elements with substitute shear strain fields. *Computers & Structures*, 23(3):409–431, 1986.

[31] K. J. Bathe and F. Brezzi. A simplified analysis of two plate bending elements — the MITC4 and MITC9 elements. In G. N. Pande and J. Middleton, editors, *Proceedings of the International Conference on Numerical Methods in Engineering (NUMETA 87)*, page D46, Wales, 1987. University College of Swansea.

[32] F. Brezzi, K. J. Bathe, and M. Fortin. Mixed-Interpolated elements for Reissner-Mindlin plates. *International Journal for Numerical Methods in Engineering*, 28:1787–1801, 1989.

[33] K. J. Bathe, S. W. Cho, M. L. Bucalem, and F. Brezzi. On our MITC plate bending/shell elements. In A. Noor et al., editors, *Analytical and Computational Models of Shells*, pages 261–278. ASME Special Publication, 1989. CED–3.

[34] K. J. Bathe, M. L. Bucalem, and F. Brezzi. Displacement and stress convergence of our MITC plate bending elements. *Engineering Computations*, 7(4):291–302, 1990.

[35] F. Brezzi, M. Fortin, and R. Stenberg. Error analysis of mixed–interpolated elements for Reissner-Mindlin plates. *Mathematical Models and Methods in Applied Sciences.* to appear.

[36] F. Brezzi and M. Fortin. *Mixed and hybrid finite element methods.* Springer-Verlag, 1991.

[37] Johnson, C. and Pitkäranta, J. Analysis of some mixed methods related to reduced integration. *Mathematics of Computation*, 38:375–400, 1982.

[38] K. J. Bathe, F. Brezzi, and S. W. Cho. The MITC7 and MITC9 plate bending elements. *Computers & Structures*, 32(3/4):797–814, 1989.

[39] P. A. Raviart and J. M. Thomas. *A Mixed Finite Element Method for Second-Order Elliptic Problems*, volume 606 of *Lecture Notes in Mathematics*, pages 292–315. Springer-Verlag, Berlin, 1975.

[40] M. Crouzeix and P. A. Raviart. Conforming and nonconforming finite element methods for solving the stationary stokes equations. *RAIRO, Anal. Numer.*, R3:33–76, 1973.

[41] F. Brezzi, J. Douglas, Jr., M. Fortin, and L. D. Marini. Efficient rectangular mixed finite elements in two and three space variables. *RAIRO MAN, Mathematical Modeling and Numerical Analysis*, 21:581–604, 1987.

[42] T. Sussman and K. J. Bathe. A finite element formulation for nonlinear incompressible elastic and inelastic analysis. *Computers & Structures*, 26:357–409, 1987.

[43] B. Häggblad and K. J. Bathe. Specifications of boundary conditions for Reissner-Mindlin plate bending finite elements. *International Journal for Numerical Methods in Engineering*, 30:981–1011, 1990.

[44] D. N. Arnold and Falk. R. S. Edge effects in Reissner–Mindlin plate theory. In A. Noor et al., editors, *Analytical and Computational Models of Shells.* ASME Special Publication, 1989. CED–3.

[45] Symbolics Inc. VAX UNIX MACSYMA reference manual. Report SM10501030.011, , 1985.

[46] Pitkäranta, J. The problem of membrane locking in finite element analysis of cylindrical shells. Report, Helsinki University of Technology, Otakaari 1, SF-02150 Espoo, Finland, 1991.

[47] K. C. Park, E. Pramono, and H. A. Stanley, G. M. Cabiness. The ANS shell elements: Earlier developments and recent improvements. In A. Noor et al., editors, *Analytical and Computational Models of Shells*, pages 217–239. ASME Special Publication, 1989. CED–3.

[48] ADINA R&D. ADINA—A finite element program for automatic dynamic incremental nonlinear analysis. Report 90–1, ADINA R&D, Watertown, MA., 1990.

[49] G. M. Lindberg, M. D. Olson, and E. R. Cowper. New developments in the finite element analysis of shells. *National Research Council of Canada, Quarterly*

Bulletin of the Division of Mechanical Engineering and the National Aeronautical Establishment, 4:1–38, 1969.

[50] T. J. R. Hughes and M. Cohen. The heterosis finite element for plate bending. *Computers & Structures*, 9:445–450, 1978.

[51] T. Sussman and K. J. Bathe. Studies of finite element procedures. stress band plots and the evaluation of finite element meshes. *Engineering Computations*, 3:178–191, 1986.

[52] L. S. D. Morley and A. J. Morris. Conflict between finite elements and shell theory. Technical report, Royal Aicraft Establishment Report, London, 1978.

[53] L. S. D. Morley. *Skew Plates and Structures.* Pergamon Press, Oxford, 1963.

[54] K. J. Bathe and E. N. Dvorkin. On the automatic solution of nonlinear finite element equations. *Computers & Structures*, 17(5-6):871–879, 1983.

[55] R. H. Leicester. Finite deformations of shallow shells. In *Proceedings of American Society of Civil Engineers*, pages 1409–1423, 1968. Vol. 94, (EM6).